THE JOURNAL OF THE INSTITUTION OF ENGINEERS, MALAYSIA
KDN PP5476/10/2012 (030203) | ISSN 0126-513X

IEM
The Institution of Engineers, Malaysia

VOL. 86, NO. 2
JUNE 2025

Vol. 86, No. 2, June 2025
KDN PP5476/10/2012 (030203) ISSN 0126-513X

IEM COUNCIL SESSION 2025/2026

President
Ir. Prof. Dr. Jeffrey Chiang Choong Luin

Deputy President
Ir. Yau Chau Fong

Vice Presidents
Ir. Prof. Dr. David Chuah Joon Huang, Y.Bhg. Dato' Ir. Wan Nazari Wan Jusoh, Ir. Dr. Bernard Lim Kee Weng, Ir. Prof. Dr. Tan Chee Fai, Ir. Prof. Dr. Lau Hieng Ho, Ir. Yeong Chin Chow, Simon, Ir. Abdul Razak Yakob

Honorary Secretary
Ir. Chen Harn Shean

Honorary Treasurer
Ir. Prof. Dr. Wong Yew Hoong

Immediate Past President
Ir. Prof. Dr. Norlida Buniyamin

Past Presidents
YBhg. Datuk Ir. Prof. Ow Chee Sheng, Y.Bhg. Academician Tan Sri Dato' Ir. Prof. Em. Dr. Chuah Hean Teik, Y.Bhg. Dato' Ir. Dr. Lim Chow Hock, Ir. Dr. Tan Yean Chin, Ir. Ong Ching Loon

Civil Representative
Ir. Tu Yong Eng

Mechanical Representative
Ir. Ng Yong Kong

Electrical Representative
Ir. Mohd. Aman Hj. Idris

Structural Representative
Ir. Dr. Tan Kuang Leong

Chemical Representative
Ir. Kim Kek Seong

Other Disciplines Representative
Ir. Dr. Dhakshyani Ratnadurai

Multimedia Representative
Ir. Assoc. Prof. Dr. Lai Khin Wee

Women Engineers Representative
Ir. Dr. Syuhaida Ismail

Young Engineers Section Representatives
Mr. Lim Yiren, Mr. Darshan a/l Balasubramaniam, Ms. Ong Ye Shian, Mr. Chuah Pei Lim, Mr. Teoh Chi Yang

Council Members
Ir. Sharifah Azlina Raja Kamal Pasmah, Ir. Ts. Dr. Wan Syakirah Wan Abdullah, Ir. Dr. Mui Kai Yin, Ir. Shamil Abu Hassan, Ir. Ts. Wan Rizaluddin Abdullah Wan Ali, Ir. Dr. Aidil Chee Tahir, Ir. Dr. Angelia Liew San Chuin, Ir. Prof. Dr. Zuhaina Zakaria, Ir. Begum Irdawati Dowlad Rahuman, Ir. Chong Chee Yen, Ir. Khoo Chee Min, Ir. Ahmad Rafidi Mohayiddin *(casual vacancy for Ir. Abdul Razak Yakob)*, Ir. Dr. Chan Swee Huat, Ir. Alex Looi Tink Huey, Ir. Sukhairul Nizam Abdul Razak, Y.Bhg. Dato' Ir. Ting Chek Choon, Ir. Dr. Norashikin M Thamrin, Ir. Lee Cheng Pay, Datuk Ir. Chin Tet Fu @Willy, Ir. Ts. Gs. Br. Dr. Zarabizan Zakaria, Ir. Choo Lay Guat, Ir. Dr. Siow Chun Lim, Ir. Assoc. Prof. Dr. Leong Kah Hon, Ir. Ts. Dr. Sara Lee Kit Yee, Ir. Chan Wah Cheong, Ir. Dr. Marianah Masrie

Council Members by Invitation
Datuk Ir. Ho Hon Sang, Dato' Ir. Ahmad Sabirin Arshad, Ir. Dr. Sanjayan K.V. Velautham

Branch Chairman

1.	Penang	: Ir. Dr. Lee Choo Yong
2.	Southern	: Ir. David Puen Ming Shen
3.	Perak	: Ir. Dr. Tiah Oon Han
4.	Pahang	: Ir. Harzah Mazni Ramli
5.	Kedah-Perlis	: Ir. Jamaluddin Abdullah
6.	Negeri Sembilan	: Ir. Richard Khoo Nee Keong
7.	Kelantan	: Ir. Hj. Nik Burhanuddin Nik Yusoff
8.	Terengganu	: Ir. Zakaria Abdullah
9.	Melaka	: Ir. Lim Su Hian
10.	Sarawak	: Ir. Dr. Angelia Liew San Chuin
11.	Miri	: Ir. Meheron Selowara Joo
12.	Sabah	: Datuk Ir. Ts. Mohd Yaakob Hj. Jaafar

STANDING COMMITTEE ON INFORMATION AND PUBLICATIONS 2025/2026
Chairman: Ir. Prof. Dr. Lau Hieng Ho
Vice Chairman: Ir. Wan Rizaluddin Abdullah Wan Ali
Secretary: Ir. Assoc. Prof. Dr. Hum Yan Chai
Chief Editor: Ir. Prof. Dr. Lau Hieng Ho
Principal Bulletin Editor: Ir. Wan Rizaluddin Abdullah Wan Ali
Editor-In-Chief: Ir. Prof. Dr. Teo Fang Yenn
Chairman Webportal: Ir. Assoc. Prof. Dr. Hasril Hasini
Resource Centre Chairman: Ir. Tay Siang Hui
Committee Members: Ir. Lee Chang Quan, Ir. Lau Tai Onn, Ir. Yee Thien Seng, Ir. Dr. Tan Kim Seah, Ir. Dr. Bhuvendhraa Rudrusamy, Ir. Dr. Nor Ilia Anisa Aris, Ir. Ts. Wong Chee Fui, Ir. Dr. Moey Lip Kean, Ir. Begum Irdawati Dowlad Rahuman, Ms. Michelle Lau Chui Chui, Ir. Dr. Marianah Masrie

JOURNAL EDITORIAL BOARD 2025/2026
Editor-In-Chief: Ir. Ts. Prof. Dr. Teo Fang Yenn
Committee Members: Ir. Dr. Bhuvendhraa Rudrusamy, Ir. Ts. Dr. Hong Kai Sze, Ir. Ts. Wong Chee Fui, Ts. Assoc. Prof. Dr. Tee Boon Tuan, Ir. Assoc. Prof. Dr. Hassimi Abu Hasan, Ir. Ts. Assoc. Prof. Dr. Hum Yan Chai, Ir. Assoc. Prof. Dr. Lim Siong Kang, Ir. Assoc. Prof. Dr. Moey Lip Kean, Ir. Dr. Sara Lee Kit Yee, Ir. Dr. Assoc. Prof. Dr. Hasril Hasini, Ir. Ts. Dr. Syuhaida Ismail, Ir. Dr. Nor Ilia Anisa Aris, Dr. Suchithra Thangalazhy Gopakumar, Ir. Assoc. Prof. Dr. Syamsul Rizal Abd Shukor

CONTENTS

THIS ISSUE WAS PUBLISHED IN SEPTEMBER 2025

For advertisement placements and subscriptions, please contact:
DIMENSION PUBLISHING SDN. BHD. (449732-T)
Level 18-01, PJX-HM Shah Tower, No.16A, Persiaran Barat,
46050 Petaling Jaya, Selangor Darul Ehsan, Malaysia.
Tel: +(603) 7493 1049 Fax: +(603) 7493 1047
E-mail: info@dimensionpublishing.com

Printed by
DIMENSION PUBLISHING SDN. BHD. (449732-T)

PRINT QUANTITY: *500 COPIES*

INFLUENCE OF CEMENT TYPES ON COMPRESSIVE STRENGTH AND TEMPERATURE OF NORMAL GRADE CONCRETE

Siong Kang Lim[1*], Wai Man Loke[2], Ze Long Lim[3], Jee Hock Lim[4], Ming Kun Yew[5], You Wai Kuan[6]

Abstract

C20/25 concrete is known as normal strength concrete which has the cylinder and cube strength of 20 MPa and 25 MPa respectively, and it is a common concrete grade used in buildings and infrastructures. This study has investigated the workability, compressive strength and concrete temperature prepared by four types of local cement namely 42.5 N OPC, 52.5 N OPC, 32.5 N PLC and 32.5 R PFAC. XRD analysis were underwent to determine the composition phases of the four types of cement. Based on the slump, Vebe time and compacting factor tests, the results revealed that the concrete cast with 32.5 N PLC has the highest workability, followed by 32.5 R PFAC, 52.5 N OPC and lastly the 42.5 N OPC. In terms of compressive strength, 52.5 N OPC concrete has recorded the highest value of the compressive strengths at every curing ages of 7 days, 28 days, and 56 days, followed by 42.5 N OPC, 32.5 R PFAC, whereas 32.5 N PLC achieved the lowest compressive strength. Besides, the concrete temperature results showed that the concrete cast with 52.5 N OPC obtained the highest peak temperature, followed by 42.5 N OPC, 32.5 N PLC, and the 32.5 R PFAC obtained the lowest concrete temperature. The concrete temperature results were tally with the amount of heat of hydration calculated based on the composition phases percentage determined by XRD and Rietveld Refinement method. In short, the study provides an insight for the cements used in production of normal strength concrete to achieve designated strength and temperature control.

Received: *4 December, 2024*
Revised: *6 February, 2025*
Accepted: *1 April, 2025*

[1,2,3,4,5]Department of Civil Engineering, Lee Kong Chian Faculty of Engineering & Science, Universiti Tunku Abdul Rahman (UTAR), Sungai Long Campus, Jalan Sungai Long, 43000 Kajang, Malaysia.

[6]PKN Building Solutions Sdn Bhd, 1st Floor, Phase 2 Petronas Station, Lot 36904, Jalan Kolam Air ampang, 68000 Kuala Lumpur, Malaysia.

****Corresponding author:***
sklim@utar.edu.my

DOI: *https://10.54552/v86i2.271*

Keywords:
Compressive strength, Concrete temperature, Normal strength concrete, XRD analysis

1.0 INTRODUCTION

In construction industry, concrete has been used for a period of over 20 decades due to its lengthy stability and durability. From the other perspectives, concrete also provides great energy performance, adaptability, and ecologically favourable requirements (Mojtaba, Azin and Omidreza, 2013). The performance of concrete is influenced by numerous factors, including component materials, mix proportions, curing conditions, and environmental considerations. Among these, temperature is a crucial environmental factor affecting concrete behaviour. Variations in temperature can significantly impact the strength development, durability, and overall performance of concrete during its curing and service life. Concrete temperature is influenced not only by the ambient temperature but also by the cement content in the mix, which can be managed to control the temperature. Concrete construction in Malaysia faces significant challenges due to the country's tropical climate, characterised by high humidity and substantial temperature fluctuations. The curing temperature plays a crucial role in influencing the strength development and durability of the concrete. Excessive heat during curing might cause thermal cracking and deterioration in durability. It becomes feasible to regulate the curing process properly while managing the concrete temperature within acceptable ranges through studying the concrete temperature in relation to different cement types. Understanding the strength and thermal characteristics of concrete is essential to prevent issues such as thermal cracking during the curing process (Poudyal, Adhikari and Won, 2021).

The characteristics of Portland cement are determined by the fineness of grinding and the relative quantities of four major chemical components, which account for approximately 90% of the cement by weight (Hamad, 1995). Tricalcium silicate (C_3S), dicalcium silicate (C_2S), tricalcium aluminate (C_3A), and tetracalcium aluminoferrite (C_4AF) are the principal compounds of cement (Neville, 2011). When cement reacts with water, a chemical reaction, which is known as the heat of hydration is released by cement, thus altering the temperature of the concrete (Miguel and Rui, 2008). It is important to ensure there was no tremendous amount of heat liberated as negative repercussions such as thermal cracking and reduced long-term durability may occur. Besides that, various types of cement are associated with distinct heat of hydration properties, which have an immediate impact on the temperature of concrete (Mojtaba, Azin and Omidreza, 2013). In the case study on temperatures and stresses due to cement hydration on reinforced foundation by Miguel and Rui (2008), the authors stated that the temperature of the concrete must be considered throughout the curing process. Therefore, in order to effectively regulate

the curing process and maintain the concrete temperature within the acceptable ranges, it is critical to familiarise with the liberation of heat for each type of cement.

In Malaysia, there are limited study on concrete temperature and hydration heat in normal grade concrete used in buildings and infrastructure work, this research aims to study the strength properties and concrete temperature of C20/25 concrete that was prepared by various types of cement in Malaysia, namely the CEM I 42.5 N OPC, CEM I 52.5 N OPC, CEM II / B-L 32.5 N PLC and 32.5 R PFA cement. The fresh properties were evaluated through the fresh properties tests namely slump test, Vebe test, and compacting factor test. For hardened properties, compressive strength test was performed on concrete cubes at curing ages of 7, 28, and 56 days, and on concrete cylinders at 28 days. Additionally, concrete temperature test was conducted to determine the peak temperature generated by each concrete mix, and calculation for total heat of cement hydration was performed, whereas the phase compositions namely C_3S, C_2S, C_3A and C_4AF were determined through XRD scanning, and phase quantification by Rietveld refinement method (Karen, Ruben and Barbara, 2016; Evans and Evans, 2021).

2.0 DETAILS EXPERIMENTAL

This section describes raw materials preparation, screening of trial mixes, adopted method for workability test of fresh concrete, compression test of concrete cubes and cylinders, measurement of concrete temperature, and phase composition determination and quantification of various types of cement.

2.1 Raw Materials Preparation

The raw materials used in this research including cements, fine aggregates, 10 mm and 20 mm coarse aggregates and tap water.

Two types of local Ordinary Portland Cements and two types of local composite Cements were used in the study namely Ordinary Portland Cement- CEM I 52.5 N, Ordinary Portland Cement- CEM I 42.5 N, Portland Limestone Cement – CEM II / B-L 32.5 N, and lastly the 32.5 R Pulverised Fly Ash (PFA) Cement. These cements were sieved through a 300μm sieve opening to eliminate lumps and stored in an air-tight container before usage to prevent interaction with the external moisture (Lim *et al.,* 2024).

This research utilises the quartz sand, 10 mm and 20 mm coarse aggregates to produce the normal weight concrete. Both fine coarse aggregates were washed with clean water to remove debris and impurities, thereafter, dried under the sun prior to usage (Lim *et al.,* 2024). The sieve analysis was conducted in accordance with ASTM C33/C33M (2018) and the particle size distribution results are shown in Figure 1. The fineness modulus of 7.11 and 2.05 were obtained for coarse and fine aggregates respectively.

Tap water that comply with the ASTM C1602/C1602M (2022) was used for the casting and curing process of the concrete.

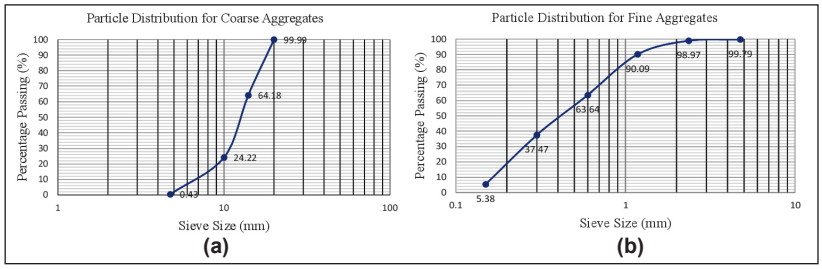

Figure 1: Particle size distribution of aggregates (a) Coarse aggregates; (b) Fine aggregates

2.2 Trial Mixes

Table 1 shows the mix proportions based on Design of Normal Concrete Mixes (2nd Edition) by Building Research Establishment (1997) for the trial mixes. The reference cement used for trial mixes was the 42.5 N local OPC. The water to cement ratio was adjusted from 0.63 to 0.72 to obtain cube compressive strength of 25 MPa. The concrete cubic specimens in trial mixes were prepared and underwent the compression test. Based on the compressive strength of trial mixes using 42.5N OPC depicted in Table 2, an optimal mix proportion of the reference cement has been selected for comparison study on concrete strength and temperature with those mixes prepared with different types of local cement.

Table 1: Mix Proportions for trial mixes based on 1m³ concrete volume

W/C Ratios	Mix Proportion (kg/m³)				
	Cement	Water	Aggregate		
			Fine	10mm	20mm
0.63	357.1	225	632.8	375	750.1
0.67	335.8	225	676.1	367.7	735.4
0.72*	312.5	225	721	360.5	721

**Optimal mix proportion based on compressive strength results in Table 2*

2.3 Workability Test

Slump test conducted in this study complied with the standard of ASTM C143/C143M (2018). First, a cone-shaped frustum with 300mm high was used as the mould for the slump test. The mould, with a 200mm-diameter base and a 100mm-diameter opening at the top, was placed on a flat, smooth, nonporous base plate. Fresh concrete was then poured into the mould in three layers, with each layer comprising approximately one-third of the mould's volume. Each layer was uniformly tamped with 25 strokes using the rounded end of a tamping rod. Excessive concrete was removed, and the top surface levelled with a trowel. The mould was then slowly and vertically removed, allowing the unsupported concrete to slump. The slump cone was placed next to the slumped concrete, and the tamping rod was laid across the top of the cone. The slump value was measured as the difference between the height of the slump cone and the center point of the concrete slump specimen.

Vebe test conducted in this study complied with the standard of BS EN 12350-3 (2019). The slump cone was placed into the cylindrical metal pot of the container for slump test. The procedure begun by rotating the consistometer, positioning the glass disc rider attached to the swivel arm on the surface of the unsupported concrete inside the container. The vibrating machine was then activated, causing the

concrete to consolidate within the container. The vibration continued until the original conical shape of the fresh concrete transitioned into a cylindrical form. The transformation was completed after the glass disc rider had been fully submerged in the fresh concrete, indicating the end of the compaction process. The duration of this entire process was recorded as Vebe Time.

Compacting factor test, which adhered to the BS EN 12350-4 (2019) has been conducted to determine consistency of the mixes. Fresh concrete was placed into the upper hopper using a hand scoop until it was filled and levelled. The trapdoor at the bottom of the upper hopper was opened, allowing the concrete to flow into the lower hopper. Then, the trapdoor of the lower hopper was opened, permitting the concrete to descend into a cylinder placed below. Excessive concrete above the cylinder's top level was trimmed and leveled with a trowel. The partially compacted concrete obtained was weighed and recorded. The fully compacted concrete was obtained through layered compaction with standard tamping rod. The compacting factor was computed by Equation (1) below.

$$Compacting\ Factor = \frac{Partially\ Compacted\ Concrete}{Fully\ Compacted\ Concrete} \quad (1)$$

2.4 Compression Test

The compression test conducted is complied with the standard of BS EN 12390-3 (2019) for cubic sample and ASTM C39 (2021) for cylindrical sample. The concrete samples were water cured for 7, 28, and 56 days, and subsequently the compression test were performed. The results were taken as average of triplicate.

2.5 Concrete Temperature Measurement

This temperature test which complies with ASTM C1064 (2017) was conducted to monitor changes in concrete temperature over a specified period. The temperature of freshly mixed concrete in lab scaled 250 mm concealed square mould (0.0156 m^3) was measured with a digital probe thermometer inserted at center of the fresh concrete. The temperature readings were recorded at 15-minute intervals for the first 2 hours, at 30 minutes intervals for the third hour, and at 1-hour intervals for the subsequent hours until the temperature dropped from peak temperature. The hydration heat generated by the four main cement compounds was computed based on the values in J/g recommended by Neville and Brooks (2010), which C_3S is 502 J/g, C_2S is 260 J/g, C_3A is 867 J/g and C_4AF is 419 J/g. Equation (2) below shows the calculation of total hydration heat released by cement in kilo Joule (kJ).

$$Total\ Hydration\ Heat\ (kJ) = Cement\ used(kg) \times cement\ compound\ \% \times heat\ generated\ by\ cement\ compound\ in\ \frac{J}{g} \quad (2)$$

2.6 Chemical Composition Determination

The X-Ray Diffraction (XRD) test has been adapted to analyse the phase compositions presented in the studied cements in accordance with ASTM C1365 (2018). Each cement powder was packed into a sample holder and placed in the path of an X-ray beam scanning. The cement powder sample was scanned at diffraction angle of 2^{θ} from 5 to 85 degrees for 40 minutes. XRD raw data was generated, and subsequently Rietveld refinement method in HighScore Plus Software was adopted to perform phase identification and phase quantification for four major chemical compounds namely C_3S, C_2S, C_3A, and C_4AF in the cement sample.

3.0 RESULTS AND DISCUSSION

This section shows results of trial mixes, workability of fresh concrete, compressive strength of concrete cubes and cylinders, C20/25 concrete peak temperature, and hydration heat generated by various types of cement in this study. The results were discussed and justified accordingly.

3.1 Compresive Strength of Trial Mixes

Trial mixes with different water to cement ratio were conducted to determine the optimal water to cement ratio to be used in actual mixes. Table 2 illustrates the 7-day and 28-day compressive strengths of concrete cubes from three trial mixes tabulated in Table 1. Based on the results, the water-to-cement ratio of 0.72 was treated as optimal ratio for this study, as it yielded an average 28-day cube strength of 25.72 MPa, aligning closely with the designated strength, and more economical compared with the other two mixes.

Table 2: Compressive strength of trial mixes

W/C Ratios	7 Days Strengths (MPa)				28 Days Strengths (MPa)			
	1	2	3	Average	1	2	3	Average
0.63	24.37	22.72	23.56	23.55	36.20	33.93	34.86	35.00
0.67	20.09	22.21	23.11	21.80	30.10	30.19	31.22	30.50
0.72	18.45	20.76	19.57	19.59	25.10	26.44	25.63	25.72

3.2 Workability

The slump test results in Table 3 reveal the slump values are ranged between 100 mm and 175 mm, confirming the exceptional workability of the concrete. It's worth noting that the concrete cast with 32.5 N PLC recorded the highest slump value, reaching 173 mm. The finding by Poudyal, Adhikari and Won (2021) stated that when compared with OPC concrete, higher slump value was achieved by PLC at same w/b ratio. In blended cement systems with higher packing density due to well distribution of Nano limestone powder particles, less water is trapped between the particles, making more water available to lubricate the particles, increasing the flow and workability of the fresh cement paste (Knop, Peled and Cohen, 2014). The Vebe time and compacting factor in Table 3 below further proven that the 32.5N PLC mix possesses the highest level of workability.

Based on Table 3, the 32.5 R PFAC mix is ranked as the second most workable concrete among the all mixes. The slump tests, vebe test, and compacting factor test yielded values of 140 mm, 5.59 seconds, and 0.9734, respectively. The findings align with the study by Nkomo, Masu and Nziu (2019), which concluded that incorporating fly ash into concrete positively affects its rheological properties and enhancing workability. Fly ash increases the paste volume, enhancing plasticity and cohesion. Moreover, the spherical shape of fly ash particles acts as a lubricant at the aggregate interface, reducing friction

and improving workability. Generally, a higher fly ash volume fraction correlates with superior workability in the concrete mix. The spherical morphology of fly ash particles also facilitates easier handling, placement, and finishing of concrete, promoting smooth flow within the mixture and significantly enhancing workability (Nkomo, Masu and Nziu, 2019). The both 42.5 N OPC and 52.5 N OPC mixes exhibited lower slump values, longer Vebe time, and lower compacting factor values compared with that of 32.5 N PLC and 32.5 R PFAC mixes.

Table 3: Workability test results of C20/25 concrete cast with different types of cement

Cement Types	Slump Value (mm)			Vebe Time (s)			Compacting Factor		
	1	2	Average	1	2	Average	1	2	Average
42.5 N OPC	118	112	115	6.98	6.54	6.76	0.9676	0.9719	0.9698
52.5 N OPC	124	129	126.5	6.03	5.87	5.95	0.9726	0.9682	0.9704
32.5 N PLC	175	169	173	4.57	5.24	4.91	0.9774	0.9804	0.9789
32.5 R PFAC	136	144	140	5.81	5.37	5.59	0.9708	0.9759	0.9734

3.3 Density

There were two types of densities studied in this research, namely the fresh and hardened density. Based on Table 4, it is observed that 52.5 N OPC had the highest values for both fresh and hardened density, followed by 42.5 N OPC, 32.5 R PFAC, and finally 32.5 N PLC. Comparing 42.5 N OPC and 52.5 N OPC, the concrete cast with 52.5 N OPC recorded the highest fresh and hardened densities of 2283.16 kg/m³ and 2258.17 kg/m³, respectively. This could be due to the higher specific gravity of 52.5 N OPC compared to the PLC and PFAC as shown in Table 4. Besides, Table 5 shows that 52.5 N OPC has the highest chemical compounds which may lead to fast chemical reaction, thus contribute to slight increase of density.

For the concrete cast using 32.5 N PLC, the lowest fresh and hardened densities were recorded at 2254.02 kg/m³ and 2245.04 kg/m³, respectively. The inclusion of Nano size limestone particles with smaller average size and higher surface area compared to OPC suggesting higher packing density of blended cement systems (Knop, Peled and Cohen, 2014; Poudyal, Adhikari and Won, 2021). However, limestone particles are lighter than cement clinker particles, potentially leading to a lighter concrete mixture overall (Knop, Peled and Cohen, 2014). Table 4 shows that the 32.5 N PLC obtained lowest measured specific gravity at 2.57. On the other hand, the concrete cast with 32.5 R PFAC showed slightly higher fresh and hardened densities compared to 32.5 N PLC concrete, at 2256.20 kg/m³ and 2248.00 kg/m³, respectively. Adabu, Mohammed and Shafiq (2017) stated that specific gravity of local fly ash is 2.30 while that of local 42.5 N OPC is 3.15. Experimental results in Table 4 reveal that 32.5 R PFAC has smaller SG than that of both OPCs, which resulted in a lighter density concrete mixture compared to that of OPC concrete.

Table 4: Fresh and hardened densities of C20/25 concrete cast with different types of cement

Types of Cement	Fresh Density (kg/m³)	Hardened Density (kg/m³)	Specific Gravity (SG)*
42.5 N OPC	2265.68	2253.43	3.22
52.5 N OPC	2283.16	2258.17	3.09
32.5 N PLC	2254.02	2245.04	2.57
32.5 R PFAC	2256.20	2248.00	2.62

**Le Chatelier Flask method was adopted to measure specific gravity in accordance with ASTM C188 (2023), the values are the average of two measurements.*

3.4 Compressive Strength of Actual Mixes

The optimal water to cement ratio was determined as 0.72 based on the trial mixes results. In actual mixes, both concrete cubes and cylinders were cast and tested for compression test. As depicted in Figure 1, concrete cast with 52.5 N OPC cement exhibited the highest compressive strength across all curing periods, followed by mixes with 42.5 N OPC, 32.5 R PFA, and 32.5 N PLC, which demonstrated the lowest compressive strength throughout the curing periods. The use of a higher strength class of cement typically results in concrete cubes with greater compressive strength (Gupta, 2019). Therefore, the results for the compressive strength tests accurately reflected the trend.

Based on phase quantification results in Table 6, it is evident that the 52.5 N OPC contains a higher proportion of cement clinker compared to that of 42.5 N OPC. Since cement clinker contributes to concrete strength, thus higher cement clinker content in 52.5 N OPC resulted in greater compressive strength than that of 42.5 N OPC. On the other hand, the compressive strength of the concrete cast with 32.5 N PLC were the lowest. Although both PFAC and PLC have similar total cement clinker content as shown in Table 6, but 32.5 N PLC mix possesses the lowest C3S compound. Wang (2018) mentioned that the reactivity of limestone powder is much lower compared to cement and fly ash. Besides, pozzolanic behaviour of PFAC further contributed to medium to long term strength gain through pozzolanic activity, which proven by strength development shown in Figure 2.

Based on Figure 2, the increase in 7-day strengths to 28-day strengths for 42.5 N OPC, 52.5 N OPC, 32.5 N PLC, and 32.5 R PFAC mixes were 64.05%, 59.54%, 29.36%, and 50.59%, respectively. When fly ash was used as a partial replacement for cement in the studied concrete, it decreased the compressive strength at the ages of 7-day and 28-day compared to that of the OPC mixes, which is tally with the findings by Poudyal, Adhikari and Won (2021). However, fly ash's pozzolanic behaviour contribute positively to the concrete's long-term compressive strength. The strength development results in Figure 2 show that the 32.5 R PFA mix exhibited the most significant increment in compressive strength from ages of 28 days to 56 days. Specifically, the compressive strength of 32.5 R PFAC increased by 38.15%, rising from 17.98 MPa to 24.84 MPa during the period. On the other hand, the percentage increments of compressive strength from ages of 28 days to 56 days for 42.5 N OPC, 52.5 N OPC, and 32.5 N PLC mixes were 14.19%, 11.38%, and 14.79%, respectively, which are lower than the increment of 32.5 R PFAC mix.

According to the results depicted in Figure 3 above, the 28-day compressive strengths of the concrete cylinders possessed

a similar pattern to that of the concrete cubes cast with the four types of cement. The strengths increased in ascending order from 32.5 N PLC, 32.5 R PFAC, 42.5 N OPC mixes, and finally, 52.5 N OPC mix. Among these, the concrete cylinders cast with 52.5 N OPC exhibited the highest 28-day compressive strength at 23.47 MPa, while those cast with 32.5 N PLC showed the lowest 28-day compressive strength at 11.78 MPa. Generally, the strengths of the concrete cylinders were 85 to 90 percent corresponded to that of concrete cubes as shown in Table 5 below.

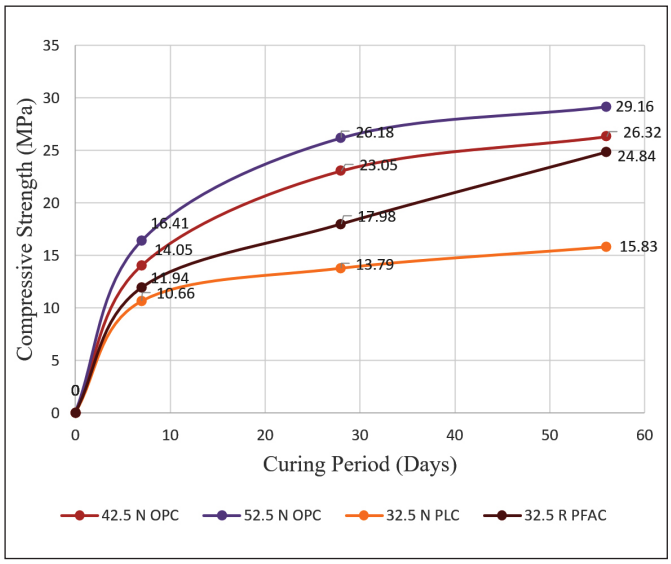

Figure 2: Compressive strength at 7, 28 and 56 days of concrete cubes cast with different cement

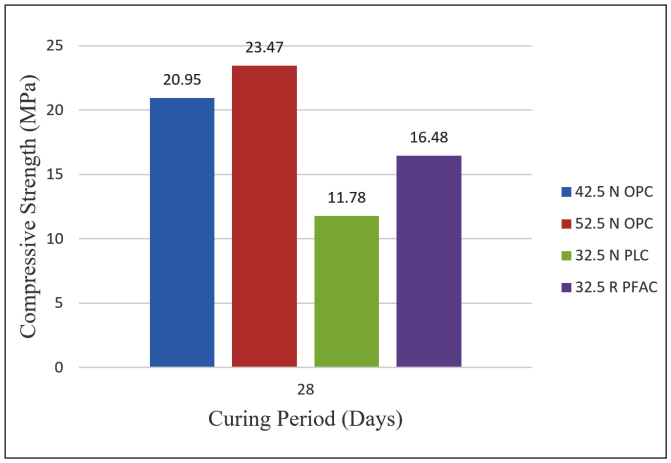

Figure 3: 28 days compressive strength of concrete cylinders cast with different types of cement

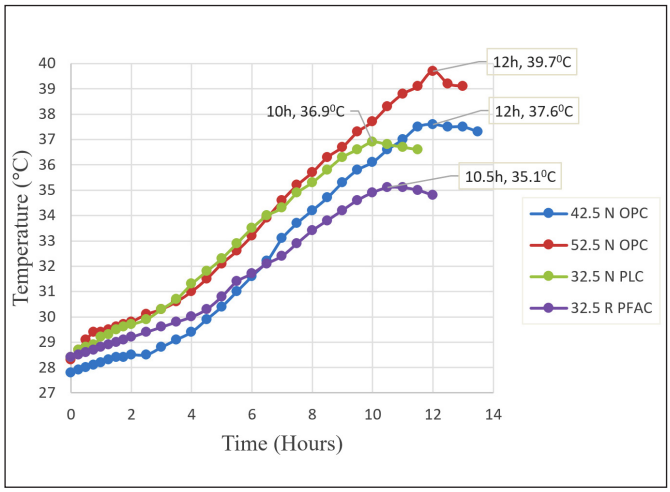

Figure 4: Temperature of concrete cast with different types of cement

3.5 Concrete Temperature

Based on optimal mix proportion shown in Table 1, at 0.72 w/c, cement used is 312.5 kg/m³. Thus, at 0.0156 m³ concrete volume, cement used in this study was 4.875 kg. It was evident that the concrete cast with 52.5 N OPC had reached the highest peak temperature of 39.7°C at 12 hours, and followed by 42.5 N OPC fresh mix reached its peak temperature of 37.6°C at 12 hours, 32.5 N PLC fresh mix reached 36.9°C at 10 hours, and lastly 32.5 R PFAC fresh mix obtained the lowest peak temperature of 35.1 °C at 10.5 hours. Based on Table 6, the increments of concrete temperature were recorded at 9.8°C, 11.4°C, 8.5°C and 6.7°C for 42.5 N OPC, 52.5 N OPC, 32.5 N PLC and 32.5 R PFAC fresh mixes respectively. Based on Table 7, it shows both ordinary Portland cement contain a greater proportion of tricalcium silicate (C_3S) and dicalcium silicate (C_2S) compared to both composite cements. The 52.5 N OPC possesses the highest amount of tricalcium aluminate (C_3A) and tricalcium silicate (C_3S), therefore accelerated the heat generation, leading to the highest peak temperature and highest temperature increment as shown in Figure 4 and Table 6 respectively. On the other hand, the PLC concrete recorded the 2nd lowest increment in temperature due to the lower C3S content compared to that of 42.5 N and 52.5 N OPCs. The incorporation of limestone powder has diluted the Portland cement clinker. Lastly, the fresh mix cast with 32.5 R PFAC recorded the lowest increment in temperature of 6.7°C due to the lowest C_3A and cement clinker content. A study by Nkomo, Masu and Nziu (2019) concluded that ground fly ash lowered the heat generated during hydration compared to pure cement.

Table 5: Comparison of cube strength and cylinder strength of C20/25 concrete cast with different types of cement

Types of Cement Mixture	28-Day Cube Strength (MPa)	28-Day Cylinder Strength (MPa)	Difference in MPa*	Cylinder Strength Corresponding to Cube Strength (%)
42.5 N OPC	23.05	20.95	2.10	90.89
52.5 N OPC	26.18	23.47	2.71	89.65
32.5 N PLC	13.79	11.78	2.01	85.42
32.5 R PFAC	17.98	16.48	1.50	91.66

**Compressive strength of concrete cube subtracts compressive strength of concrete cylinder*

As the proportion of fly ash in the concrete increased, there was a progressive reduction in heat release during hydration. Furthermore, the increased fly ash volume enlarged the surface area available for interaction, resulting in higher absorption of calcium ions. This increased absorption slowed down the accumulation of calcium ions in the early stages of hydration, thereby reducing the overall heat of hydration.

Table 6: Comparison of hydration temperature of C20/25 concrete cast with different types of cement

Types of Cement Mixture	Initial Concrete Temperature (°C)	Peak Concrete Temperature (°C)	Increment in Concrete Temperature (°C)	Increment in Percentage (%) *
42.5 N OPC	27.8	37.6	9.8	35.3
52.5 N OPC	28.3	39.7	11.4	40.3
32.5 N PLC	28.4	36.9	8.5	29.9
32.5 R PFAC	28.4	35.1	6.7	23.6

**Increment in °C corresponded to initial concrete temperature*

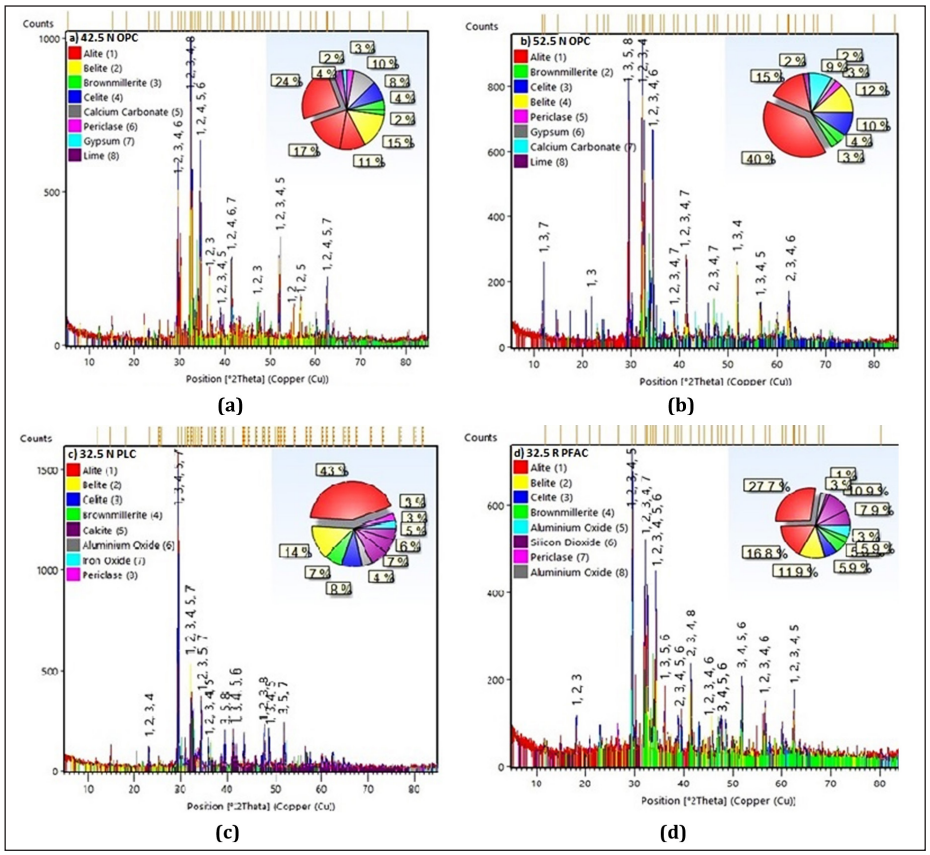

Figure 5: Phase composition of different types of cement powder. (a) 42.5 N OPC; (b) 52.5 N OPC;(c) 32.5 N PLC; (d) 32.5 R PFAC

3.6 Phase Quantification and Hydration Heat

XRD analysis was performed, and Rietveld refinement method has been adopted to determine the phase composition and quantification of respective cement powder as shown in Figure 5. The percentage of each chemical compound is crucial, as it was used to calculate the total heat of hydration generated by cements used in this study. The various types of cement used were assumed fully hydrated and the calculation of total hydration heat was computed using Equation 2 above, subsequently the results are presented in Table 7 below. Based on the results shown, the total heat of hydration for 52.5 N OPC is the highest, followed by 42.5 N OPC, 32.5 N PLC and lastly 32.5 R PFAC. The hydration heat results are tally with the respective peak temperature recorded in Figure 4 above.

4.0 CONCLUSION

Some conclusions can be drawn based on the study:

1. The incorporation of pulverised fly ash and limestone powder in concrete could increase workability of fresh concrete compared to that of the OPC mixes.
2. The incorporation of pulverised fly ash and limestone powder in concrete could slightly decrease fresh and hardened densities of concrete compared to that of the OPC mixes.
3. At the same mix proportion, compression test results revealed that 52.5 N OPC C20/25 mix exhibited the highest 28-day compressive strength among all cements, followed by 42.5 N OPC mix, 32.5 R PFA mix, and lastly 32.5 N PLC mix.
4. The compressive strength of the concrete cylinders from the studied mixes were 85 to 90 percent corresponded to that of concrete cubes.

Table 7: Chemical compounds and total heat of hydration of different types of cement

Types of Cement	C_3S Content (%)	C_2S Content (%)	C_3A Content (%)	C_4AF Content (%)	Total Cement Clinker (%)	Total Heat of Hydration (kJ)*
42.5 N OPC	52.0	15.0	8.0	6.0	81	1923.4
52.5 N OPC	55.0	12.0	14.0	11.9	92.9	2332.9
32.5 N PLC	43.0	14.0	8.0	7.0	72	1710.9
32.5 R PFAC	44.5	11.9	5.9	8.9	71.2	1671.0

**The calculated total heat of cement hydration is based on 0.0156 m^3 concrete volume, whereas 4.875 kg cement is used*

5. The incorporation of pulverised fly ash and limestone powder in concrete could reduce the peak temperature and temperature increment of concrete, whereas the dilution of principal compounds in the composite cements has reduced the total hydration heat generated by the cements.

ACKNOWLEDGMENT

The authors gratefully acknowledge Universiti Tunku Abdul Rahman for providing facilities support, and PKN Building Solution Sdn Bhd for financial assistance to this study in the form of a research grant (Vote No.: 8173/0001).

AUTHORS CONTRIBUTION

- **Siong Kang Lim and You Wai Kuan:** Conceptualisation, study design, and supervision.
- **Wai Mun Loke and Ze Long Lim:** Data collection, methodology, and formal analysis.
- **Ming Kun Yew and Jee Hock Lim:** Writing original draft preparation and literature review. ■

REFERENCES

[1] Adabu M., Mohammed B. S. & Shafiq N. (2017) Mechanical performance of roller compacted rubbercrete with different mineral filler. *Jurnal Teknologi, 79(6),* pp.75-88.

[2] American Society for Testing and Materials. (2017). *ASTM C1064 Standard Test Method for Temperature of Freshly Mixed Hydraulic-Cement Concrete.* West Conshohocken, United States: ASTM.

[3] American Society for Testing and Materials. (2018). *ASTM C33/C33M Standard Specification for Concrete Aggregate.* West Conshohocken, United States: ASTM.

[4] American Society for Testing and Materials. (2018). *ASTM C143/C143M Standard Specification for Concrete Aggregates.* West Conshohocken, United States: ASTM.

[5] American Society for Testing and Materials.(2018). *ASTM C1365 Determination of the Proportion of Phases in Portland Cement and Portland-Cement Clinker.* West Conshohocken, United States: ASTM.

[6] American Society for Testing and Materials. (2021). *ASTM C39 Standard Test Method for Compressive Strength of Cylindrical Concrete Specimens.* West Conshohocken, United States: ASTM.

[7] American Society for Testing and Materials.(2022). *ASTM C1602/C1602M Standard Specification for Concrete Aggregates.* West Conshohocken, United States: ASTM.

[8] British Standards Institution. (2019). *BS EN 12350-3 Testing fresh concrete Part 3: Vebe test.* London: BSI.

[9] British Standards Institution. (2019). *BS EN 12350-4 Testing fresh concrete Part 4: Degree of Compactibility*. London: BSI.

[10] British Standards Institution. (2019). BS EN 12390-3 *Testing hardened concrete Part 3: Compressive strength of test specimens.* London: BSI.

[11] Building Research Establishment. (1997). *Design of normal concrete mixes, 2nd edition.* BR 331, Garston, CRC.

[12] Evans, J. S. O. & Evans, I. R. (2021). Structure analysis from powder diffraction data: rietveld refinement in excel. *Journal of Chemical Education, 98(2):* 495-505.https://doi.org/10.1021/acs.jchemed.0c01016

[13] Gupta, C. (2019). Effect of grade of cement on strength of concrete. Retrieved on 17 April 2024. https://www.researchgate.net/publication/331099515_effect_of_grade_of_cement_on_strength_of_concrete

[14] Hamad, B. S. (1995). Investigations of chemical and physical properties of white cement concrete. *Advanced cement based material, 2(4):* 161-167. https://doi.org/10.1016/1065-7355(95)90017-9

[15] Karen, S., Ruben, S., & Barbara, L. (2016). *A practical guide to microstructural analysis of cementitious materials.* 1st Ed. Boca Raton: CRC Press.

[16] Knop, Y., Peled, A., & Cohen R. (2014). Influences of limestone particles size distributions and contents on blended cement properties. *Construction and Building Materials, [e-journal] 166:* 26-34. https://doi.org/10.1016/j.conbuildmat.2014.08.004

[17] Lim, S. K., Eng, L. Y., Lim, J. H., Yew, M. K., Lee, Y. L., & Lim, M. H. (2024). Enhancing Strength and Impact Resistance of Latex Rubberized Concrete through Steel Fiber Incorporation. *Journal of Advanced Research in Applied Mechanics, 112(1)*: 125-136. https://doi.org/10.37934/aram.112.1.125136

[18] Miguel, A.,& Rui, F. (2008). Temperatures and stresses due to cement hydration on the R/C foundation of a wind tower—A case study. *Engineering Structures,* 30: 2392–2400. https://doi.org/10.1016/j.engstruct.2008.01.018

[19] Mojtaba, V. S., Azin, S. B.& Omidreza A.(2013). Assessment of the roles of various cement replacement in achieving the sustainable and high performance concrete. *International Journal of Advances in Engineering & Technology, 6(1):* 68-77.

[20] Neville, A. M., & Brooks, J. J. (2010). *Concrete Technology.* 2nd Ed. Prentice Hall: Pearson Education Ltd.

[21] Neville, A. M. (2011). *Properties of concrete.* 5th ed. Harlow: Pearson Education Ltd.

[22] Nkomo, N. Z., Masu, L. M. & Nziu, P. K. (2019). The effect of fly ash on the workability and mechanical properties of concrete slabs: a review. *International Journal of Mechanical and Production Engineering Research and Development (IJMPERD) 9(5):* 591-610.

[23] Poudyal, L., Adhikari, K. & Won. M.(2021). Mechanical and durability properties of portland limestone cement (PLC) incorporated with nano calcium carbonate ($CaCO_3$). *Materials, 14(4):* 905. https://doi.org/10.3390/ma14040905

[24] Wang, X. Y. (2018). Analysis of hydration and strength optimization of cement-fly ash-limestone ternary blended. *Concrete Construction and Building Materials, 66:* 130-140. https://doi.org/10.1016/j.conbuildmat.2018.01.058

PROFILES

SIONG KANG LIM received his B.Eng. in (Civil Engineering), M.Eng. (Construction Management) and Ph.D. (Civil Engineering) degrees from University of Technology (UTM), Malaysia in 2001, 2002 and 2008, respectively. He is now the associate professor in the Lee Kong Chian Faculty of Engineering and Sciences, Universiti Tunku Abdul Rahman (UTAR), Malaysia. He is a member of The Institution of Engineers, Malaysia (IEM), Committee member of IEM Journal Editorial Board, and Professional Engineer of Board of Engineers, Malaysia (BEM).
Email address: sklim@utar.edu.my

WAI MAN LOKE earned his B.Eng in Civil Engineering from Universiti Tunku Abdul Rahman (UTAR), Malaysia in 2024. He is currently working as a civil engineering consultant, where the company is specialised in providing structural design services and various engineering consultancy services. He is also registered as Graduate Engineer (GE) under Board of Engineers, Malaysia (BEM).
Email address: brynlokewaiman@yahoo.com

ZE LONG LIM attained his B.Eng. in (Civil Engineering) from Universiti Tunku Abdul Rahman (UTAR), Malaysia in 2024. He is now currently working at a civil engineering consultancy firm, specialising in structural design and project management. Passionate about delivering innovative and sustainable engineering solutions while maintaining high-quality standards. He is a Graduate Engineer (GE) of Board of Engineers, Malaysia (BEM).
Email address: limzelong727@gmail.com

JEE HOCK LIM received his B.Eng. in (Civil Engineering) and Ph.D. (Civil Engineering) degrees from University of Technology (UTM), Malaysia in 2006 and 2014, respectively. He is now the associate professor in the Lee Kong Chian Faculty of Engineering and Sciences, Universiti Tunku Abdul Rahman (UTAR), Malaysia. He is a member of The Institution of Engineers, Malaysia (IEM) and Professional Engineer of Board of Engineers, Malaysia (BEM).
Email address: limjh@utar.edu.my

MING KUN YEW earned his degree in Mechanical Engineering from the Faculty of Mechanical Engineering, UM (Manufacturing). He pursued further education at the same university, attaining both his MSc. Eng. and Ph.D. in Civil and Environmental Engineering with a collaboration in Mechanical Engineering (Materials). He currently holds the position of Associate Professor at the Lee Kong Chian Faculty of Engineering and Sciences, Universiti Tunku Abdul Rahman (UTAR), Malaysia. He is affiliated with The Institution of Engineers, Malaysia (IEM) and is recognised as a Professional Engineer by the Board of Engineers, Malaysia (BEM). He actively participates in The Institution of Engineers, Malaysia (IEM) under Material Engineering Technical Division (MaTD), serving as ordinary committee member. In this role, he takes a leading role and contributes to organising competitions for Integrated Design Projects (IDP) involving various institutes across Malaysia.
Email address: yewmk@utar.edu.my

YOU WAI KUAN is a specialist contractor in building repair and rectification for the past 25 years. His intuition in trouble-shooting and urge to go extra miles in search for causes and solutions particularly in leakage, leak detection, concrete repair and protection has led him to develop holistic insight into building pathology in the buildings in Malaysia. His expertise has been recognised and he has been appointed as an instructor in Inter-floor Leakage by the Tribunal of Home Buyer Claim and Strata Management, various Commissioners of Buildings, University of Malaya and a number of professional bodies. Additionally, he also writes regularly as an industry expert in building leakage, indoor mold, concrete repair and protection (EN1504), building pathology, defect management and building resiliency to numerous industrial bulletins, journals, magazines and newspapers. To-date, his credentials have enabled him to become a building forensic expert and expert witness in courts or tribunals.
Email address: kuanyouwai@gmail.com

A COMPARISON BETWEEN PERFORMANCE OF EC GEOBLOCK WITH CONVENTIONAL GEOGRID USED AS SOFT GROUND IMPROVEMENT METHODS

Yan Ho Loke[1], Nik Norsyahariati Nik Daud[2*], Wyn Shern Loke[3]

Abstract

As urban development advances, population increases which leads to more demand in structures such as roads, houses and more. Most structures are built with some sort of ground improvement or foundation. One of the most common techniques is to use geogrid to reinforce the structure and the ground due to its performance and cost effectiveness. In the current study a new arrangement of EC Geoblock is proposed for ground improvement and the performance are compared with geogrid. The study consists of two phases: First Phase begins with the simulation through PLAXIS 3D by excavation with depth of 0.55m then laying of geogrid or EC Geoblock and backfilled with selected filling material and ends with application of surface load on top of the strengthened area. Second Phase was proceeded with the variation of 5 scenarios; Scenario I – unreinforced soil, Scenario II – soil reinforced with 2 layers of geogrid with sand backfill, Scenario III – soil reinforced with 5 layers of geogrid with sand backfill, Scenario IV – soil reinforced with EC Geoblock with sand backfill and lastly Scenario V – soil reinforced with EC Geoblock with sand backfill and collapse load of case III. From the results, the best performing method in improving the mechanical properties is Scenario V with the least settlements among all simulations. Therefore, the new arrangement of EC Geoblock is feasible to be used in strengthening the ground in required places before construction of superstructure.

Received: *19 October, 2024*
Revised: *25 February, 2025*
Accepted: *2 April, 2025*

[1,2]Department of Civil Engineering, Faculty of Engineering, Universiti Putra Malaysia, 43400 Serdang, Selangor, Malaysia.

[1,3]GEOCO SDN BHD, 43300 Seri Kembangan, Selangor, Malaysia.

[2]Housing Research Center (HRC), Faculty of Engineering, Universiti Putra Malaysia, 43400 Serdang, Selangor, Malaysia.

****Corresponding author:***
niknor@upm.edu.my

DOI: *https://10.54552/v86i2.266*

Keywords:
EC geoblock, Geogrid, Soft clay, Soil reinforcement

1.0 INTRODUCTION

As more structures are required to be built on critical ground condition such as soft soil due to reasons such as land scarcity, population growth and to prevent landslides and other ground hazards; a cost-effective way of improving the ground to accommodate the structures are necessary.

Figure 1 shows a soft soil location in Peninsular Malaysia. Two major groups of alluvial deposits have been identified as riverine deposits and the marine, estuarine and brackish deposits. Soft clay which is part of soft soil that has low shear strength, low permeability and highly compressible. This has been experienced by Mohamad *et al.,* (2016) who had studied two sites in Malaysia deals with soft clay. They found out that the instability of the ground during construction works had caused delay and cost overrun in completion of the project in Selangor, whereas occurrence of continuous post construction settlement had affected the integrity and serviceability of the building in Sabah. Structure on unreinforced soft clay will experience high settlement due to the high compressibility property of soft clay. In addition, due to its low permeability, the ability to drain water especially during rain is very poor, thus lead to soil instability.

Currently, many methods have been used to strengthen the stiffness and strength of the soil in its initial states and when subjected to loading. Geogrid is popular due to its cost efficiency and environmentally friendly nature. The study of geogrid can be dated back to as early as the late 1980 (Barker, 1987; Haas *et al.,* 1988). Some examples of using Geogrid includes to prevent damage to road pavement (Ooi *et al.,* 2022), reinforcing embankment on foundation (Mohammed *et al.,* 2022) and more.

The selection of materials used in backfilling after excavation and ground reinforcing is important. Concrete or cement is a common material used in backfilling with good performance but comes with high cost. On the other hand, the surrounding soil which is soft clay is the case is also a feasible choice even though the performance is not as good as concrete. In addition, soft clay can also be mixed with air and cement to form a lightweight material that can be used as backfill material as the performance of the lightweight material performs well as embankment material (Chaiyaput *et al.,* 2023).

In this study, a new method for improving weak ground by using EC Geoblock precast concrete block is proposed and compared with geogrid to assess its performance on ground improvement on soft clay. Finite Element Modelling is a great and cost-efficient way to test the performance of the new proposal. PLAXIS 3D is a great user-friendly commercial software package that have been used to simulate various scenarios involving geogrid, pile, foundation and more (Al Ghanim *et al.,* 2019; Alsirawan, 2021; Salih *et al.,* 2022). Hence, PLAXIS 3D is used to perform the simulation for the current study.

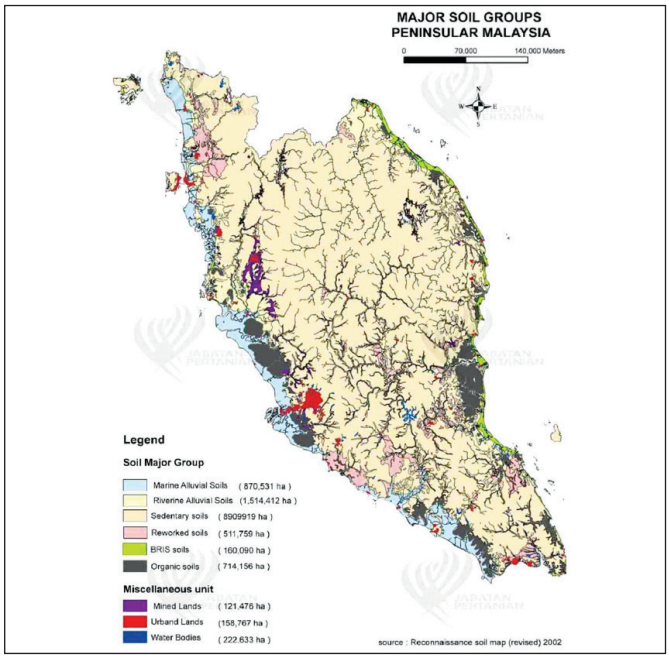

Figure 1: Soft soil location in Peninsular Malaysia (Source: Reconnaissance soil map, 2002 – revised)

2.0 MATERIALS

2.1 Soil Properties

The soil constitutive model used to model two of the soil is hardening soil model. Even though, Mohr's coulomb model has been a popular choice in modelling soil due to its simplicity, it is not chosen for the current study as it failed to account for the non-linearity of soil and stress-dependency of soil stiffness which might lead to erroneous computation of strain that led to bad accuracy in soil deformation modelling. On the other hand, hardening soil model which is an elastic-plastic model is an advance soil model which is capable of simulating both non-linearity and stress-dependency of soil based on power law. Hence, it is the better choice for modeling soil, so the hardening soil model is chosen for the current study. Table 1 summarised the two soil properties, which are soft clay, the main soil profile, and gravel, the filling material of the newly proposed foundation.

Table 1: Properties of soils

Parameters	Unit	Soil Type	
		Soft Clay	Sand
Drainage type	-	Undrained	Drained
Unsaturated unit weight, Y_{unsat}	kN/m^3	16	17.0
Saturated unit weight, Y_{sat}	kN/m^3	17	20.0
Effective cohesion, c'_{ref}	kN/m^2	5	0
Effective friction angle, φ'	°	25	33
Dilatancy angle, ψ	°	0	3
Ref. secant stiffness, E^{ref}_{50}	kN/m^2	2x10^3	35x10^3
Ref. tangential stiffness, E^{ref}_{oed}	kN/m^2	2x10^3	35x10^3
Ref. unloading/reloading stiffness, E^{ref}_{ur}	kN/m^2	1x10^4	105x10^3
Power (stress-level dependency of stiffness)	m	1.0	0.5
Unloading-reloading Poisson's ratio, v_{ur}	-	0.2	0.2

2.2 Specification of EC Geoblock

The "E" and "C" in the name of the blocks represent the shape of the blocks. The C block is half the size of the E block and both of the dimensions are illustrated in Figure 2. The precast blocks are designed to fulfill the following criteria; i) lightweight and small enough to be carried by people, ii) self-interlocking mechanism and iii) able to contain infill materials to create porous or impermeable structure.

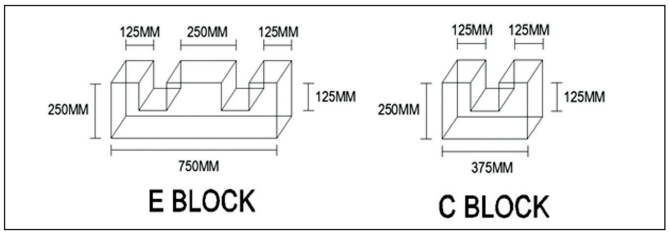

Figure 2: Dimensions of E and C Blocks

2.3 Specification of Geogrid

The axial stiffness, EA of the geogrid used for the study is 950kN/m. The value adopted is based on (Nezamabadi *et al.,* 2017) and also used in (Abdul Halim *et al.,* 2021).

3.0 METHODS

As the study area consists of clay and groundwater level is 1m below ground level, ground improvement is necessary before any forms of construction that exerts load to the ground can happen. In this study, the newly proposed ground improvement technique using EC Geoblock arrangement is compared with geogrid which is a common geosynthetic material used to strengthen soil. The study employs approach similar with study (GeoStruct Academy, 2024). Hence, this approach is deemed effective in determining the bearing capacity.

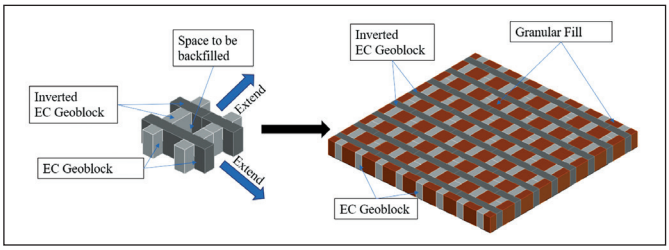

Figure 3: Installation of EC Geoblock

3.1 Geogrid

The process of applying Geogrid begins with excavation of soft clay up to 0.55m below ground surface. Subsequently, geogrid reinforcement is installed at the bottom of the excavated area, followed by backfilling of sand. Lastly, a surface load is exerted to the reinforced area through a 1.2 by 1.2m plate. This section includes a total of three analyses. The three will focus on geogrid, varying the spacing and number of geogrid layers.

3.2 EC Geoblock

The proposed EC Geoblock can be arranged in a way where each block is interlocked together without the use of adhesive. The arrangement

will leave a few square voids in which good drainage material in this case gravel can be filled for better draining. The proposed foundation consist of E and C shape block and the installation process starts with excavation of 0.55m. Subsequently, laying the block in vertical direction before inverting the block and placing the blocks in horizontal direction on top of the block in vertical direction as shown in Figure 4. The blocks in the second layer can also be non-inverted so more layers can be added to improve ground stability if necessary. After placing the blocks, the space above and in between block is backfilled with sand before application of surface load through a 1.2 by 1.2 m steel plate.

4.0 RESULTS AND DISCUSSION

4.1 Vertical Settlement

Clay is a type of soil that can be easily compresses, therefore when a structure is built or load is applied on it, there may be severe settling. This could result in soil collapse which is a severe ground hazard. Maximum settlement for the four cases before soil collapse are shown in Figure 4 and Figure 5. It can be seen that, high settlements are observed at the center for initial and geogrid reinforced ground whereas upward soil movement can be seen at EC Geoblock reinforced ground.

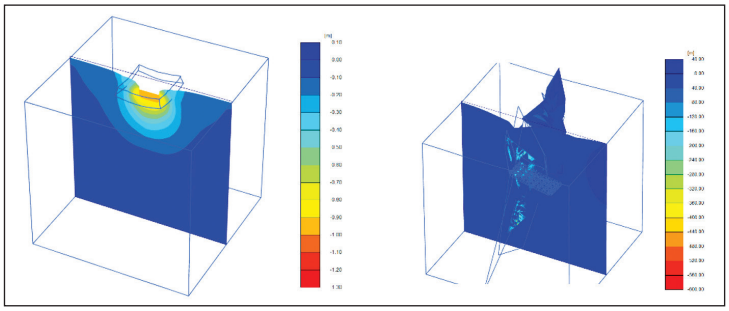

Figure 4: Vertical settlement of 5 layers of geogrid reinforced ground and EC geoblock reinforced ground

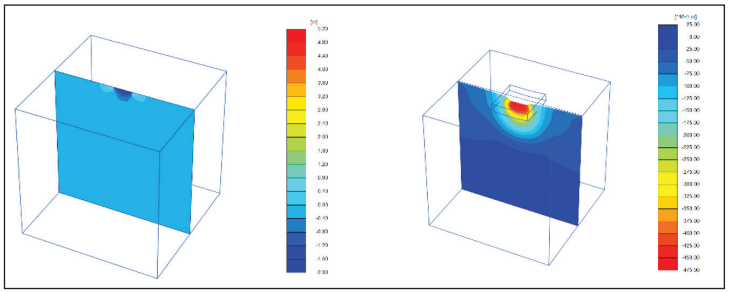

Figure 5: Vertical settlement of unreinforced ground and 2 layers of geogrid reinforced ground

Soil collapses of all four cases are believed to be due to excessive load as each case was loaded until failure. All reinforcements experience large vertical settlement. Upward movement can be seen at the corner of geogrids and geogrid settle at the center without much movement. On the other hand, The settlement of EC Geoblock exhibits a significant offset from the center.

A general total settlement of designing shallow foundation is around 25mm from empirical evidence (Gholamreza Mesri *et al.,* 1996) and current practice (Das, 2023). Settlement exiting the stated limit can lead to structural distress. Based on the load

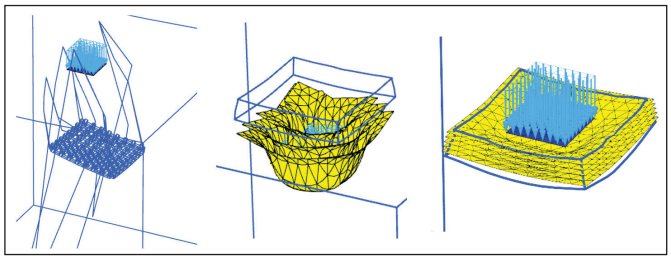

Figure 6: Failure behaviour of geogrid and EC Geoblock

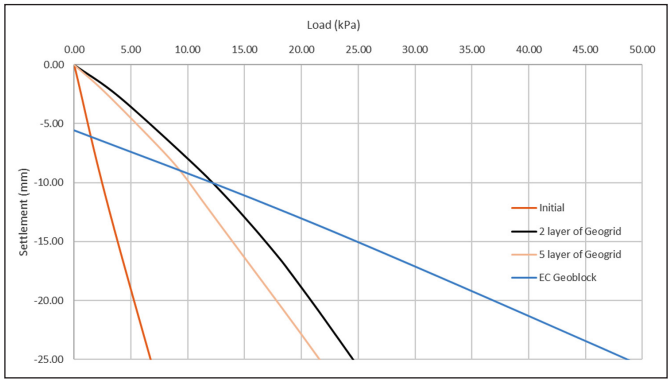

Figure 7: Load-settlement curve

settlement curve illustrated in Figure 7, EC Geoblock is able to withstand close to 50kPa load while the ground reinforced with 2 layer of geogrid can only tolerate close to 25 kPa load. The difference is over between 2 layer of geogrid and EC Geoblock is more than twice. Therefore, EC Geoblock is more efficient and reliable than geogrid which may reach 25mm settlement limit at lower load.

4.2 Bearing Capacity

Soil bearing capacity describe the maximum load that a soil can withstand before it collapses and it is crucial in designing foundation or ground improvement techniques. By using double tangent method on the displacement vs load graph, the bearing capacities of all five cases are determined and summarised in Table 2. In this method, two tangents are drawn: one at the beginning of the load-settlement curve and the other at the point where the curve's curvature changes. The double tangent method is a feasible method as this method have been used in recent articles (Jaiswal & Chauhan, 2021; Mohamed *et al.,* 2023).While double tangent method is able to provide quick estimate, it has limitation when compared to load-settlement curve obtained from simulation where the soil collapse from incremental loading as this method heavily depends on the tangent line drawn which can vary between various individuals. Hence, the bearing capacity for the current study is obtained using the second method.

The soil reinforced with EC Geoblock has the highest soil bearing capacity and soil without reinforcement has the lowest soil bearing capacity. The result revealed that bearing capacity increase with geogrid layers and ground reinforced with EC Geoblock has the highest bearing capacity and settlement. The high bearing capacity from EC Geoblock reinforced ground are mainly due to concrete being a more rigid material than geogrid

and great confinement effect provided through the fill material within the spaces of the structure which can assist in reducing lateral spreading (Krishna & Latha, 2023).

Since it is not practical and not common to design shallow ground reinforcement to withstand load close to 10000kPa, the settlement of EC Geoblock reinforced with failure load of case III will be compared against the settlement of case III. The settlement recorded for EC Geoblock reinforced ground is around 0.5554m whereas ground reinforced with 5 layers of geogrid experience 0.9262m of settlement. The settlement of case III is almost twice more than the EC geoblock reinforced ground with same loading applied.

Table 2: Bearing capacity values of each scenario

Scenario	Description	Bearing capacity, *q* (kPa)
I	No reinforcement	150.72
II	2 layers of Geogrid with sand backfill	436.97
III	5 layers of Geogrid with sand backfill	1103.18
IV	EC Geoblock with sand backfill	9925.08

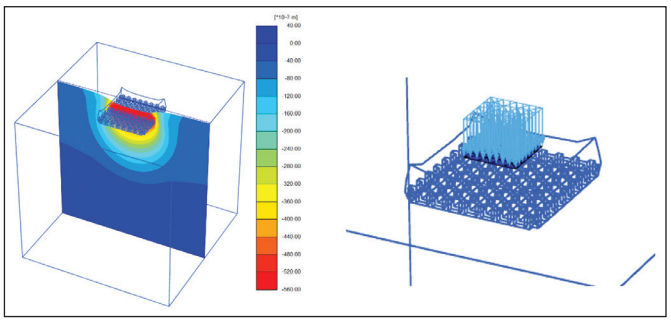

Figure 8: Settlement and deformation behavior of EC Geoblock under collapse load of case III

5.0 CONCLUSION AND FUTURE RESEARCH

FEA of five different scenarios with load application to failure are done in this study. From the simulation, it is proven that EC Geoblock has better performance in vertical settlement and bearing capacity to Geogrid. The data show remarkable almost tenfold increase in bearing capacity than using 5 layers of geogrids. In addition, EC Geoblock exhibited significantly higher load bearing capacity at a defined settlement limit of 25mm capable of withstanding nearly twice the load compared to a five-layer geogrid reinforcement configuration. Furthermore, the interlocking nature of EC Geoblock ensure effective load distribution over a wide area and the voids in between the formation allow great drainage ability to mitigate the risk of soil collapse. Therefore, the evidence supports the adoption of EC Geoblock for ground improvement as a equivalent or better alternative to geogrid reinforcement. Future research can include the testing of multiple layers of the new arrangement of EC GeoBlock or a model test related to the new system.

ACKNOWLEDGMENT

Authors would like to acknowledge and thanks to Civil Engineering Department, Engineering Faculty, Universiti Putra Malaysia, Malaysia and GEOCO Sdn. Bhd.

APPENDIX

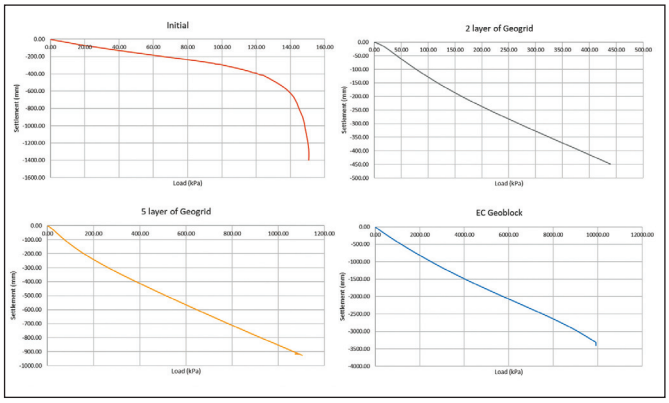

Figure A1: Full load-settlement curve for case I to IV

AUTHOR CONTRIBUTIONS

- **Yan Ho Loke:** Conceptualisation, data collection, methodology, and formal analysis.
- **Nik Norsyahariati Nik Daud:** Conceptualisation, study design, and supervision.
- **Wyn Shern Loke:** Writing—original draft preparation and literature review. ■

REFERENCES

[1] Abdul Halim, M. F., Yahya, N. F., Tuan Ismail, T. N. H., & Abd Latif, M. F. (2021). Numerical Analysis of Geogrid Reinforced Embankment on Soft Clay. *Progress in Engineering Application and Technology, 2(2),* 223–230. https://publisher.uthm.edu.my/periodicals/index.php/peat/article/view/993

[2] Al Ghanim, A. A., Shafiqu, Q. S. M., & Ibraheem, A. T. (2019). Finite element analysis of the geogrid-pile foundation system under earthquake loading. *Al-Nahrain Journal for Engineering Sciences, 22(3),* 202-207.

[3] Alsirawan, R. (2021). Analysis of Embankment Supported by Rigid Inclusions Using Plaxis 3D. *Acta Technica Jaurinensis, 14(4),* 455-476.

[4] Barker, W. R. (1987). Open-graded bases for airfield pavements.

[5] Chaiyaput, S., Ayawanna, J., Jongpradist, P., Poorahong, H., Sukkarak, R., & Jamsawang, P. (2023). Application of a cement–clay–air foam mixture as a lightweight embankment material for construction on soft clay. Case Studies in Construction Materials, e02188.

[6] Das, B. M. (2023). Principles of Foundation Engineering, Si. Cengage Learning.

[7] GeoStruct Academy. (2024, June 10). Lesson 32. Bearing Capacity of Foundation on Two Layered Soil Using PLAXIS 3D. YouTube: https://www.youtube.com/watch?v=zD1hN81fMME

[8] Gholamreza Mesri, Terzaghi, K., & Brazelton, R. (1996). *Soil mechanics in engineering practice.* Wiley.

[9] Haas, R., Walls, J., & Carroll, R. (1988). Geogrid reinforcement of granular bases in flexible pavements. *Transportation research record, 1188(1),* 19-27.

[10] Jaiswal, S., & Chauhan, V. B. (2021). Ultimate bearing capacity of strip footing resting on rock mass using adaptive finite element method. *Journal of King Saud University-Engineering Sciences, 36(4),* 235-248.

[11] Krishna, A., & Latha, G. M. (2023). Evolution of Geocells as Sustainable Support to Transportation Infrastructure. *Sustainability, 15(15),* 11773. https://doi.org/10.3390/su151511773

[12] Mohamad, N., Razali, C., Hadi, A., Som, P., Eng, B., Rusli, M., & Mohamad, F. (2016). Challenges in construction over soft soil-case studies in Malaysia. *IOP conference series: materials science and engineering, 136(1):* 012002.

[13] Mohamed, M. K., Sakr, M. A., & Azzam, W. R. (2023). Geotechnical behavior of encased stone columns in soft clay soil. *Innovative Infrastructure Solutions, 8(80).*

[14] Mohammed, S. A., Naimi, S., & Abdul Kareem, A. H. (2022). The effect of geogrid reinforcement of embankment over soft foundation. *Periodicals of Engineering and Natural Sciences (PEN) 10(6):* 5-27. doi:10.21533/pen.v10i6.3345

[15] Nezamabadi, M. F., Lajevardi, S. H., & Sadeghi, M. (2017). Effect of different category of geogrid and sand layer on pull-out behaviour. *The 2nd World Congress on Civil, Structural, and Environmental Engineering.* doi: 10.11159/icgre17.175

[16] Ooi, T., Tee, R., Chan, C., & Lau, J. (2022). Case Histories of Performance of Geogrids in Soft Ground. *International Symposium on Practical Applications of Ground Engineering for Embankments on Soft Soils (GEESS2022,* Kuala Lumpur.

[17] Reconnaissance soil map (2002). Access via: https://geotanih.doa.gov.my/about/peninsular?print=1

[18] Salih, A. G., Rashid, A. S., & Salih, N. B. (2022). Finite Element Analysis of the Load-Settlement Behavior of Large-Scale Shallow Foundations on Fine-Grained Soil Utilizing Plaxis 3D. *Current Trends in Geotechnical Engineering and Construction* (pp.249-260).

PROFILES

YAN HO LOKE (Dip. Civil Eng. (UTM), B.E.Civil (UPM)) is currently a professional engineer with practising certificate. He is currently managing director of Geoco Sdn Bhd. He employs his leadership and skills, guides the company in providing sound engineering solutions in ground engineering works such as site investigations, slope stabilisations, earth retaining structures, underpinning, shallow and deep foundations and deep excavation works. His interest and vast experience spanning over 30 years in the field of geotechnical engineering, have led him to invent the innovative EC GeoBlock.
Email address: lokeyanho@gmail.com

NIK NORSYAHARIATI NIK DAUD has a PhD in Civil Engineering and a senior lecturer at the Universiti Putra Malaysia (UPM), Malaysia. She is a registered Graduate Engineer under the Board of Engineers Malaysia (BEM) and The Institution of Engineers, Malaysia (IEM). She also served as the Head of Geotechnical and Geological Engineering Unit and Head of Soil Mechanics Laboratory at the department. She has several publications and awards in both national and international levels. Her research interests are geotechnical engineering and environmental geotechnics.
Email address: niknor@upm.edu.my

WYN SHERN LOKE graduated with a degree in Civil Engineering with honours from Monash University Malaysia (MUM) in 2022. He has developed a solid foundation in finite element analysis through his final year project involving slope and pile elements. He is a graduate engineer registered under the Board of Engineers Malaysia (BEM) and he also served as a project engineer in Geoco Sdn. Bhd. His research interests are geotechnical engineering and numerical analysis.
Email address: ws.loke8@gmail.com

SEPARATION OF METHANOL AND ACETONITRILE MIXTURE VIA EXTRACTIVE DISTILLATION USING IMIDAZOLIUM-BASED IONIC LIQUIDS AND CONVENTIONAL SOLVENTS AS ENTRAINERS: A SIMULATION APPROACH

Zhi Ting Ang[1], Ianatul Khoiroh[2*]

Abstract

In this work, a comparative simulation study of extractive distillation using imidazolium-based ionic liquids and conventional solvents for the separation of methanol and acetonitrile was conducted using Aspen HYSYS. The ionic liquids selected were 1-ethyl-3-methylimidazolium bis(trifluoromethylsulfonyl)-imide or [EMIM][BTI], 1-butyl-3-methylimidazolium or bis(trifluoromethylsulfonyl)-imide [BMIM][TFSI], and 1-butyl-3-methylimidazolium acetate or [BMIM][OAc], while the conventional solvents were aniline, ethylene glycol, and glycerol. A case study on the solvent feed conditions was conducted to determine the optimum operating temperature and pressure for the extractive distillation columns. The simulation results show that the application of ionic liquid as the entrainer is more effective in eliminating the azeotropic point of methanol and acetonitrile as compared to the conventional solvents under the same specifications for the extractive distillation column and solvent recovery column.

Received: *9 October, 2024*
Revised: *9 April, 2025*
Accepted: *9 May, 2025*

[1,2]Department of Chemical & Environmental Engineering, Faculty of Science and Engineering, University of Nottingham Malaysia, Jalan Broga, 43500 Semenyih, Selangor Darul Ehsan, Malaysia.

****Corresponding author:***
Ianatul.Khoiroh@nottingham.edu.my

DOI: *https://10.54552/v86i2.265*

Keywords:
Azeotrope, Entrainer, Extractive distillation, Ionic liquids, Simulation

1.0 INTRODUCTION

The distillation process, one of the major separation processes in the chemical industry, accounts for 10-15% of the total energy consumption in chemical plants (Ma *et al.,* 2019). Despite its extensive energy consumption in the chemical industry, distillation remains the most widely used method in separating a mixture into pure components (Sinnot *et al.,* 2019). The principle of distillation is based on the differences in volatility between the components present in the liquid mixtures (Ma *et al.,* 2019). Acetonitrile and methanol are two of the most widely used chemicals in the chemical and pharmaceutical industries due to their high solubility in organic materials (Joshi *et al.,* 2019). For example, large amounts of acetonitrile and methanol are utilised during the manufacture of peptide drugs (Hintzen *et al.,* 2014). Therefore, the separation of mixtures consist of methanol and acetonitrile must be carried out to minimise the environmental impacts, as well as recycling the methanol and acetonitrile (Zhu *et al.,* 2016).

Unfortunately, the methanol and acetonitrile mixture cannot be separated via conventional distillation processes, as the mixture forms a minimum boiling homogeneous azeotrope at 336.7 K and atmospheric pressure, containing 81% methanol (Luyben, 2013). Several distillation technologies, including pressure-swing distillation, reactive distillation, extractive distillation, and azeotropic distillation, have been proposed to separate azeotropic mixtures (Ma *et al.,* 2019). Pressure-swing distillation is commonly used for the homogenous azeotropic mixtures that are sensitive to changes in pressure (Sinnot *et al.,* 2019). On the other hand, reactive distillation involves a complex separation process, as it separates the components in the mixture while performing the chemical reaction (Ma *et al.,* 2019). Extractive distillation involves the addition of separating agent or entrainer to alter the relative volatility between the key components without forming an azeotrope (Coker, 2010). Extractive distillation is similar to azeotropic distillation; however, no azeotropes are formed upon the addition of the entrainer, and the entrainer added is essentially non-volatile (Coker, 2010).

The entrainer used for the separation processes typically possesses a significantly higher boiling point than the mixture components and can induce a salting-out effect, thereby reducing the volatility of the component that interacts with the entrainer (Wankat, 2012). The remaining component present in the mixture is then become relatively more volatile and easier to be separated and removed as the distillate (Wankat, 2012). Apart from affecting the relative volatilities of the key components, several characteristics are important for selecting a suitable entrainer. These include low latent heat, non-reactivity, non-corrosiveness, non-toxicity, and solubility with the components in the mixture (Coker, 2010). Several conventional solvents have been used as entrainers, such as aniline, dimethylformamide (DMF), glycerol, and ethylene glycol. These solvents have also been studied for the separation of azeotropic mixture of methanol and acetonitrile (Li *et al.,* 2012). However, these entrainers have several disadvantages, such as causing environmental pollution due to volatile emissions and presenting significant challenges

in recycling due to their complex separation and purification processes (Cai *et al.,* 2013).

Ionic liquids (ILs) possess various unique physic-chemical properties to replace the conventional solvents, including good chemical and thermal stability, excellent dissolving capacity, and non-volatility (Seiler *et al.,* 2014). Numerous studies have been conducted to investigate and review the utilisation of ILs as entrainers for extractive distillation (Shen *et al.,* 2023: You *et al.,* 2022; Martínez-Galmiche *et al.,* 2022; and Vilas-Boas *et al.,* 2024). Ionic liquid consisting of cations such as imidazolium and alkyl quaternary coupled with anions such as hydrogen sulphate, halogen, and acetate are commonly used to separate polar-polar systems, including alcohol/water, nitrile/water, and alcohol/nitrile mixtures (Pereiro *et al.,* 2012). On the other hand, ILs consisting cations such as imidazolium and pyridine coupled with anions such as tetrafluoroborate (BF4), bis(trifluoromethyl-sulfonyl)imide (NTf2) and dicyanamide are commonly selected to separate nonpolar-nonpolar systems, including alkane/alkene and aliphatic/aromatics mixtures (Pereiro *et al.,* 2012). While ILs consisting of imidazolium cation and sulphate anion are commonly used to separate polar-nonpolar systems, including alcohol/aliphatic mixtures (Pereiro *et al.,* 2012).

A study was conducted by Li *et al.* (2016) to investigate the effects of 1-octyl-3-methylimidazolium tetrafluoroborate, [OMIM][BF_4], and 1-ethyl-3-methylimidazolium tetrafluoroborate, [EMIM][BF_4], on the vapor-liquid equilibrium behaviour of the methanol-acetonitrile system. It was reported that [OMIM][BF_4] has a stronger salting-out effect on methanol compared to [EMIM][BF_4]. However, ILs with the [BF_4]- anion are difficult to synthesise, and corrosive hydrogen fluoride could be emitted upon contact with water (Cai *et al.,* 2013). On the other hand, Zhang *et al.* (2016)] investigated the performance of separating methanol and acetonitrile mixture using 1-ethyl-3-methylimidazolium bis(trifluoromethylsulfonyl)imide or [EMIM][NTf_2]. It was found that the azeotropic phenomenon could be eliminated using this ionic liquid. However, the current production cost of ionic liquids containing [NTf_2]- is economically unfavourable, making them less viable for large-scale use (Nasirpour *et al,* 2020).

Another study by Z. Zhang *et al.* (2018) compared the performance of 1-butyl-3-methylimidazolium chloride or [BMIM][Cl], 1-butyl-3-methylimidazolium bromide or [BMIM][Br] and 1-butyl-3-methylimidazolium acetate or [BMIM][OAc] as entrainers to separate methanol and acetonitrile at atmospheric pressure. The finding reveals that these three ionic liquids produced a significant salting-effect and enhanced the relative volatility of acetonitrile to methanol. A directly proportional relationship between the amount of ILs and the salting-out effect was determined in the study (Zhang *et al.,* 2018). It was also concluded that the [BMIM][OAc] has the best separation performance compared to [BMIM][Cl] and [BMIM][Br].

In this work, three ionic liquids, namely 1-ethyl-3-methylimidazolium bis(trifluoromethylsulfonyl)-imide or [EMIM][BTI], 1-butyl-3-methylimidazolium bis(trifluoromethylsulfonyl)-imide or [BMIM][TFSI], 1-butyl-3-methylimidazolium acetate or [BMIM][OAc] were tested as entrainers to separate binary mixture composed of methanol and acetonitrile via simulation approaches using Aspen HYSYS V11. The effects and performance of these ILs and three conventional solvents were compared and evaluated to determine the optimum operating temperature and pressure for the extractive distillation column. The solvents studied include aniline, ethylene glycol and glycerol. The results obtained from simulation and case studies aim to corroborate the feasibility of utilising ILs as entrainers to separate methanol and acetonitrile.

2.0 METHODOLOGY

The non-random two-liquid (NRTL) model (Renon *et al.,* 1968) was selected as the thermodynamic package to evaluate the vapor-liquid equilibrium of the mixture in Aspen HYSYS V11 software. The hypothetical functions available in Aspen HYSYS were utilised to estimate the properties of ionic liquids. The performance of these ionic liquids and conventional solvents were compared using the same columns specifications including the number of stages, solvent to feed ratio, feed stage as well as the solvent feed stage for both columns. These specifications were adapted from the study conducted by Wang *et al.* (2019). Fig. 1 shows the flowsheet for the extractive distillation process whereas Table 1 shows the specifications for both extractive distillation column (EDC) and solvent recovery column (SRC).

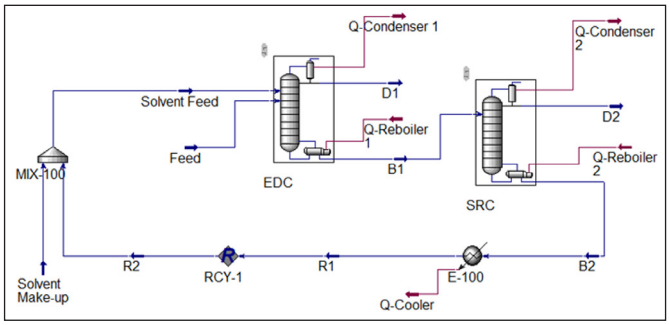

Figure 1: Process flowsheet for extractive distillation of methanol and acetonitrile

Table 1: Specifications of extractive distillation column (EDC) and solvent recovery column (SRC)

Specifications	EDC	SRC
Number of Stages	48	8
Solvent to Feed Ratio	1	-
Feed Stage	4	-
Solvent Feed Stage	33	5

The operating conditions for solvent feed including temperature and pressure were optimised by conducting individual case studies on each of the parameters. The effect of each parameter on the separation performance was investigated through case studies. The best settings for both columns were evaluated based on the purity of methanol and acetonitrile recovered.

3.0 RESULTS AND DISCUSSION

3.1 Simulation of Extractive Distillation Process

The results obtained from the simulation of extractive distillation for methanol and acetonitrile using conventional solvents and ionic liquids are tabulated in Table 2 and Table 3.

Table 2: Simulation results for extractive distillation of methanol-acetonitrile using conventional solvents

Parameters	Unit	Aniline		Ethylene Glycol		Glycerol	
		EDC	SRC	EDC	SRC	EDC	SRC
Reflux Ratio	-	0.205	0.450	1.458	2.060	2.092	0.004
Distillate Flow Rate	kmol/h	85.0	16.0	85.0	16.0	85.0	15.1
Bottom Flow Rate	kmol/h	116.0	100.0	116.0	100.0	115.1	100.0
Purity of Methanol/ Acetonitrile	%	94.0	86.7	94.0	86.9	94.0	92.1
Purity of Solvent Recovered	%	-	99.0	-	96.0	-	99.9

Table 3: Simulation results for extractive distillation of methanol-acetonitrile using ionic liquids

Parameters	Unit	[EMIM][BTI]		[BMIM][TFSI]		[BMIM][OAc]	
		EDC	SRC	EDC	SRC	EDC	SRC
Reflux Ratio	-	1.176	0.047	1.176	0.047	1.176	0.047
Distillate Flow Rate	kmol/h	85.0	15.0	85	15	85.0	15.0
Bottom Flow Rate	kmol/h	115.0	100.0	115	100	115.0	100.0
Purity of Methanol/ Acetonitrile	%	94.8	97.1	95.2	99.5	94.8	97.1
Purity of Solvent Recovered	%	-	100.0	-	100.0	-	100.0

According to the simulation results tabulated in Table 2, the use of glycerol as the entrainer for extractive distillation achieves the best separation performance among the conventional solvents. However, the comparison between the simulation results for both conventional solvents and ionic liquids (Table 3) shows that the use of ionic liquids as an entrainer can achieve higher purity for methanol, acetonitrile, as well as the solvent recovered. It is found that the highest purity of the binary mixture in extractive distillation column is achieved using [BMIM][TFSI] with 95.2% purity. This increase in relative volatility may be attributed to the properties of ionic liquids, including their ability to modify the thermodynamics and molecular interactions within the system. By introducing [BMIM][TFSI] into the extractive distillation process, the separation between the two components becomes more pronounced, resulting in higher selectivity and purity of acetonitrile. Furthermore, the addition of ionic liquids shifts the azeotropic point towards higher methanol concentrations similar to study by Boli *et al.* (2020). This means that the presence of ILs can alter the composition of the azeotrope formed by the methanol-acetonitrile mixture, allowing for easier separation by extractive distillation. Shifting the azeotropic point is a desirable outcome as it overcomes the limitations imposed by azeotropic behaviour (Sofea *et al.,* 2022).

On the other hand, a higher loss of solvents through the distillate of the extractive distillation column and the solvent recovery column is observed for the extractive distillation process that utilises conventional solvents (Table 2) as an entrainer compared to ILs (Table 3). Consequently, a larger amount of make-up solvent is required for the process, resulting in higher operating costs (Wang *et al.,* 2023).

These findings emphasise the advantageous role of ionic liquids, such as [BMIM][TFSI], in extractive distillation processes. Their unique properties and interactions with the mixture components contribute to enhanced separation performance, higher selectivity, and the ability to modify azeotropic behavior. However, it is important to consider factors such as the cost, availability, and environmental impact of ionic liquids when evaluating their suitability for large-scale industrial applications (Berton *et al.,* 2022). Further research and experimentation are necessary to fully explore the potential of [BMIM][TFSI] and other ionic liquids in extractive distillation and other separation processes.

It is worth noting that these results were fully based on simulation data, and further experimental investigations are required to validate these findings. Nonetheless, comparative analysis provides valuable insights into the potential benefits of employing ionic liquids in extractive distillation processes, emphasising their superior performance in terms of both separation efficiency and cost-effectiveness.

3.2 Optimisation of Solvent Feed Conditions

The optimum operating temperature and pressure of the solvent for the extractive distillation process using [BMIM][TFSI] as entrainer were further determined by using the case study function available in Aspen HYSYS. The determination of the optimum operating temperature and pressure for the extractive distillation process employing [BMIM][TFSI] as an entrainer can be accomplished by utilising the case study function available in Aspen HYSYS, a widely used process simulation software. This function allows for the exploration of various operating conditions and provides valuable insights into the process of performance. Fig 2 and Fig. 3 show the results determined from the case studies.

According to the results obtained from the case studies on solvent feed temperature and pressure, there is no appreciable reduction observed (almost constant) in the molar flow of methanol and acetonitrile recovered from the distillate of the extractive distillation column and solvent recovery column as the solvent feed temperature and pressure increase. However, it is important to note that lower feed temperature and pressure are generally more favoured to reduce the cost of utilities and equipment, as a higher solvent feed temperature and pressure will require more heating utilities and additional equipment such as pump and compressor. Further investigations on the top temperature, bottom temperature of both columns, as well as economic analysis on the capital and operating costs can be carried out to optimise the extractive distillation using [BMIM][TFSI] as entrainer (Wang *et al.,* 2023). These may involve exploring the optimal top and bottom temperatures of both columns, as well as performing an economic analysis to evaluate the capital and operating costs associated with the chosen operating conditions. Such analyses can provide a comprehensive understanding of the process and guide the decision-making process in designing an efficient and cost-effective extraction system.

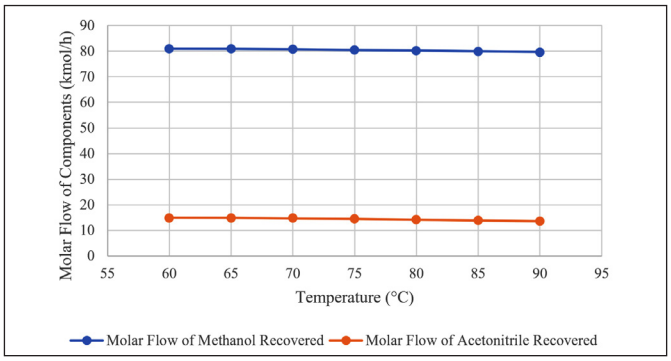

Figure 2: Case study on the solvent feed temperature

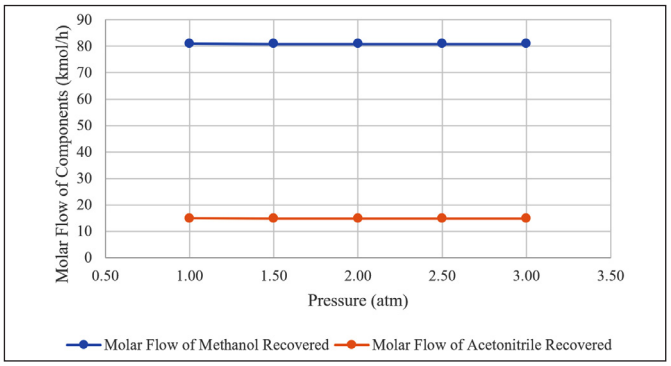

Figure 3: Case study on the solvent feed pressure

4.0 CONCLUSION

The Aspen HYSYS simulation using the NRTL model has been performed to simulate the extractive distillation process for the azeotropic mixture containing methanol and acetonitrile. According to the simulation results, 1-butyl-3-methylimidazolium bis(trifluoromethylsulfonyl)-imide [BMIM][TFSI] is the most efficient solvent for the extractive distillation process. Besides that, the simulation results also showed that the application of ionic liquids as entrainer for the extractive distillation of methanol and acetonitrile are feasible. It is generally more desirable to operate the extractive distillation column at lower temperature and pressure to reduce the operating cost and capital costs. Further improvements can be made by integrating heat integration technology and heat pump technology to reduce the utilities cost for the extractive distillation process. Apart from that, life cycle analysis can be conducted to further evaluate and compare the environmental impacts of the extractive distillation process using conventional solvents and ionic liquids.

ACKNOWLEDGEMENT

This work was supported by the Ministry of Higher Education Malaysia under Fundamental Research Grant Scheme (FRGS) through Grant No. FRGS/1/2019/STG07/UNIM/02/3 and FRGS/1/2023/STG05/UNIM/02/2.

AUTHOR CONTRIBUTION

- **Zhi Ting Ang:** Data Curation, Formal Analysis, Methodology, Visualisation, Writing (Original Draft)
- **Ianatul Khoiroh:** Conceptualisation, Resources, Funding Acquisition, Supervision, Writing (review & editing). ■

REFERENCES

[1] Ma, Y., Cui, P., Wang, Y., Zhu, Z., Wang, Y., & Gao, J. (2019). A review of extractive distillation from an azeotropic phenomenon for dynamic control. *Chinese Journal of Chemical Engineering, 27,* 1510–22. https://doi.org/10.1016/j.cjche.2018.08.015.

[2] Sinnott, R., & Towler, G. (2019). *Chemical Engineering Design.* 6th ed., Elsevier. https://doi.org/10.1016/b978-0-08-102599-4.09980-x.

[3] Joshi, D. R. & Adhikari, N. (2019). An overview on common organic solvents and their toxicity. *Journal of Pharmaceutical Research International, 28(3),* 1–18. doi: 10.9734/jpri/2019/v28i330203.

[4] Hintzen, F., Perera, G., Hauptstein, S., Müller, C., Laffleur, F., & Bernkop-Schnürch A. (2014). In vivo evaluation of an oral self-microemulsifying drug delivery system (SMEDDS) for leuprorelin. *International Journal of Pharmaceutics, 472,* 20–6. https://doi.org/10.1016/j.ijpharm.2014.05.047.

[5] Zhu, Z., Xu, D., Liu, X., Zhang, Z., & Wang, Y. (2016). Separation of acetonitrile/methanol/benzene ternary azeotrope via triple column pressure-swing distillation. *Separation and Purification Technology, 169,* 66–77. https://doi.org/10.1016/j.seppur.2016.06.009.

[6] Luyben, W.L. (2013). Comparison of extractive distillation and pressure-swing distillation for acetone/chloroform separation. *Computers & Chemical Engineering. 50,* 1–7. https://doi.org/10.1016/j.compchemeng.2012.10.014.

[7] Coker, A.K. (2010). Ludwig's Applied Process Design for Chemical and Petrochemical Plants: Distillation, Packed Towers, Petroleum Fractionation, Gas Processing and Dehydration.

[8] Wankat, P.C. (2012). Separation process engineering: includes mass transfer analysis. 3rd ed. Prentice Hall.

[9] Li, G., Yu, Y., & Bai, P. (2012). Batch extractive distillation of mixture methanol-acetonitrile using aniline as a asolvent. *Polish Journal of Chemical Technology, 14,* 48–53. https://doi.org/10.2478/v10026-012-0083-4.

[10] Cai, F., Wu. X., Chen. C., Chen. X., Asumana. C, & Haque, M. R. (2013). Isobaric vapor-liquid equilibrium for methanol+dimethyl carbonate+phosphoric-based ionic liquids. *Fluid Phase Equilibria, 352,* 47–53. https://doi.org/10.1016/j.fluid.2013.05.021.

[11] Seiler, M., Jork, C., Kavarnou, A., Arlt W., & Hirsch, R. (2004). Separation of azeotropic mixtures using hyperbranched polymers or ionic liquids. *AIChE Journal, 50,* 2439–2454. https://doi.org/10.1002/aic.10249.

[12] Shen, T., Teng, L., Hu, Y. & Shen W. (2023). Systematic screening procedure and innovative energy-saving design for ionic liquid-based extractive distillation process, *Frontiers of Chemical Science and Engineering, 17,* 34–45. https://doi.org/10.1007/s11705-022-2234-3

[13] You, X., Zhao. K., Li, L., & Qiu, T. (2022). Ionic liquids as entrainer in extractive distillation for effectively separating 1-propanol–water azeotropic mixture. *Chinese Journal of Chemical Engineering, 49,* 224-233. https://doi.org/10.1016/j.cjche.2021.12.007

[14] Martínez-Galmiche, I. F., Ramírez-Corona, N., Conde-Mejía, C., Sánchez-Sánchez, K. Gani, B., & Jiménez-Gutiérrez, R. (2022). Design of energy-efficient ionic liquid-based extractive distillation systems for ethanol dehydration including alternatives for ionic liquid recovery. *Chemical Engineering Research and Design, 188,* 238-248. https://doi.org/10.1016/j.cherd.2022.09.035

[15] Vilas-Boas, S. M., Batista, F. R. M., Dias, R. F., Coutinho, J. A. P., Ferreira, O da, Costs M. C., & Pinho. (2024). Deterpenation of citrus essential oil via extractive distillation using imidazolium-based ionic liquids as entrainers. *Journal of the Taiwan Institute of Chemical Engineers, 156,* 105367 https://doi.org/10.1016/j.jtice.2024.105367.

[16] Pereiro, A.B., Araújo, J. M. M., Esperança, J. M. S. S., Marrucho, I. M., & Rebelo, L. P. N. (2012). Ionic liquids in separations of azeotropic systems - A review. *The Journal of Chemical Thermodynamics, 46,* 2–28. https://doi.org/10.1016/j.jct.2011.05.026.

[17] Li, Q., Zhu, W., Liu, B., Fan, Z., Zhu, Y., & Gao, Z. (2016). Measurement and correlation of the vapor-liquid equilibrium for methanol + acetonitrile + imidazolium-based ionic liquids at 101.3 kPa. *The Journal of Chemical Thermodynamic, 101,* 25–30. https://doi.org/10.1016/j.jct.2016.05.011.

[18] Zhang, Y., Yu, D., Guo, F., Shen, Y,, Zhou, J,, Li, Z., & Li, Q. (2016). Vapor-Liquid Equilibria Measurement of (Methanol + Ethanenitrile + Bis(trifluoromethylsulfonyl) Imide)-Based Ionic Liquids at 101.3 kPa. *Journal of Chemical & Engineering Data, 61,* 2202–8. https://doi.org/10.1021/acs.jced.5b00796.

[19] Nasirpour, N., Mohammadpourfard, M., & Heris, S. Z. (2020). Ionic liquids: Promising compounds for sustainable chemical processes and applications. *Chemical Engineering Research and Design, 160,* 264-300. https://doi.org/10.1016/j.cherd.2020.06.006

[20] Zhang, Z., Yang, R., Li, W., Zhang, T., Zhang, D., & Zhang, Q. (2018). Separation of acetonitrile and methanol azeotropic mixture using imidazolium-based ionic liquids as entrainers. *Fluid Phase Equilibria, 477,* 12–8. https://doi.org/10.1016/j.fluid.2018.08.009.

[21] Renon, H., & Prausnitz, J. M. (1968). Local Compositions in Thermodynamic Excess Functions for Liquid Mixtures. *AICHE Journal, 14,* 135–44. https://doi.org/10.1002/aic.690140124

[22] Wang, Y., Bu, G., Geng, X., Zhu, Z., Cui, P., & Liao, Z. (2019). Design optimization and operating pressure effects in the separation of acetonitrile/methanol/water mixture by ternary extractive distillation. *Journal of Cleaner Production, 218,* 212–24. https://doi.org/10.1016/j.jclepro.2019.01.324.

[23] Boli, E., & Vautsas, E. (2020). Ionic liquids as entrainers for the separation of azeotropic mixtures: Experimental measurements and COSMO-RS predictions. *Chemical Engineering Science, 219,* 115579. https://doi.org/10.1016/j.ces.2020.115579.

[24] Sofea, J., Wong, W. N., Yee, J. T. H., Lee, T. H.W. , Lau, P. L., & Khoiroh. I. (2022). Separation of Azeotrope Mixture Composed of Acetone and Methanol using Various Entrainers. *Journal of Applied Science and Engineering, 25,* 945-950. https://doi.org/10.6180/jase.202210_25(5).0010.

[25] Wang, Y., Ye, Q., Li, J., Rui Q., & Yu, A. (2023). Economic and entropy production evaluation of extractive distillation and solvent-assisted pressure-swing distillation by multi-objective optimization. *Chinese Journal of Chemical Engineering, 63,* 246-259. https://doi.org/10.1016/j.cjche.2023.04.017.

[26] Berton, P., Abidi, N., & Shamshina, J. L. (2022). Ionic liquids: Implementing objectives of sustainability for the next generation chemical processes and industrial applications. *Current Opinion in Green and Sustainable Chemistry, 35,* 100625. https://doi.org/10.1016/j.cogsc.2022.100625.

PROFILES

ZHI TING ANG graduated with a degree in Chemical and Environmental Engineering from the University of Nottingham Malaysia in 2021. During his time at university, he developed a strong foundation in both chemical processes and environmental sustainability, which has greatly influenced his career path. Currently, he is employed as a Project & Design Engineer in Singapore, where he applies his expertise to manage and design engineering projects.
Email address: angzhiting98@gmail.com

IANATUL KHOIROH obtained her PhD in Chemical Engineering from the National Taiwan University of Science and Technology (NTUST), Taiwan, in 2012. She has been with the University of Nottingham Malaysia since 2013, where she is currently an Associate Professor. Ianatul's research focuses on the greener separation processes using bio-based solvents. Her research interests also extend to the fields of carbon dioxide capture and sequestration, passive cooling, and the development of safer Li-ion batteries.
Email address: Ianatul.Khoiroh@nottingham.edu.my

TUNNELLING IN NEGATIVE FACE LOSS ENVIRONMENT – FROM RISK TO OPPORTUNITY

Chee Min Khoo[1*], Hisham Mohamad[2]

Abstract

In conventional tunnelling scenario, the face pressure exerted by the Tunnel Boring Machine (TBM) is typically lower than the mobilised earth pressure, resulting in controlled ground movement towards the tunnel face, known as positive face loss. However, negative face loss poses a distinct challenge where the face pressure exceeds the mobilised earth pressure, causing the ground to move away from the tunnel face. This paper presents a full-scale field investigation on tunnel-soil-pile interaction under negative face loss tunnelling environments. The study integrates field measurements with numerical analysis to assess the transient effects of shield tunnelling on a fully instrumented experiment pile, which was pre-loaded and equipped with strain gauges, an inclinometer, and distributed fibre optic sensing. Real-time monitoring was conducted throughout the tunnel advancement, while three-dimensional finite element modelling was developed using actual TBM driving data to simulate pile responses as various tunnelling stages. The field observations and numerical results validate the hypothesised movement paths of the pile under negative face loss and offer new insights into the pile's behaviour. The study highlights the importance of controlling tunnel volume loss, with an optimal TBM face pressure range recommended between 0.8 and 1.1 times the overburden pressure, and grouting pressure between 1.1 and 1.5 times the overburden pressure to mitigate ground settlement. The validated numerical framework serves as a basis for further parametric studies and provides practical recommendations for risk mitigation and enhanced tunnelling efficiency. These findings mark a significant advancement in understanding tunnelling-induced effects on piles, transforming negative face loss from a mere risk into a potential opportunity for optimised tunnelling performance.

Received: *21 January, 2025*
Revised: *3 March, 2025*
Accepted: *15 April, 2025*

[1,2]Department of Civil and Environmental Engineering, Universiti Teknologi PETRONAS, 32610 Seri Iskandar, Perak, Malaysia.

****Corresponding author:***
khoocheemin@gmail.com

DOI: *https://10.54552/v86i2.272*

Keywords:
Tunnel-soil-pile interaction, Tunnelling-induced pile responses, Transient effects, Negative face loss, Distributed fibre optic sensing

List of Notations

y is the distance between the TBM face and the experiment pile
D is the tunnel diameter
p_f is the face pressure
p_g is the tail skin grouting pressure
σ is the overburden pressure

1.0 INTRODUCTION

Shield tunnelling using pressurised face Tunnel Boring Machines (TBMs), such as Earth Pressure Balance (EPB) and slurry shields, is a highly mechanised, relatively safe, and fast tunnel construction method. In a typical tunnelling scenario, the face pressure exerted by the TBM remains lower than the mobilised earth pressure, allowing for controlled advancement as the ground moves towards the machine. This phenomenon generally results in predictable surface settlement, consistent with the principle of positive face loss. In contrast, negative face loss presents a unique challenge. Here, the face pressure exceeds the mobilised earth pressure, pushing the ground away from the TBM face and potentially causing surface heave. This can pose risks to underground utilities, above-ground structures, and the environment if not managed effectively.

In the case of a tunnelling adjacent to a pile foundation, where the pile is initially in equilibrium with long-term external loads and soil consolidation before tunnel excavation, the excavation disrupts this balance, causing additional deformation and stress adjustments in both the surrounding soil mass and the pile foundation. Due to the redistribution of deformation and stress induced by tunnel excavation, the pile experiences displacements in various directions based on its location relative to the TBM and the magnitude of ground loss components, such as face loss, shield loss, and tail loss (Loganathan, 2016). In the context of negative face loss condition, the pile moves outward as the TBM approaches. After the TBM passes, positive shield and tail loss occurs, causing the pile to move toward the tunnel. Figure 1 depicts the pile movement path in this scenario. Therefore, understanding the dynamics of TBM operating pressures and volume loss is crucial for tunnelling projects, as it governs ground behaviour and pile movement patterns. Both the capacity and serviceability of the piles in response to tunnelling-induced transient effects must be carefully evaluated.

Considerable research has been conducted on tunnelling beneath or adjacent to piles, employing various methodologies including field studies, laboratory centrifuge tests, empirical, analytical, and numerical approaches. However, most of these studies focus on frictional or frictional-end bearing piles, with the exception of a socketed pile modelled in one of the centrifuge

tests by Ong (2009). In full-scale field studies, pile responses to nearby tunnelling have often been evaluated indirectly through monitoring of structures and ground instrumentation. Direct in-pile instrumentation, however, has been limited, presenting opportunities for more in-depth investigations. Some notable in-pile instrumentation field studies are summarised in Table 1, where the instrumented piles had their toe levels terminated either above the tunnel crown or beside the tunnel extrados at varying depths.

Results from in-pile instrumentation revealed distinct zones of influence around tunnels during construction. Within these zones, both the ground and piles experienced varying degrees and directions of relative displacements. As the TBM approached, passed beneath or adjacent to, and continued beyond the pile, notable redistributions of load along the pile lengths were observed. This phenomenon induced lateral pile deflections and bending moments, some of which were transient and reversible, depending on the prevalence of several factors (Khoo, 2024). However, few researchers have focused on pile lateral deflection. Loganathan's (2016) hypothesis on the settlement influence zone and pile movement paths remains an area worth exploring.

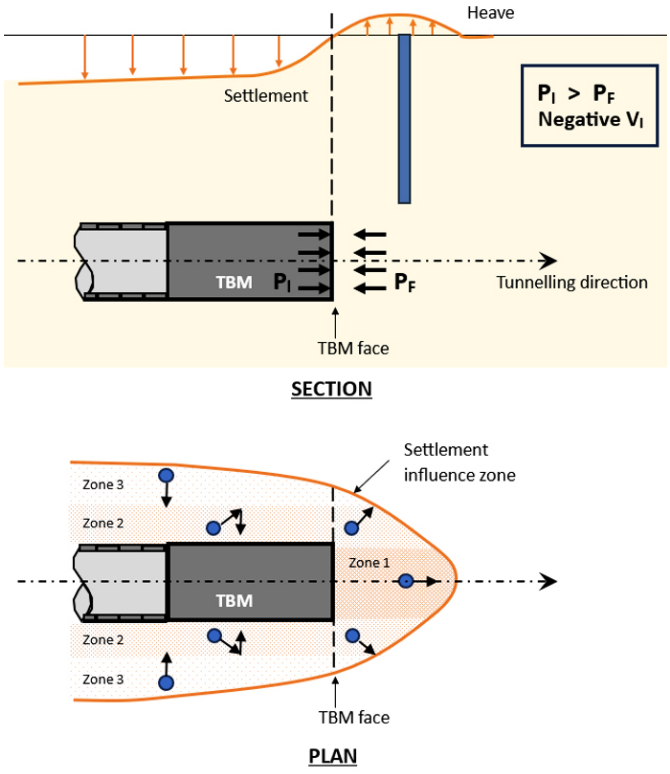

Figure 1: Ground response and pile movement path in negative face loss scenario (Loganathan, 2016)

To contribute to this body of knowledge, full-scale field research was recently conducted at Malaysia's Klang Valley Mass Rapid Transit (KVMRT) - Putrajaya Line. The study builds on previous efforts and addresses gaps in knowledge by employing distributed fibre optic sensing technology based on stimulated Brillouin scattering, using the Brillouin Optical Time Domain Analysis (BOTDA) technique, to monitor real-time strain in a pre-loaded experiment micropile in close proximity to twin bored tunnels excavated using Variable Density (multimode) TBMs. This novel technique offers several advantages over conventional point-based sensors (e.g. strain gauges) for assessing tunnel-soil-pile interactions (Soga *et al.,* 2008). It is also effective in identifying anomalies in cast-in-situ concrete piles (Mohamad *et al.,* 2016). The integrated sensors measure three-dimensional deformations, including bending and lateral displacements, providing more precise data on tunnel-soil-pile interaction and pile responses throughout the entire pile length during the transient effects of shield tunnelling. This advanced technology has proven effective in monitoring various large civil and geotechnical structures, including piles (Ohno *et al.,*2002, Klar *et al.,* 2006), test piles (Mohamad *et al,* 2009; Tee *et al.,* 2016; Tee *et al.,* 2017), retaining walls (Mohamad *et al.,* 2011), as well as bridges and tunnels (Mohamad *et al.,* 2010; Mohamad *et al.,* 2012).

Field data from the research site were interpreted and back-analysed using three-dimensional finite element modelling, alongside TBM driving data recorded during tunnelling. Numerical results from the tunnel-soil-pile interaction analysis were validated with field measurements. The validated framework has opened avenues for further exploration through numerical parametric studies. This paper aims to deepen the understanding of the transient effects of shield tunnelling on a loaded pile in a negative face loss environment, offering valuable insights for the scientific and tunnelling community, along with recommendations and strategies to mitigate risks

Table 1: Summary of reported field studies with in-pile instrumentation

Citation	Project	Soil Type	Tunnel Type	Pile Type	In-Pile Monitoring
Mair (1993) Lee *et al.* (1994)	Angel Underground Station, London	London clay	Hand-dug tunnel	Bored pile (under-reamed)	Inclinometer
Teunissen & Hutteman (1998) Kaalberg *et al.* (2005)	North/South Line, Amsterdam	Very soft silty clay overlying sand layer	Shield tunnel	Timber pile, concrete pile	Pile top pressure sensor, precise levelling
Coutts & Wong (2000) Pang *et al.* (2005)	North-East Line C704, Singapore	Bukit Timah granitic residual soil	EPB shield tunnel	Bored pile	Vibrating wire strain gauge
Jacobsz *et al.* (2005) Selematas *et al.* (2005)	Channel Tunnel Rail Link C250, Essex, UK	Terrace gravel and London clay	EPB shield tunnel	Driven pile, bored pile	Vibrating wire strain gauge, base load cell, electrolevel inclinometer
Cham (2007)	Circle Line C852, Singapore	Bukit Timah granitic residual soil	EPB shield tunnel	Bored pile	Vibrating wire strain gauge
Mohamad *et al.* (2022)	Grand Paris Express Line 16, France	Fine clayey sand overlying limestone	EPB shield tunnel	Cast-in-situ pile	Strain gauge, optical fibre cable

associated with pile responses during various stages of tunnel excavation. The findings underscore the delicate balance in negative face loss tunnelling, where careful management can mitigate risks while enhancing tunnelling safety and efficiency.

2.0 BACKGROUND OF THE STUDY

2.1 The Research Site

The research site is located at the Education Quarters in the central business district of Kuala Lumpur and was designated for a full-scale field investigation. This is part of the KVMRT Putrajaya Line project, where twin bored tunnels, each with a diameter of 6.35 m, were driven partially beneath the Quarters. The tunnelling commenced from the northwest at Hospital Kuala Lumpur (HKL) Cross-over and extended southeastward to Raja Uda Station, as illustrated in Figure 2. Notably, the southbound tunnel passed directly beneath a 5-storey building, presenting significant challenges due to the presence of the existing building foundations.

To mitigate this challenge, the affected piles were removed, and underpinning work was carried out ahead of the TBM passage. The underpinning process involved the installation of micropiles capped under a reinforced concrete transfer structure, which spanned across the tunnel. Given the anticipated complexities of the tunnel construction, an additional 'experiment' micropile was strategically installed. Figure 3 provides a plan view and cross-section of the tunnel relative to the existing building foundation, newly installed underpinning

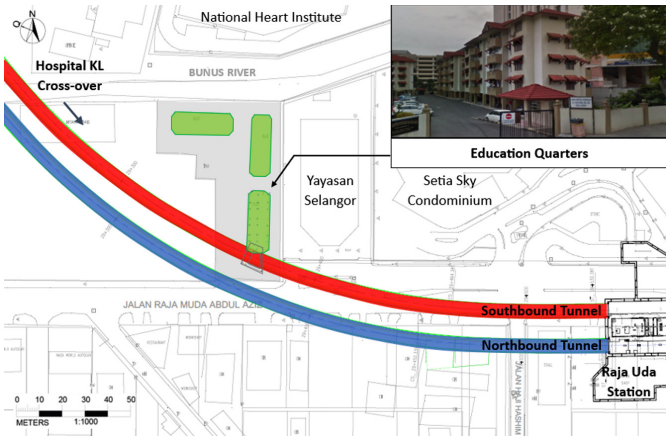

Figure 2: Location plan of the research site

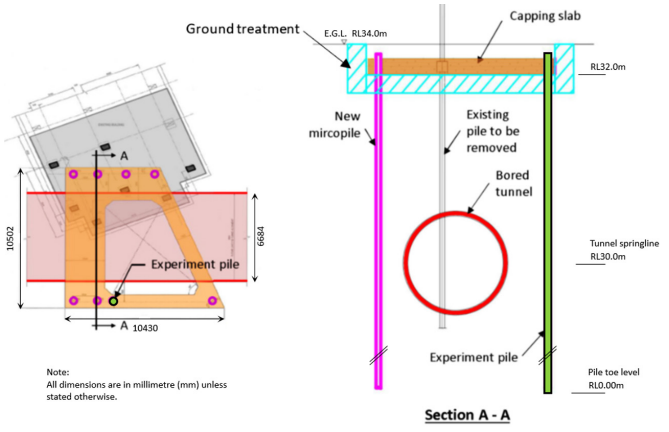

Figure 3: Plan view and cross-section of the underpinning works

piles, and the experiment pile. Detailed information of the pile removal and underpinning works can be found in the references (Tan *et al.,* 2019, Khoo *et al.,* 2024a). This strategic decision enabled comprehensive in-pile instrumentation and real-time monitoring throughout the tunnelling process, with the experiment pile playing a critical role in providing insights into the interactions and transient responses of the pile-tunnel system.

2.2 Ground Characterisation

The site is located within the Kuala Lumpur Limestone formation, characterised by flat terrain with an average elevation of Reduced Level (RL) 34 m. Site investigations confirmed the expected regional geological setting, revealing alluvium overlying limestone bedrock. However, the bedrock levels at the site were predicted to be erratic, with potential cavities due to the karstic features inherent in the limestone formation. The alluvium consists mainly of interbedded layers of loose sand and soft clay/silt. Groundwater was encountered at a depth of 4 m at the research site, with a typical seasonal fluctuation of ±0.5 m. Figure 4 illustrates the interpreted geological profile along the southbound tunnel alignment, where the tunnel is located, with cover-to-diameter ratios ranging from approximately 1.6 to 2.0.

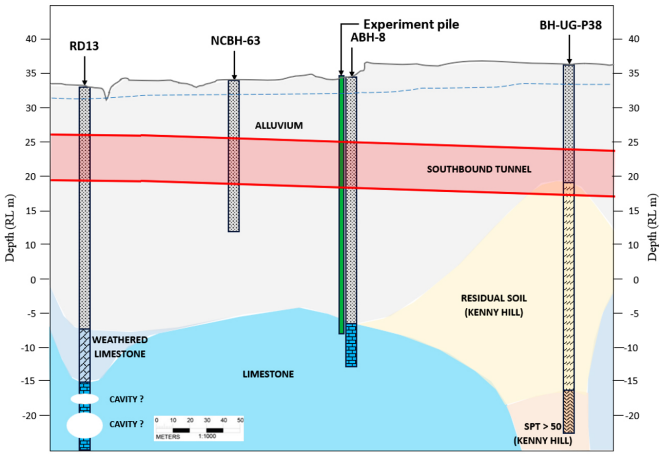

Figure 4: Interpreted geological profile along the southbound tunnel alignment

The ground stratification consists of alluvium overlying limestone bedrock, and the pile, being socketed int the bedrock, provides a controlled environment with a fixed-end condition. This feature represents a novel aspect to the research, as, to the best of the authors' knowledge, no prior studies have specifically investigated this scenario.

2.3 The Experiment Pile and Instrumentation

The experiment pile, with a diameter of 300 mm, was positioned 1.5 m away from the extrados of the southbound tunnel. It is reinforced with an API (American Petroleum Institute) pipe, measuring 177.8 mm in outer diameter and 10.36 mm in wall thickness. The pile was installed to a depth of 1.5 m into the limestone bedrock at 32.3 m below ground level. The micropile (Grade G30) is designed with a working capacity of 600 kN. Key details of the experiment pile are summarised in Table 2. A detailed account on the pile head setup for pre-loading can be found in Khoo *et al.* (2024a).

Table 2: Details of the experiment pile

Parameter	Unit	Value
Pile diameter	mm	300
Pile working load	kN	600
Pile reinforcement	-	API pipe (177.8 mm O.D. with 10.36 mm wall thickness)
Cement grout grade	MN/m^2	30
Water cement ratio	-	0.45
Rock socket length	m	1.5
Total pile length	m	33.8
Date of installation	-	16 March 2018

The in-pile instrumentation was meticulously designed to provide real-time data on the tunnelling-induced transient pile responses, including vertical displacement at the pile head, horizontal deformation of the pile shaft, axial load distribution, and internal forces within the pile. This instrumentation incorporated both conventional vibrating wire strain gauges and inclinometer, as well as advanced fiber optic distributed sensors. The integration of both conventional and advanced sensing technologies enhances the reliability and accuracy of measurements, enabling a comprehensive evaluation of the pile's response to tunnelling-induced transient effects. Details of the in-pile instrumentation and arrangement are illustrated in Figure 5.

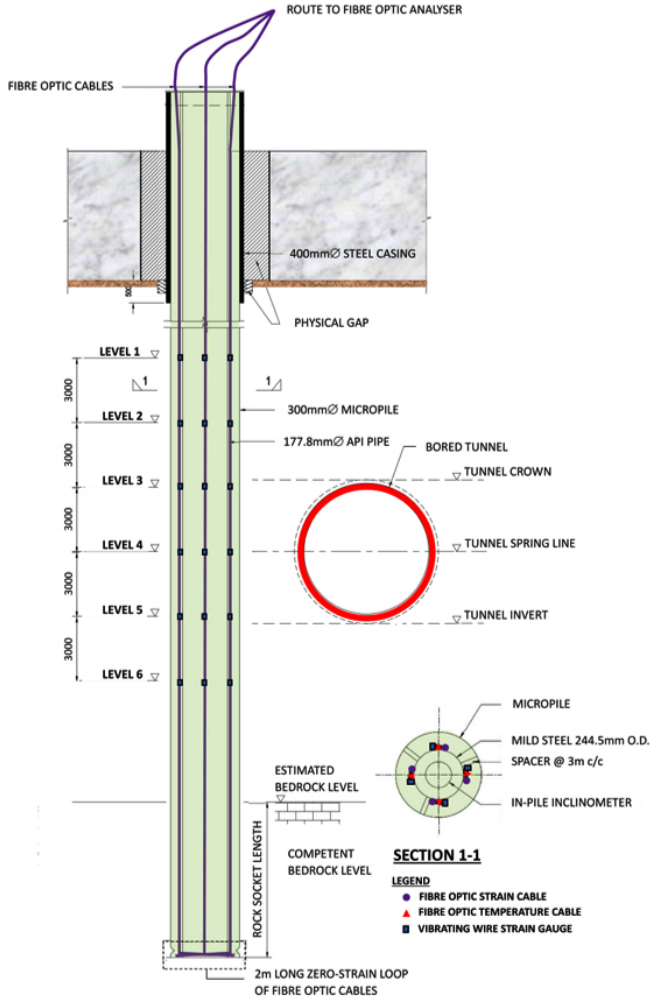

Figure 5: In-pile instrumentation and arrangement

Six levels of vibrating wire strain gauges were strategically affixed to the pile reinforcement (API pipe). These gauges were placed at 3-meter intervals, beginning from a depth of 4 m below the ground surface. Each level corresponds to significant measuring points. Level 1 – 6 m above the tunnel crown, Level 2 – 3 m above the tunnel crown, Level 3 – tunnel crown, Level 4, tunnel springline, Level 5 – tunnel invert, and Level 6 – 3 m below tunnel invert. At every level, the strain gauges were arranged on four sides (two pairs per level), with each pair aligned parallel and perpendicular to the tunnel orientation. These strain gauges were spot-welded on 10 mm steel bands and securely fastened to the designated levels on the API pipe. Unfortunately, some sensors did not survive the installation process.

Additionally, an inclinometer casing was pre-installed inside the API pile during the grouting process, providing redundancy for pile deflection measurements and ensuring comprehensive data collection on the pile's behaviour during the tunnelling process. The baseline measurement, which was used for interpretation, was conducted one month before the TBM reached the target, to eliminate any strain induced by the installation process.

In addition to the in-pile instrumentation, settlement markers, inclinometers, and piezometers were installed in the ground adjacent to the experiment pile. The building that the tunnel undercrossed was also closely monitored. This comprehensive instrumentation regime enabled a thorough investigation of tunnelling-induced effects and tunnel-soil-pile interaction. Figure 6 illustrates the ground and structure instrumentation surrounding the experiment pile.

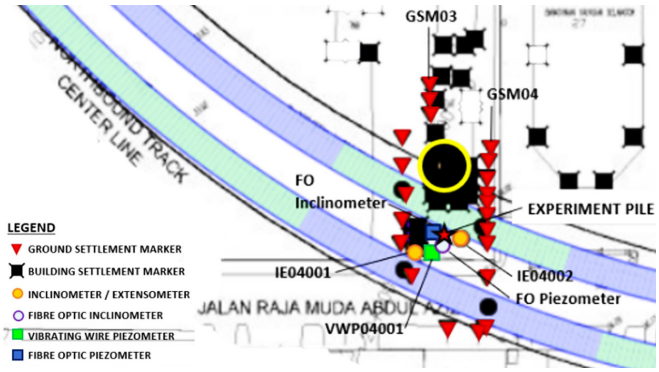

Figure 6: Ground and structure instrumentation

3.0 FIELD MEASUREMENTS AND NUMERICAL ANALYSIS

3.1 Key Tunnelling Data

The installation of the instrumented experiment pile was completed in March 2018, followed by pile removal work ahead of the passage of the TBMs. Construction activities were carefully coordinated to ensure that the underpinning and pile removal did not interfere with tunnelling operations or affect the permanent tunnel lining. Consolidation due to the piling and ground treatment works was assumed to be complete prior to TBM advancement, given the high permeability of the alluvium sandy soil.

This study specifically focused on the southbound tunnelling over a distance of approximately between y = -10D and +10D from the experiment pile, as illustrated by the time-location of

the TBM in Figure 7, where y represents the distance between the TBM face and the experiment pile, normalised by the tunnel diameter (D). Positive values of y indicate distance where the TBM has passed beyond the pile. This section of tunnel was completed between 3 May 2019 and 16 May 2019. It is important to note that the TBM stopped for planned cutterhead intervention on 6 and 7 May 2019, which took place within a grout block.

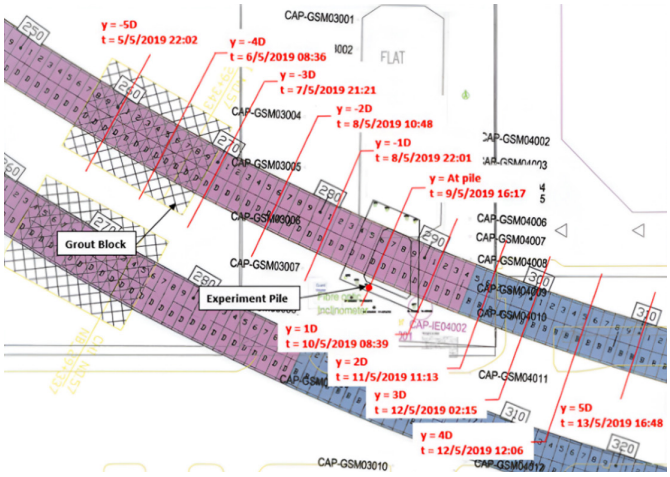

Figure 7: Time-location of the southbound TBM in relation to the experiment pile

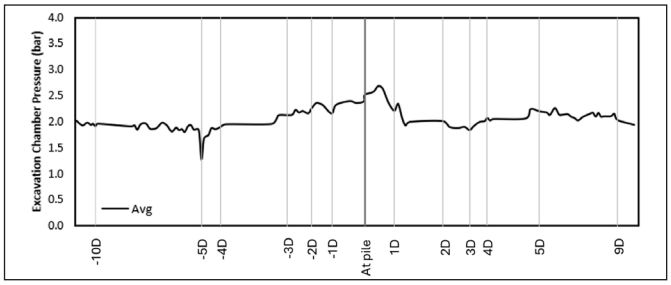

Figure 8: Recorded excavation chamber pressures

Variable density tunnel boring machines were selected for excavating the tunnels from HKL Cross-over to Raja Uda Station, operating in the earth pressure balance (EPB) mode. During the TBM progress, a continuous range of face support pressure was provided. Figure 8 shows the recorded average face pressure in the excavation chamber. It is evident that a higher face pressure was applied ahead of the experiment pile. The face pressure gradually increased from 2 bar (at a distance of y = -3D) to a maximum of 2.6 bar as the TBM cutterhead reached the experiment pile location, eventually decreasing to the normal face pressure at a distance of 1D away.

As part of the key tunnelling data, the normal range of advance speed was between 20 – 50 mm/min, with an average of 34.5 mm/min for this length of the bored section. Advance thrust forces and group pressures fluctuated between 10 – 17 MN and 50 – 150 bar, respectively. The grouting pressure at the grout ports remained relatively constant throughout the tunnel drive, with average pressures approximately 2 - 4 bar.

3.2 Numerical Simulation

The three-dimensional numerical modelling and simulation were conducted using a commercially available finite element program, PLAXIS 3D, to replicate tunnel advancement in a manner closely resembling actual excavation processes. A comprehensive 3D model with dimensions of 140m in length, 40 m in height, and 100 m in width was employed for the analysis, consisting of 56,584 elements and 88,440 nodes, as shown in Figure 9. Readers are referred to Khoo *et al.* (2024b, 2025) for further details on the model set-up, soil constitutive model, and material properties. This paper reiterates some of the key simulation techniques adopted.

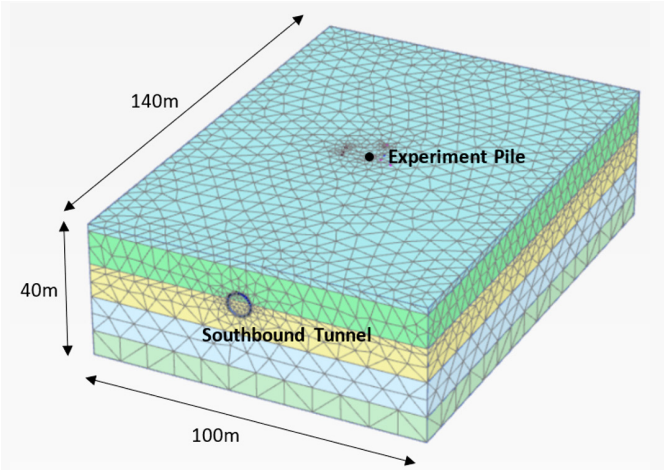

Figure 9: Perspective view of the developed 3D model

The model simulated the first 42 m of tunnels modelled using the "all-in-once installation" approach (Vermeer *et al.,* 2002), followed by a step-by-step simulation to represent sequential tunnel advancement. The recorded face pressures from the TBM excavation chamber were applied to the tunnel face using a multi-segmental trapezoidal profile instead of the conventional triangular earth pressure (Khoo *et al.,* 2024b). This approach accounted for pressure loss along the screw conveyor in EPB tunnelling, where the pressure gradually decreases, and reaching zero at the discharging outlet. According to Herrenknecht & Rehm (2003), as reproduced in Figure 10, the pressure at the screw conveyor inlet reduces to 80% of the applied face pressure, with the pressure gradient influenced by the fluidity and impermeability of the muck. The irregular pressure distribution reflects the inherent challenges in maintaining a classical earth pressure profile during excavation.

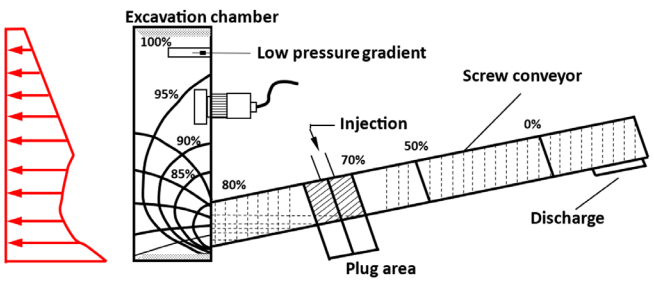

Figure 10: Earth pressure distribution diagram (Herrenknecht and Rehm, 2003)

As shown in Figure 11, tail void grouting was modelled by applying radially distribution isotropic pressure around the tunnel periphery to replicate the injection pressure of grout in its fluid state. This grouting simulation method has been widely adopted by researchers, including Kasper & Meschke (2004)

and Mollon *et al.* (2013). The recorded grouting pressures during tunnel advancement were incorporated into the numerical model to improve the simulation's realism and accuracy.

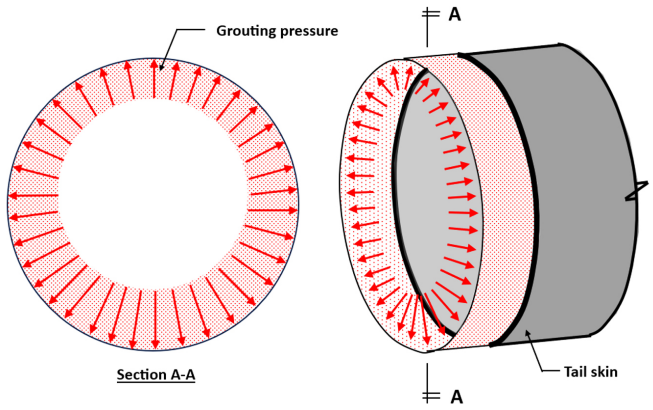

Figure 11: Profile of radial distribution grouting increasing with depth adopted in the simulation

3.3 Field Measurements and Numerical Analysis Results

The initial step in the study involved comprehensive calibration and validation of the numerical model to verify the experiment pile's load-settlement behaviour and axial load distribution during the pre-loading stage, before being subjected to tunnelling effects. The observed agreement (> 95%) between computed and measured pile head settlements (Figure 12), as well as pile load distributions (Figure 13), underscores the validity of the numerical framework established in this study (Khoo, 2024).

The numerical analysis results were subsequently compared with field measurements, focusing on transient pile responses such as pile head movement, axial load distribution, bending moments, and lateral deflection. This comprehensive comparison demonstrates the numerical simulations' accuracy and reliability in capturing the dynamic behaviour of the pile under tunnelling-induced effects. For detailed comparisons of pile head movement, axial load distribution, and bending moments between field measurements and numerical back-analysis, readers are referred to Khoo *et al.* (2025). This paper provides a summary of the key findings related to pile lateral deflection.

Figure 14 presents a detailed view of the time-based movement path of the pile at six critical depths. In this illustration, the positive direction of Axis-A indicates movement away from the tunnel in the transverse direction, while the positive direction of Axis-B denotes movement away from the tunnel face in the longitudinal direction.

Both the field measurements and numerical results consistently demonstrate that as the TBM approached the target, the pile generally experienced outward movement, with the exception of Level 1 in the numerical analysis. This anomaly may be attributed to the numerically simulated top-loaded fixed-end pile behaving as a slender bending element. Once the TBM face passed the pile, the lateral deflection at tunnel level promptly shifted back towards the tunnel as the distance increased, although the numerical analysis indicated slight variations in direction.

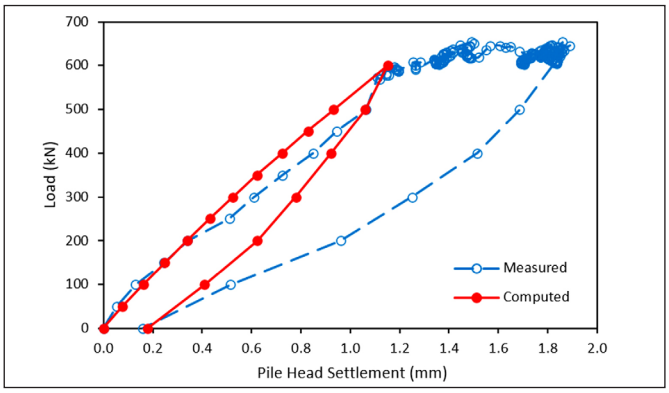

Figure 12: Load settlement behaviour of the experiment pile

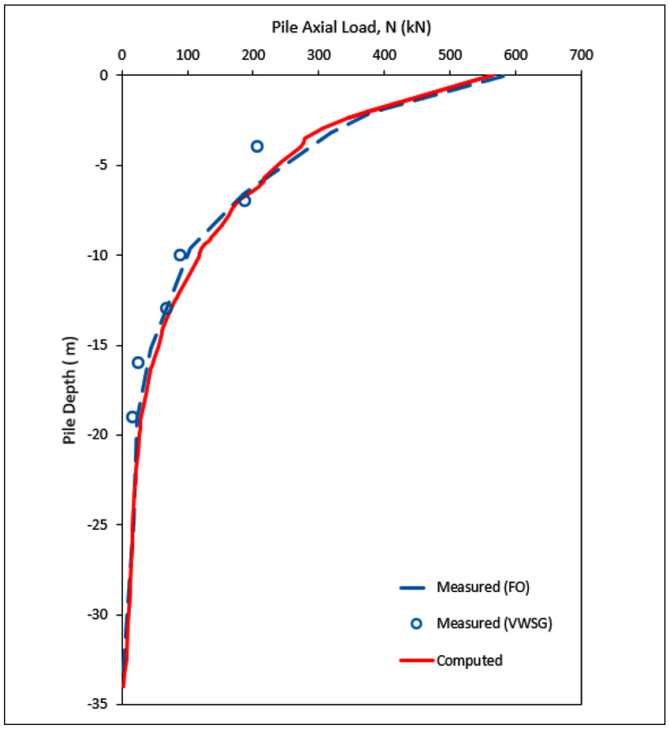

Figure 13: Axial load distribution along the experiment pile

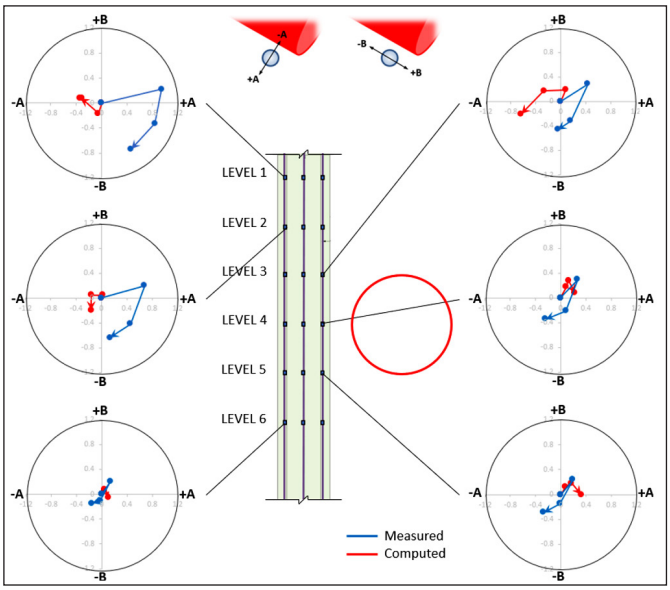

Figure 14: Incremental pile movement during the tunnel advance

These findings align with the hypothesis proposed by Loganathan (2016) regarding pile movement paths in a negative face loss scenario. According to this hypothesis, when the TBM face pressure exceeds the mobilised earth pressure at the face, the ground is pushed away from the TBM face, inducing heave at the surface and sub-surface ground movement away from the TBM face. Subsequently, when the TBM has passed, a positive shield and tail loss occurs, signalling the closing of the physical gap. This results in the ground moving toward the tunnel, leading to ground settlement. This entire phenomenon was evidenced by the measured ground surface movements as depicted in Figure 15. Additionally, the measurement of building settlement, shown in Figure 16, further validates these observations. Refer Figure 6 for the locations of the instrumentation.

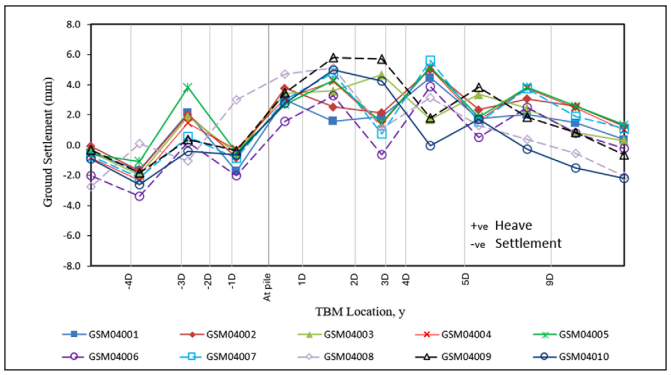

Figure 15: Measured ground surface movements

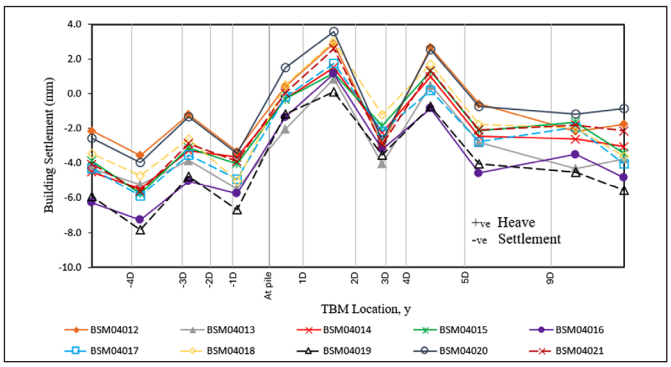

Figure 16: Measured building settlements

4.0 PARAMETRIC STUDY

Following the successful back-analysis and validation of the three-dimensional (3D) finite element model using valuable TBM operating data and field measurements from the research site, a series of parametric studies has been implemented to identify an optimum range of tunnelling parameters for controlling ground loss and minimising the impacts on the adjacent pile during various stages of tunnel excavation. Specifically, the influence of face support pressure and tail skin grouting pressure is assessed, providing insights into the significance of each parameter concerning the pile responses induced by tunnelling.

4.1 Effects of Face Support Pressure

The application of face support pressure is normalised to the overburden pressure (p_f/σ) at the tunnel crown level, with specified variations as outlined in Table 3. These diverse ranges are calibrated to the validated research site data to observe pile responses and the magnitude of ground surface settlement while maintaining consistent soil properties, pile properties, and other TBM driving parameters. The analyses aim to ascertain the relationship between applied face pressure and key effects on pile responses, including pile head displacement, pile lateral deflections (perpendicular and parallel to the tunnel), and pile axial load.

Table 3: Variation of face support pressure

Face Pressure, p_f (kN/m^2)	Ratio to Baseline	p_f/σ
48.75	0.25	0.3
97.50	0.50	0.5
146.50	0.75	0.8
195.00	1.00	1.1
243.75	1.25	1.4
292.50	1.50	1.6
341.25	1.75	1.9
390.00	2.00	2.2

When the normalised face pressure (p_f/σ) exceeds 1.0, a negative face loss scenario occurs. Otherwise, it is considered as positive face loss, where the face pressure is within the range of overburden pressure or significantly lower than the overburden pressure.

For each applied face pressure, the evolution of the impacts is studied for a distance of TBM advance from y = -2D up to y = 9D from the experiment pile, where y is the distance between the TBM face and the experiment pile, normalised by the tunnel diameter (D). The negative distance signifies the TBM's position prior to reaching the pile. This range of distance is selected considering the recommended zone of influence from the research study (Khoo *et al.*, 2025) as well as a sufficiently long distance for stabilising the equilibrium of tunnelling effects.

4.1.1 Pile Head Displacement

Figure 17 illustrates the pile head settlement at various p_f/σ values. Generally, it can be observed that the pile head experiences a lesser magnitude of settlement within the range of p_f/σ between 0.8 and 1.1. This trend is evident as the TBM passes by the pile until a distance of y = 3D. However, there is a noticeable increase in pile head settlement when p_f/σ exceeds 1.1.

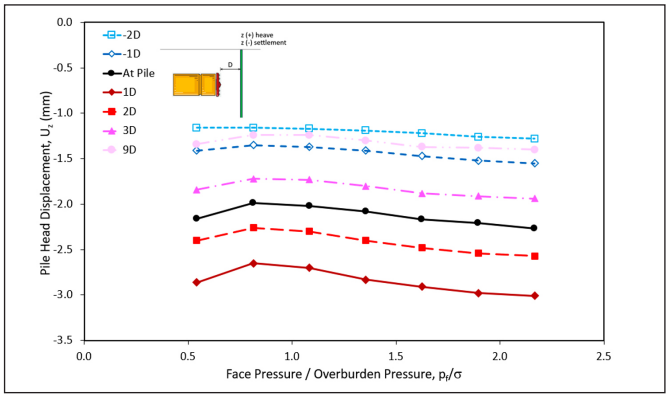

Figure 17: Pile head displacement, U_z vs. face pressure/overburden pressure, p_f/σ

It should be emphasised, however, that the numerical model fails to converge if p_f/σ is less than 0.5. This implies that a minimum face support pressure is required for the successful simulation of this project case study. In practice, if the face support pressure decreases further, significant deformation or total collapse of the soil body may occur.

4.1.2 Pile Lateral Deflections

Figure 18 illustrates the maximum pile lateral deflections at various p_f/σ values for the transverse direction (perpendicular to the tunnel). Positive values indicate movement away from the tunnel extrados. Generally, the pile lateral deflection becomes noticeable in the transverse direction when the p_f/σ ratio is about 1.4 or higher. The same trend is observed for an approaching TBM at y = -1D, with the magnitude of deflection continuously increasing until the TBM has passed far beyond the pile.

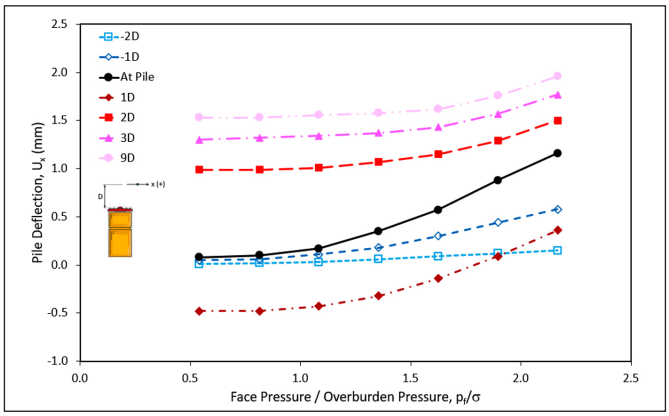

Figure 18: Pile lateral deflection, U_x vs. face pressure/overburden pressure, p_f/σ

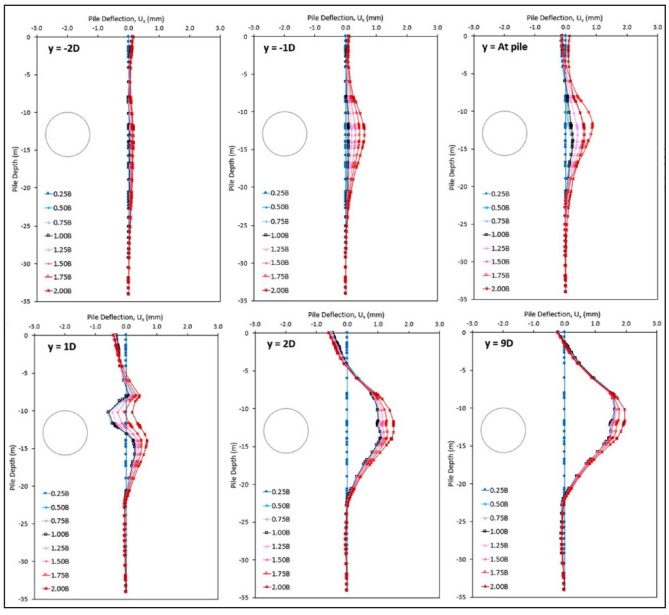

Figure 19: Evolution of pile lateral deflection, U_x profile

The evolution of pile lateral deflection profiles is illustrated in Figure 19. From here, we can see that the pile movement path is obvious, especially for the case of negative face loss ($p_f/\sigma > 1.0$), where the pile is being pushed away when the TBM is approaching and being pulled inward at y = 1D (where the shield is passing through the pile) temporarily before release outward after the entire TBM shield has passed beyond the pile a distance of y = 2D. The maximum pile lateral deflection occurs in a zone above the tunnel springline to the tunnel crown.

Opposite to the transverse direction, the magnitude of pile lateral deflection in the longitudinal direction significantly and linearly increases with the increased p_f/σ ratio, even from a lower ratio of 0.5, as shown in Figure 20. Logically, a higher face pressure applied will directly push the pile forward along the tunnel alignment. The pile lateral deflection reaches its peak when the TBM face approaches the pile and starts to decrease after the TBM passed beyond.

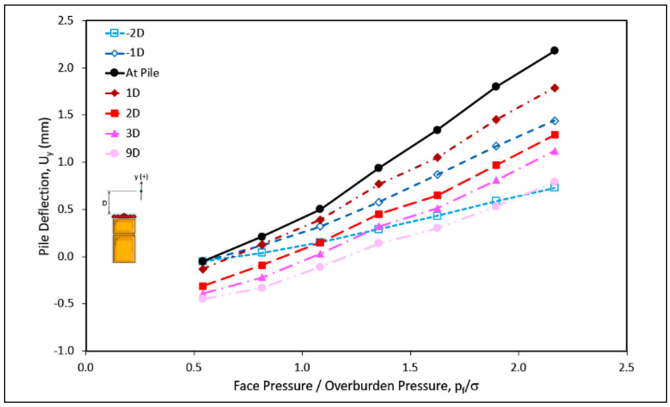

Figure 20: Pile lateral deflection, U_y vs. face pressure/overburden pressure, p_f/σ

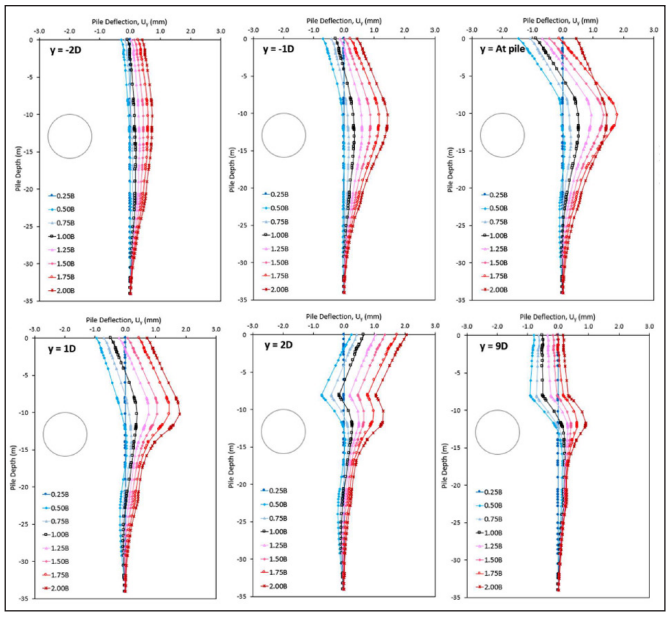

Figure 21: Evolution of pile lateral deflection, U_y

In a similar presentation, Figure 21 illustrates the evolution of pile lateral deflection in the longitudinal direction. Similar pile movement behaviour is noted except that the incurred inward movements are irreversible as observed when TBM passed far beyond the pile, y = 9D. This observation tallies with the hypothesis proposed by Loganathan (2016) for a negative face loss tunnelling environment, where the ground is pushed away from the TBM face, may induce heave at the surface and subsurface ground movement away from the TBM face,

subsequently, when the TBM has passed, a positive shield and tail loss occurs, signifying the closing of the physical gap. This results in the ground movement toward the tunnel, leading to ground settlement.

4.1.3 Pile Axial Load

Regarding the pile axial load, the evaluation focuses on the maximum value occurring in the critical zone between one time diameter above and below the tunnel horizon. This is crucial as the maximum axial load, attributed to the additional drag load due to tunnelling-induced ground settlement, typically occurs at the tunnel horizon.

Figure 22 illustrates the impacts on pile axial load in response to the varying applied face pressure. Despite the pile axial load generally being unresponsive to higher face pressure, a reduced load is obtained when the p_f/σ ratio is around 0.8 to 1.1 as observed when the TBM is at y = 1D, as shown in Figure 22.

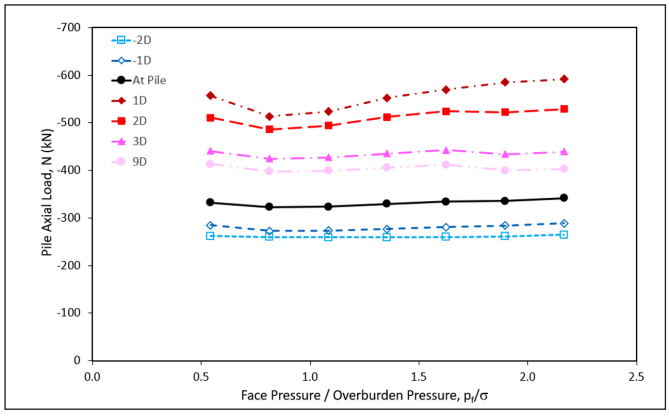

Figure 22: Pile axial force vs. face pressure/overburden pressure, p_f/σ

4.1.4 Ground Surface Settlement

Figure 23 illustrates the general trend of maximum ground settlement and ground loss obtained for the range of p_f/σ ratio adopted in this study. Clearly, the recommended optimum face pressure is between 0.8 to 1.1 times the overburden pressure, aligning with the earlier observations.

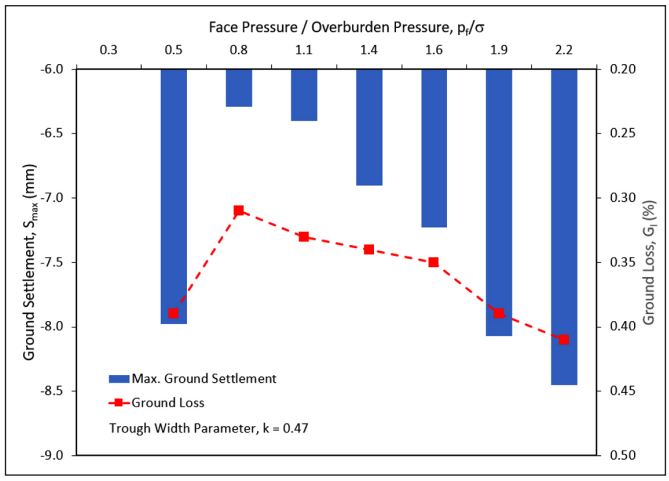

Figure 23: Ground settlement vs. face pressure/overburden pressure, p_f/σ

4.2 Effects of Tail Skin Grouting Pressure

Similar to the face support pressure analyses, this set of studies will vary the normalised grouting pressure to assess its impact on pile responses. The applied pressure will be increased up to three times the overburden pressure to explore potential beneficial effects. The relationship between applied grouting pressure and variables such as pile head displacement, pile lateral deflections, axial load and ground surface settlement will be examined.

In exploring the impact of tail skin grouting, grouting pressure is normalised to the overburden pressure at the tunnel axis level, spanning a specified range (Table 5).

Table 5: Variation of tail skin grouting pressure

Grouting Pressure, p_g (kN/m²)	Ratio to Baseline	p_g/σ
87.5	0.25	0.4
175.5	0.50	0.7
262.5	0.75	1.1
350.0	1.00	1.5
437.5	1.25	1.9
525.0	1.50	2.2
612.5	1.75	2.6
700.0	2.00	3.0

4.2.1 Pile Head Displacement

Figure 24 illustrates the results of pile head settlement at various p_g/σ values. The pile exhibits responsiveness to tail skin grouting effects when the TBM face is at y = 2D, aligning with the shield tail coinciding with the pile position. Generally, pile head settlement diminishes with an increasing p_g/σ ratio, indicating pile rebound. Notably, the pile may experience an upward heave with substantial grouting pressure, particularly when the p_g/σ ratio exceeds 2.0.

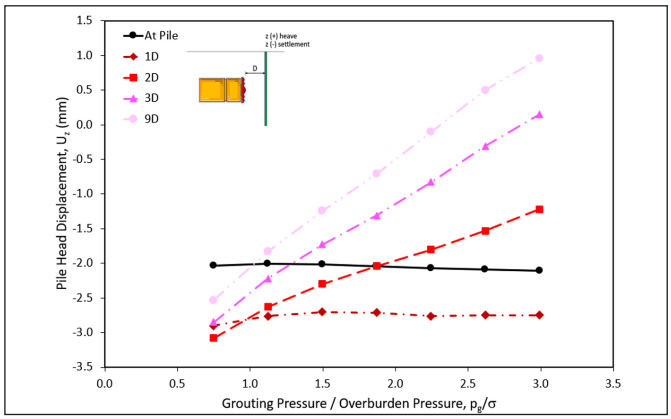

Figure 24: Pile head displacement, U_z vs. grouting pressure/overburden pressure, p_g/σ

It is essential to highlight that the simulation adopted radially distributed pressure around a tunnel ring (perpendicular to the ground), deviating from real-word scenarios where grouting pressure is applied to the annulus gap between the lining and surrounding soil. Additionally, the study observes temporary compression of the pile due to downdrag load generated during TBM passage, with subsequent release after the TBM surpasses y = 3D. The rate of pile rebound consistently heightens as the TBM moves farther away.

Similar to the prior face pressures study, convergence issues arise if p_g/σ is less than 0.5, underscoring the need for a minimum grouting pressure for successful simulation in this project case study.

4.2.2 Pile Lateral Deflection

Figure 25 provides an overview of pile lateral deflections at various p_g/σ values for the transverse direction (perpendicular to the tunnel).

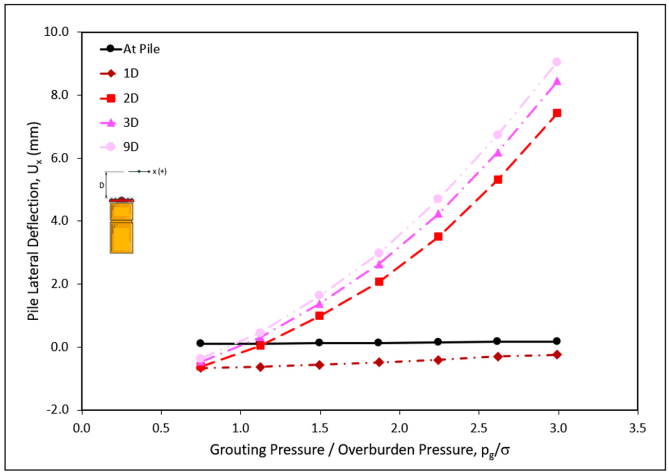

Figure 25: Pile lateral deflection, U_x vs. grouting pressure/overburden pressure, p_g/σ

The behaviour of pile lateral deflection in the transverse direction mirrors that of pile head settlement, given the adoption of radially distributed pressure in simulating tail skin grouting pressure. Notably, lateral deflection exhibits exponential growth with an increasing p_g/σ ratio. Similar patterns are observed in the longitudinal direction, as depicted in Figure 26.

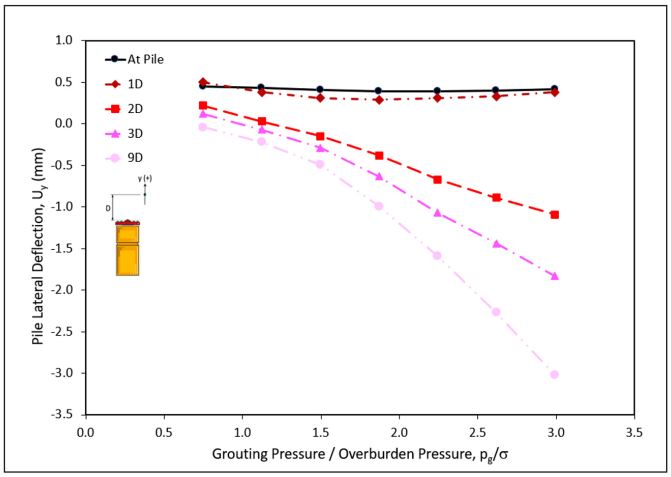

Figure 26: Pile lateral deflection, U_y vs. grouting pressure/overburden pressure, p_g/σ

4.2.3 Pile Axial Load

Figure 27 offers insights into the development and distribution of pile axial load during the TBM passage under varying applied grouting pressures. Additionally, Figure 28 presents the maximum axial load (compression) experienced by the pile in response to the effects of grouting pressure. As anticipated, downdrag load resulting from negative skin friction, caused by

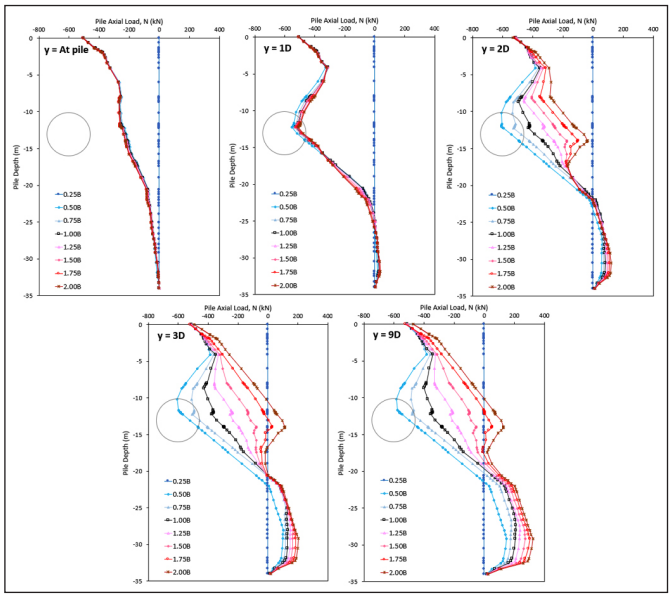

Figure 27: Development and distribution of pile axial load

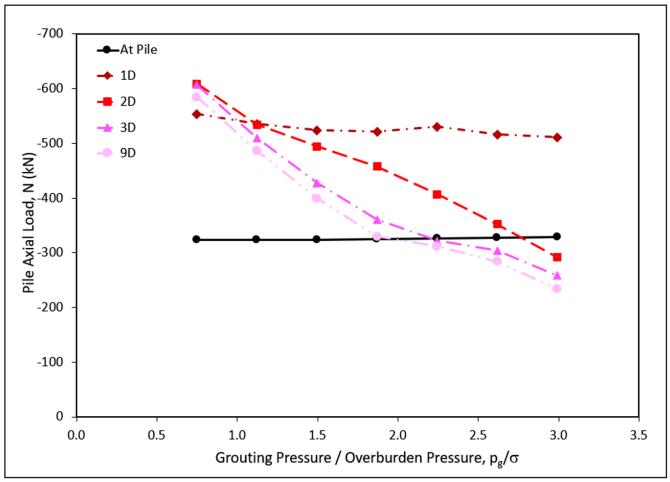

Figure 28: Pile axial load vs. grouting pressure/overburden pressure, p_g/σ

tunnelling-induced ground settlement, is generated. The pile demonstrates responsiveness to this, influence when the TBM is positioned at y = 2D and beyond.

The primary observation suggests that higher grouting pressure induces ground heaving, including pile head rebound, as depicted in Figure 24. This effect proves advantageous in swiftly counteracting negative skin friction quickly. It is plausible that the resulting additional positive skin friction contributes to enhancing the geotechnical capacity of the pile. Conversely, lower grouting pressure (p_g/σ < 1.0) leads to increased downdrag load compared to the baseline scenario.

4.2.4 Ground Surface Settlement

Figure 29 illustrates the overall trend of maximum ground settlement and ground loss within the range of p_g/σ ratio considered in this study. Notably, the recommended optimum grouting pressure is identified between 1.1 to 1.5 times the overburden pressure. This range correlates with the lowest magnitudes of ground settlement and ground loss, demonstrating its effectiveness in minimising the impact on the

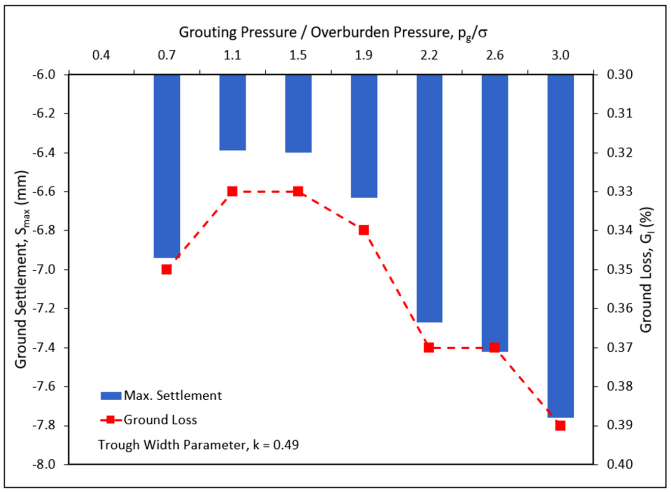

Figure 29: Ground settlement vs. grouting pressure/overburden pressure, p_g/σ

adjacent pile and surrounding ground. It is crucial, however, to consider the implications of applying higher grouting pressure in the design of the tunnel lining design.

4.0 CONCLUSIONS

This study conducted a comprehensive numerical investigation to evaluate the effects of varying face support pressures and tail skin grouting pressures on tunnelling-induced pile responses and ground surface settlement. The three-dimensional finite element model, calibrated and validated using field measurements and tunnelling data from a full-scale field research study, provided valuable insights into tunnel-soil-pile interactions.

The parametric analysis revealed distinctions tunnelling behaviours, particularly between negative face loss - occurring when normalised face pressure exceeds 1.0 - and positive face loss, when face pressure falls within or below the overburden pressure. This distinction highlights the critical influence of both face support and tail skin grouting pressures on pile responses and ground settlement during tunnelling operations.

Significant patterns in pile displacements were observed, notably in pile head settlement and lateral deflections, which varied across different tunnel excavation stages. The study also examined pile axial load distribution and ground settlement within the critical tunnel influence zone. The findings emphasise the importance of maintaining adequate face support pressures to mitigate excessive ground settlements and pile deformations. An optimum face support pressure range of 0.8 to 1.1 times the overburden pressure was identified, minimising pile responses and ground settlement.

Regarding tail skin grouting pressure, increasing grouting pressure was found to reduce pile head settlement while inducing exponential transverse lateral deflections and longitudinal pile rotation. Axial force analyses suggested that higher grouting pressure could induce ground heaving, counteracting negative skin friction and resulting in reduced axial loads. An optimum grouting pressure range of 1.1 to 1.5 times the overburden pressure was recommended to minimise ground loss and settlement, although the potential implications on tunnel lining design warrant careful consideration.

This research has provided an updated understanding of the transient responses of a single-loaded pile to tunnelling effects. The findings suggest that, for tunnelling in highly permeable soils, the application of negative face loss can minimise ground settlement and enhance pile performance by counteracting the stresses induced by downgrad load. This insight opens up new opportunities for optimising tunnelling performance.

ACKNOWLEDGEMENTS

The authors extend their gratitude to the management of Mass Rapid Transit Corporation Sdn. Bhd. for granting permission to publish this paper and for their positive support, which significantly contributed to the success of this work. Special thanks are also extended to Ir. Dr. Ooi Lean Hock of MMC-Gamuda KVMRT (T) Sdn. Bhd. for his insightful suggestions and guidance, without which the full-scale field measurement would not have been possible. The support rendered by Dr. Tee Bun Pin of Smart Sensing Technology Sdn. Bhd. in the installation of the in-pile instrumentation, including fibre optic cables and vibrating wire strain gauges, is highly appreciated.

AUTHORS' CONTRIBUTIONS

- **Chee Min Khoo:** Data collection, methodology, analysis, interpretation, writing.
- **Hisham Mohamad:** Conceptualisation, study design, and supervision. ■

REFERENCES

[1] Cham, W. M. (2007). *The response of piles to tunnelling*. MSc thesis, Imperial College, London.

[2] Couts, D. R., & Wang, J. (2000). Monitoring of reinforced concrete piles under horizontal and vertical loads due to tunnelling. In J. Zhao, N. Shirlaw, & R. Khrisnan (Eds.), *Tunnels and Underground Structures* (pp. 541-546).

[3] Herrenknecht, M., & Rehm, U. (2003). *Earth pressure balanced shield technology*. Internal lecture in Colorado School of Mine, USA.

[4] Jacobsz, S. W., Bowers, K. H., Moss, N. A., & Zanardo, G. (2005). The effects of tunnelling on piled structures on the CTRL. In *5th International Symposium on Geotechnical Aspects of Underground Construction in Soft Ground*, June 15-17, 2005, Amsterdam, Netherlands.

[5] Kaalberg, F. J., Teunissen, E. A. H., van Tol, A. F., & Bosch, J. W. (2005). Dutch research on the impact of shield tunnelling on pile foundations. In *5th International Symposium on Geotechnical Aspects of Underground Construction in Soft Ground,* June 15-17, 2005, Amsterdam, Netherlands.

[6] Kasper, T., & Meschke, G. (2004). A 3D finite element simulation model for TBM tunnelling in soft ground. *International Journal for Numerical and Analytical Methods in Geomechanics*, 28(14). 1441-1460.

[7] Khoo, C. M. (2024). *The transient effects of shield tunnelling on a loaded pile*. PhD thesis, Universiti Teknologi PETRONAS.

[8] Khoo, C. M., Mohamad, H., Tee, B. P., & Ghazali, M. F. (2024a). Field measurement of pile transient lateral response to advancing tunnel. In Yan et al. (eds.), *Tunnelling for a Better Life; Proceedings of the ITA-AITES World Tunnel Congress 2024 (WTC2024)*, April 19-25, -2024, Shenzhen, China. CRC Press: London, pp.2672-2680.

[9] Khoo, C. M., Mohamad, H., Beddelee, A. A. A. M., Thansirichaisree, P., Ghazali, M. F., & Mohd Nasir, M. Y. (2025), Effects of advancing tunnel on a loaded pile: numerical analysis and field measurements. *Journal of Rock Mechanics and Geotechnical Engineering*. In Press.

[10] Khoo, C. M., Mohamad, H., Mohd Nasir, M. Y., & Thansirichaisree, P. (2024b). Some insights into three-dimensional modelling of tunnel excavation. *International Journal of GEOMATE*. 27(120).

[11] Klar, A., Bennett, P. J., & Soga, K. (2006). Distributed strain measurement for pile foundations. In *Proceedings of the Institution of Civil Engineers, Geotechnical Engineering,* 159(3), 135-144.

[12] Lee, R. G., Turner, A. J., & Whitworth, L. J. (1994). Deformations caused by tunnelling beneath a piled structure. *In XIII ICSMFE*, New Delhi, India (pp. 873-878).

[13] Loganathan, N. (2016). Design charts: tunnelling-induced effects on adjacent pile foundation. In *Proceedings of 19th Southeast Asian Geotechnical Conference & 2nd AGSSEA Conference,* Kuala Lumpur, Malaysia (pp. 1125-1130).

[14] Mair, R. J. (1993). Unwin Memorial Lecture – Developments in geotechnical engineering research: application to tunnels and deep excavations. In *Proceedings of the Institution of Civil Engineers, Civil Engineering*, 97(1), 27-41.

[15] Mohamad, H., Soga, K., & Bennett P. J. (2009). Fibre optic installation techniques for pile instrumentation. In *Proceedings of the 17th International Conference on Soil Mechanics and Geotechnical Engineering: The Academia and Practice of Geotechnical Engineering*, IOS Press, 3, pp. 1873-1876.

[16] Mohamad, H., Bennett, P. J., Soga, K., Mair, R. J., & Bowers, K. (2010). Behaviour of an old masonry tunnel due to tunnelling-induced ground settlement. *Géotechnique*, 60(12), 927-938.

[17] Mohamad, H., Soga, K., Pellew, A., & Bennett, P. J. (2011). Performance monitoring of a secant piled wall using distributed fibre optic strain sensing. *Journal of Geotechnical and Geoenvironmental Engineering*, 137(12), 1236-1243.

[18] Mohamad, H, Soga, K., Bennet, P. J., Mair, R. J., & Lim, C. S. (2012). Monitoring twin tunnel interaction using distributed optical fibre strain measurements. *Journal of Geotechnical and Geoenvironmental Engineering*, 138, 957-967.

[19] Mohamad, H., Tee, B. P., Ang, K. A., & Chong, M. F. (2016). Characterizing anomalies in distributed strain measurements of cast-in-situ bored piles. *Jurnal Teknologi*, 78(8-5), 75-82.

[20] Mohamad, W., Bourgeois, E., Kouby, A. L., Szymkiewicz, F., Michalski, A., Branque, D., Berthoz, N., Soyez, L., Kreziak, C. (2022). Full scale study of pile response to EPBS tunnelling on a Grand Paris Express site. *Tunnelling and Underground Space Technology,* 124, 104492.

[21] Mollon, G., Dias, D., & Soubra, A. (2013). Probabilistic analyses of tunnelling-induced ground movements. *Acta Geotechnica,* 8. 181-199.

[22] Ohno, H., Naruse, H., Kurashima, T., & Nobiki, A. (2002). Application of Brillouin scattering-based distributed optical fibre strain sensor to actual concrete piles. *IEICE Transaction on Electronics E85*, 945-951.

[23] Pang, C. H., Yong, K. Y., Chow, Y. K., & Wang, J. (2005). Response of pile foundation subjected to shield tunnelling. In *5th International Symposium on Geotechnical Aspects of Underground Construction*, June 15-17, 2005, Amsterdam, Netherlands.

[24] Selemetas, D, Standing, R. J., & Mair, R. J. (2005). The response of full-scale piles to tunnelling. In *5th International Symposium on Geotechnical Aspects of Underground Construction in Soft Ground*, June 15-17, 2005, Amsterdam, Netherlands.

[25] Soga, K., Mohamad, H., & Bennett, P. J. (2008). Distributed fibre optics strain measurements for monitoring geotechnical structures. In *6th International Conference on Case Histories in Geotechnical Engineering* (Symposium in honour of Professor James K Mitchell), Arlington, USA.

[26] Tan, Y. C., Teh, W. S., & Gue, C. S. (2019). Special design considerations for underpinning system for existing structures due to tunnelling. In *Proceedings of ITA-AITES World Tunnel Congress 2019* (WTC2019), 3-9 May, 2019, Naples, Italy.

[27] Tee, B. P., Mohamad, H., Ang, K. A., & Chong, M.F. (2016). Load test performance of bored pile with distributed fibre optic strain sensing. In *Proceedings of 19th Southeast Asian Geotechnical Conference & 2nd AGSSEA Conference,* Kuala Lumpur, Malaysia (pp. 865-870).

[28] Tee, B. P., Rashid, A. S. A., Abdullah, R. A., Kassim, K. A., & Mohamad, H. (2017). Application of distributed fibre optic sensor in instrumented pile load test. *Asean Engineering Journal.*

[29] Teunissen, E. A. H., & Hutteman, M. (1998). Pile and surface settlement at full scale tests North/South Line metro. In *Proceedings of the World Tunnel Congress'98*, São Paulo, Brazil.

[30] Vermeer, P. A., Bonnier, P. G., & Möller, S. C. (2002). On a smart use of 3D-FEM in tunnelling. In *Proceeding of 8th International Symposium on Num. Models in Geomech–NUMOGVIII*, 361–366. Balkema, Rotterdam.

PROFILES

CHEE MIN KHOO holds a Bachelor's degree with First Class Honours from Universiti Teknologi Malaysia and both an MSc degree and PhD in Civil Engineering from Universiti Teknologi PETRONAS. With over 20 years of extensive experience, he is a recognised specialist in geotechnical and tunnel engineering, with expertise in consultancy and design management. He has published nearly 40 technical papers and received the prestigious Tan Sri Hj. Yusoff Prize in 2019, the highest recognition for outstanding civil engineering papers by corporate members of IEM.
Email address: khoocheemin@gmail.com

HISHAM MOHAMAD is the Chair of Civil & Environmental Engineering Department, Universiti Teknologi PETRONAS. He is the leading expert in Distributed Fibre Optic Sensing (DFOS) for infrastructure and structural health monitoring. His invention, Smart Geopipe (TRL-8) received multiple recognitions and as best innovative product by national and international bodies, including invited to showcase at the United Nations' COP28. At UTP, he founded Smart Infrastructure Modelling & Monitoring research centre and responsible for securing and managing multi-million ringgit industrial and consultancy projects.
Email address: hisham.mohamad@utp.edu.my

LIFE CYCLE ASSESSMENT OF PALM OIL WASTE BIOCHAR AS A PARTIAL CEMENT REPLACEMENT IN CONCRETE PRODUCTION IN MALAYSIA

Ashley Yiing Yi Chow[1*], Aan Mohammad Nusrat Aman[2], Anurita Selvarajoo[3]

Abstract

As the environmental impact of construction materials faces increased scrutiny, sustainable alternatives are garnering interest. Biochar emerged as a potential candidate for partially replacing cement in construction applications. Life cycle assessment (LCA) evaluates the environmental impacts of products, processes, and services throughout their life cycle, and identify environmental improvement opportunities. This study provides a comprehensive LCA of biochar produced from empty fruit bunches and palm kernel shells as a partial cement replacement, aiming to evaluate its environmental performance across various life cycle stages. The research includes five scenarios: 4% biochar from empty fruit bunches with pyrolysis at 500°C and 455°C, 4% biochar from palm kernel shells with pyrolysis at 500°C and 409°C, and without biochar used. This study has a cradle-to-gate approach, analysing the environmental impacts of biochar production, transportation, incorporation into cement, and the resulting concrete's life cycle. The LCA is conducted using OpenLCA software and the Tool for the Reduction and Assessment of Chemical and Other Environmental Impacts TRACI for life cycle impact assessment (LCIA). The study concludes that palm oil waste biochar as a partial cement replacement reduces greenhouse gas emissions, with 4% palm kernel shell biochar pyrolysed at 409°C showing the best results among all scenarios with the emissions of carbon dioxide gas lesser by 0.474kg CO2-Eq.

Received: *12 December, 2024*
Revised: *15 April, 2025*
Accepted: *28 May, 2025*

[1,2,3] Department of Civil Engineering, Faculty of Science and Engineering, University of Nottingham Malaysia, Selangor, Malaysia.

****Corresponding author:***
ashleyyiing27@gmail.com

DOI: *https://10.54552/v86i2.280*

Keywords:
Biochar, Cement production, Cement replacement, Empty fruit bunch, Life cycle assessment, Palm kernel shell

List of Notations

LCA	is the life cycle assessment	*GWP*	is the global warming potential
LCI	is the life cycle inventory	*AP*	is the acidification potential
LCIA	is the life cycle impact assessment	*EP*	is the eutrophication
CO_2	is the carbon dioxide	*PO*	is the photochemical oxidation
EFB	is the empty fruit bunch	*HH*	is the human health
PKS	is the palm kernel shell		

1.0 INTRODUCTION

Concrete is one of the most popular materials in the construction industry (Ding *et al.,* 2016). To reduce carbon dioxide (CO_2) emissions during concrete production, the industry is exploring the use of palm oil waste biochar as a partial replacement for cement. The cement industry is a significant source of CO_2 emissions, releasing about 900 kg of CO_2 per ton of cement produced (Benhelal *et al.,* 2013). As cement is a key component in concrete, its production indirectly contributes to CO_2 emissions during concrete production.

In 2019, global palm oil production exceeded 74.8 million tonnes, accounting for roughly 41.37% of the world's vegetable oil supply (Ritchie and Roser, 2021). Palm oil is used in various sectors, including food (68%), consumer goods (27%), and bio-energies (5%) (Ritchie, 2020). The integrated biorefinery concept in the palm oil industry shows promise by using oil palm biomass to produce bio-based products (Mora-Villalobos *et al.,* 2023). Activated carbons, which are effective at capturing CO_2, can be derived from biochar, an inexpensive source. Oil palm biomass, with a carbon content ranging from 42.7% to 57.9%, including 3.5–27% fixed carbon, is a viable source for biochar production (Zakaria *et al.,* 2023). Therefore, using palm oil waste biochar as a partial cement replacement in concrete production is a promising sustainability strategy.

Traditional concrete production methods are associated with significant carbon emissions and environmental concerns, contributing to global climate change and environmental degradation. Concrete production's high carbon dioxide emissions are mainly due to the energy-intensive cement production process and the transportation of raw materials. Additionally, disposing of palm oil waste causes environmental issues, including air and water pollution, soil degradation, and habitat destruction. The transportation of palm oil waste biochar from rural production areas to urban concrete production facilities also contributes to carbon emissions, which can offset the environmental benefits of using biochar.

To address these challenges, there needs to be a shift towards lower carbon emissions in concrete production. Integrating palm oil waste biochar as a cement substitute can help to reduce carbon emissions from both concrete production and waste management. However, challenges such as optimising biochar properties, ensuring compatibility with existing concrete mixtures, and assessing the environmental

impact of biochar incorporation must be addressed (Guspa *et al.,* 2018). This research aims to evaluate the feasibility and environmental implications of using palm oil waste biochar as a partial cement replacement in concrete production, focusing on reducing carbon emissions and managing waste in the construction industry.

The study aims to conduct a comprehensive life cycle assessment (LCA) of palm oil waste biochar as a partial cement replacement in concrete production in Malaysia. It evaluates the environmental impacts associated with the entire lifecycle of palm oil waste biochar, from production to its incorporation into concrete mixes. The study also aims to provide recommendations for optimising the environmental performance of palm oil waste biochar as a cement replacement and promote its use in concrete production in Malaysia. The intended recipients of this research include construction engineers, cement and concrete producers, and material suppliers and manufacturers.

Conducting a LCA of palm oil waste biochar as a partial cement replacement in concrete production in Malaysia is significant as it addresses critical environmental and economic challenges while promoting sustainable development in the construction industry. By assessing the entire life cycle of palm oil waste biochar, from production to incorporation into concrete mixes, the LCA can quantify the environmental benefits of using biochar as a partial cement replacement. This includes impacts such as global warming potential (GWP), acidification potential (AP), eutrophication (EP), photochemical oxidation (PO), and human health (HH) compared to traditional concrete production methods. Understanding these impacts is crucial for mitigating environmental degradation and advancing sustainable practices.

2.0 LIFE CYCLE ASSESSMENT CONCEPT

To guide the utilisation of palm oil waste biochar as cement replacement among stakeholders in the construction industry, it is essential to conduct a Life Cycle Assessment (LCA) study on the biochar in concrete production. These outcomes encompass global warming potential (GWP), acidification potential (AP), eutrophication (EP), photochemical oxidation (PO), and human health (HH).

LCA studies necessitate a collection of data to quantify the extent of these outcomes, known as the life cycle inventory (LCI). Each study focuses on distinct stages of a material's lifespan, defined by system boundaries. These delineations specify different phases, as for "cradle-to-gate," which covers the extraction of raw materials up to production. Whereas for "cradle-to-grave," encompasses extraction for production to the end of the material's lifespan. Additionally, "cradle-to-cradle" denotes extraction for production till the material is recycled and reused as raw material for production again. However, in this study, cradle-to-gate is only be considered.

2.1 LCA on Biochar

Biochar, a carbon-rich material produced through the thermal decomposition of organic biomass, has gained significant interest for its diverse applications in agriculture, environmental restoration, and carbon sequestration (Lehmann *et al.,* 2015). This study delves into biochar's concept, production methods, properties, and its role in addressing environmental challenges, with a particular focus on palm oil waste biochar. Biochar is created through pyrolysis, where biomass is heated in a low-oxygen environment. This ancient technique, used historically to enhance soil fertility, is now recognised for its broader potential. Biochar can be derived from various biomass sources like crop residues, wood chips, and organic waste. The pyrolysis process, involving temperatures from 350°C to 700°C, converts volatile organic compounds into gases, leaving a carbon-dense residue. The resulting biochar's properties—such as high permeability, large surface area, and high carbon content—depend on factors like feedstock type, pyrolysis conditions, and post-production treatments. These properties endow biochar with excellent adsorption capacity, water retention ability, and soil enhancement capabilities. Notably, biochar is stable in soil, potentially sequestering carbon for centuries to millennia (Li *et al.,* 2023).

Palm oil waste biochar, a byproduct of the palm oil industry, represents a sustainable innovation in waste management and environmental conservation. Amid growing concerns about waste disposal and climate change, palm oil waste biochar offers a solution that addresses waste management, carbon sequestration, and soil enrichment. In agriculture, it enhances soil quality by improving fertility, water retention, and nutrient availability, reducing the need for chemical fertilisers. Its porous nature allows it to store water and essential nutrients, creating optimal conditions for plant growth. Additionally, its carbon sequestration potential contributes to reducing greenhouse gas emissions, aligning with global climate change mitigation efforts. Beyond agriculture, palm oil waste biochar is used in wastewater treatment, renewable energy production, and carbon capture technologies, highlighting its versatility and importance in sustainable development. The use of biochar, including palm oil waste biochar, offers numerous benefits such as soil improvement, waste valorisation, and carbon sequestration (Guspa *et al.,* 2018). By converting organic waste into a valuable resource, biochar production supports circular economy principles and reduces environmental pollution. However, challenges like feedstock availability, scalability, and market acceptance need to be addressed to fully realise biochar technology's potential.

2.2 LCA on Concrete

Concrete is fundamental to modern construction, used globally due to its strength, durability, and versatility (Nilimaa, 2023). It is essential for various infrastructure projects, including skyscrapers, highways, and dams. Despite its benefits, concrete's environmental impact necessitates an evaluation of its sustainability using Life Cycle Assessment (LCA) methodologies. Concrete is made from aggregates (sand and gravel), cement, and water, forming a solid matrix through hydration. This composition makes it durable, fire-resistant, and cost-effective, contributing to its widespread use. It is because concrete production has significant environmental consequences, primarily from raw material extraction and processing, especially cement (Nilimaa, J. 2023). Cement production involves the calcination of limestone, which

is energy-intensive and emits substantial carbon dioxide (CO_2). Additionally, extracting aggregates disturbs land and requires energy-intensive processing, further impacting the environment. LCA of concrete considers factors affecting its sustainability, including raw material choices, production methods, transportation, and waste management. Using supplementary cementitious materials like fly ash, slag, and soil can reduce the carbon footprint by partially substituting cement. Innovations in concrete mix design, such as recycled aggregates and optimised cement content, can also significantly lower environmental impacts without sacrificing performance.

3.0 LCA METHODOLOGY

The LCA for materials adhere to the guidelines set forth in ISO 14040 and ISO 14044 standards. These standards outline LCA as the systematic gathering and evaluation of inputs, outputs, and potential environmental repercussions associated with a product system. The LCA process comprises four distinct stages: goal and scope definition, life cycle inventory, impact assessment, and interpretation, as depicted in Figure 1 below.

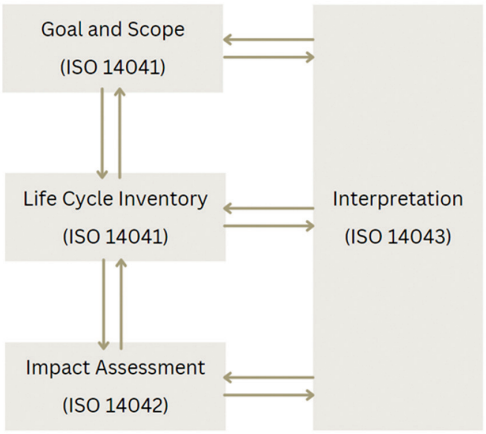

Figure 1: Life cycle assessment framework

3.1 Life Cycle Inventory Analysis

The second stage of LCA comprises compiling and quantifying data regarding the product's inputs and outputs throughout its life cycle or a specific process. All gathered data are shown in Table 1 Life Cycle Inventory Data. This inventory data is inputted into the OpenLCA software to represent the inputs and outputs of individual processes. Datas are collected from studies has been incorporated into this research, as displayed in Table 1. The utilisation of data from all the sources aims to ensure the completeness of the LCI data, thereby enabling a more dependable assessment for the developed scenarios. The emissions from diesel and from EFB and PKS belongs to midpoint category while the emissions from cement and concrete belongs to endpoint category.

3.2 Life Cycle Impact Assessment

The Environmental Impact Assessment (LCIA) method employed in this study is the Tool for the Reduction and Assessment of Chemical and Other Environmental Impacts (TRACI) method. TRACI aims to measure and assess the possible environmental impacts associated with various

Table 1: Life cycle inventory data

Inventory	Value	Unit	Reference
Average transportation distance			
From Mill to Biochar Production Plant	69.94	km	
From Biochar Production Plant to Concrete Batching Plant	30.63	km	
From Cement Batching Plant to Concrete Batching Plant	31.33	km	
Transportation by Truck			
Load	7.5-12	t	
Diesel Consumption	0.00667645	MJ/km	(Arshad, 2019)
Emissions from diesel			
CO2	5.79495134	kg/MJ	(Mustapa & Bekhet, 2016)
CO	0.003889	kg/MJ	(Anon, 1996)
HC	0.0009723	kg/MJ	(Anon, 1996)
NO	0.005004	kg/MJ	(Anon, 1996)
EFB LCI			
Electricity	92.9824564	kWh/kg	(Nasrin *et al.*, 2017)
Drying	278.947368	MJ/kg	(Nasrin *et al.*, 2017)
Emissions from EFB			
CO	0.00151047	kg	(Chan *et al.*, 2016)
CO2	0.01428132	kg	(Chan *et al.*, 2016)
CH4	0.00305622	kg	(Chan *et al.*, 2016)
PKS LCI			
Electricity	38	kWh/kg	(Rusdianasari *et al.*, 2022)
Drying	1200	kWh/kg	(Rusdianasari *et al.*, 2022)
Emissions from PKS			
CO	0.0227454	kg	(Qureshi *et al.*, 2022)
CO2	0.02454545	kg	(Qureshi *et al.*, 2022)
CH4	0.0348	kg	(Qureshi *et al.*, 2022)
Cement LCI			
Limestone	65	%	(Sutar *et al.*, 2021)
Clay	20	%	(Sutar *et al.*, 2021)
Shale	10	%	(Sutar *et al.*, 2021)
Gypsum	5	%	(Sutar *et al.*, 2021)
Emissions from Cement			
CO2	0.9	kg	(Ali *et al.*, 2011)
NO2	3000	mg	(Ali *et al.*, 2011)
NO	3000	mg	(Ali *et al.*, 2011)
O2	0.42	kg	(Ali *et al.*, 2011)
Concrete LCI			
Cement	15	%	
Water	15	%	
Aggregate	70	%	
Emissions from Concrete			
CO2	0.93	kg	(Keegan R., 2020)
CO	0.00021	kg	(Gursel & Ostertag, 2016)
NO2	0.00136	kg	(Gursel & Ostertag, 2016)
NO	0.00136	kg	(Gursel & Ostertag, 2016)
NMVOCs	0.00024	kg	(Gursel & Ostertag, 2016)
SO2	0.00199	kg	(Gursel & Ostertag, 2016)

human activities, products, and processes, particularly focusing on chemical and other pollutants that may contribute to environmental degradation. It provides a framework for assessing a wide range of environmental impact categories. TRACI methodology considers both midpoint and endpoint impact categories. Midpoint impact categories represent specific environmental stressors or pollutants, such as emissions of greenhouse gases or air pollutants. Endpoint impact categories, on the other hand, reflect broader environmental outcomes, such as human health impacts or ecosystem damage. Table 2 below shows the unit of each TRACI environmental impact categories.

Table 2: TRACI environmental impact categories

Indicator	Unit
Acidification Potential (AP)	Moles of H+-Eq
Eutrophication Potential (EP)	kg N
Global Warming Potential (GWP)	kg CO2-Eq
Photochemical Oxidation (PO)	kg NOx-Eq
Human Health (HH) (respiratory effects, average)	kg PM2.5-Eq

3.3 Modelled Scenarios

As part of this research, five scenarios will be conducted and compared which includes use of 4% of biochar from empty fruit bunch with pyrolysis process at 500°C and 455°C, 4% of biochar from palm kernel shell with pyrolysis process at 500°C and 409°C, and without biochar used. The evaluation of life cycle assessment (LCA) in this study is conducted based on the process shown in Figure 2.1 and Figure 2.2.

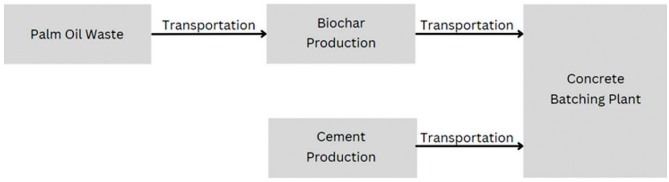

Figure 2.1: Modelled scenario with biochar

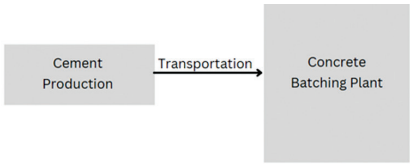

Figure 2.2: Modelled scenario without biochar

Table 3 shows the locations of palm oil mills, biochar plants, cement production plants, and concrete batching plants are chosen and taken the average distance from one point to another point.

By averaging the distance of all the locations, Table 4 presents the average distances for palm oil mill to biochar plant, biochar plant to concrete batching plant, and cement production plant to concrete batching plant. The average distance is utilised in the LCA investigation conducted in this study.

4.0 SCENARIOS OVERVIEW

Figure 3.1 to Figure 3.5 show the five scenarios that have been developed in OpenLCA software to generate environmental impact assessment. In total of 5 scenarios will be conducted and compared which includes use of 4% of biochar from empty fruit bunch with pyrolysis process at 500°C and 455°C, 4% of biochar from palm kernel shell with pyrolysis process at 500°C and 409°C, and without biochar used.

Table 3: Locations of palm oil mills, biochar plants, cement production plants, and concrete batching plants

Location	Address
Palm oil mill	Jalan Tok Mujir, Kampung Sungai Buaya, 42700 Banting Selangor
Palm oil mill	Batu 37, Jalan Raja Musa, 45600 Batang Berjuntai Selangor
Palm oil mill	Batu 24, Jalan Kuala Selangor, 47000 Sungai Buloh Selangor
Palm oil mill	LOT 334 Jalan Kepong,MUKIM, 45600 Batang Berjuntai Selangor
Biochar plant	Stesen Penyelidikan Usahama MPOB-UKM, Kajang Selangor
Biochar plant	C-01-11, Jalan Sri Kenari 12, Taman Sri Kenari, 43000 Kajang Selangor
Biochar plant	8942, Jalan Telok Gong, Kampung Telok Gong, 42000 Klang Selangor
Biochar plant	Jalan SP 2/1, Taman Serdang Perdana, Seri Kembangan Selangor
Cement production plant	8, Jalan Putra Prima 5/12, 47130 Puchong, Selangor
Cement production plant	207, Jalan Subang 6, Taman Perindustrian Subang, 47500 Subang Selangor
Cement production plant	No. 2, Jalan Kilang 51/206, Pjs 51, 46050 Petaling Jaya, Selangor
Cement production plant	Kawasan Industri Kampung Jaya Sungai Buluh, 47000 Sungai Buloh,Selangor
Concrete batching plant	Jalan Dua, Chan Sow Lin, 55200 Kuala Lumpur
Concrete batching plant	17, Jalan Tiga, Chan Sow Lin, 55200 Kuala Lumpur
Concrete batching plant	1558, Jalan Kusta, Kawasan Industri Kampung Jaya, 47000 Sungai Buloh, Selangor
Concrete batching plant	Jalan Perindustrian Balakong, Taman Balakong Jaya, 43000 Seri Kembangan Selangor

Table 4: Average distance for each route

Route	Average Distance (km)
Palm Oil Mill to Biochar Plant	69.94
Biochar Plant to Concrete Batching Plant	30.63
Cement Production Plant to Concrete Batching Plant	31.33

For scenarios with biochar used, the process starts with transportation of palm oil waste from palm mills and transported to biochar mill to undergo pyrolysis process to produce biochar. Different temperatures are taken into account during pyrolysis process as different temperatures of pyrolysis would produce different amount of greenhouse gases and different amount of energy required. The biochar produced will then be transported to concrete batching plant to act as partial cement replacement during concrete production. Cement production will take place at cement production plant and transport to concrete batching plant for final stage. During concrete production, 4% of cement will be replaced with biochar during concrete production to produce concrete with lower greenhouse gas emissions.

As for scenario without the use of biochar, the normal concrete production is adhered by starting with concrete production at concrete production plant. The produced concrete

will then be transported to concrete batching plant to produce concrete. Results are obtained for making better comparison of impact categories of global warming potential (GWP), acidification potential (AP), eutrophication (EP), photochemical oxidation (PO), and human health (HH) between used of biochar and without biochar.

4.1 TRACI Analysis

With the 5 scenarios modelled, two different comparisons are produced which is with and without transportation considered to provide a more detail results. With this comparison, impact of materials production and impact due to transportation can be shown clearly. Table 5.1 and Table 5.2 summarise the TRACI analysis results of each impact category with all 5 scenarios. Figure 4.1 and Figure 4.2 show the relative results with and without transportation.

Each impact categories assessed by TRACI is shown below for results without transportation in order to identify clearly how each scenario performs. Global Warming Potential (GWP) assess the environmental impact of greenhouse gas emissions relative to carbon dioxide (CO_2), Acidification Potential (AP) evaluates emissions of sulphur dioxide (SO_2) and nitrogen oxides (NO_x), Eutrophication Potential (EP) evaluates capacity to induce eutrophication, characterised by the influx of surplus nutrients including nitrogen and phosphorus, Photochemical Oxidation (PO) evaluates reaction of pollutants including nitrogen oxides (NO_x) and volatile organic compounds (VOCs) under sunlight, and Human Health (HH) (respiratory effects, average) assess the potential health impacts of air pollutants comprising particulate matter (PM), ozone (O_2), nitrogen dioxide (NO_2), and sulphur dioxide (SO_2).

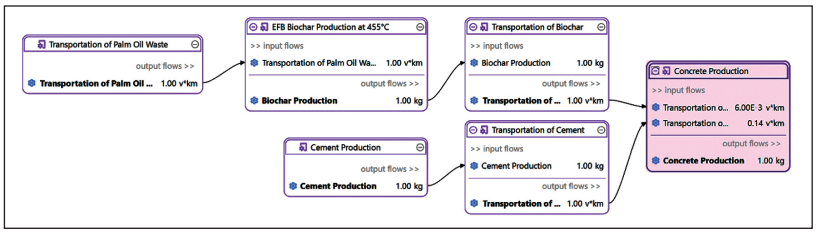

Figure 3.1: OpenLCA model: scenario of 4% empty fruit bunch at 455°C pyrolysis

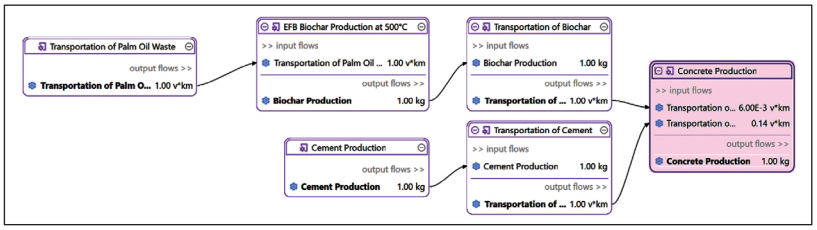

Figure 3.2: OpenLCA model: scenario of 4% empty fruit bunch at 500°C pyrolysis

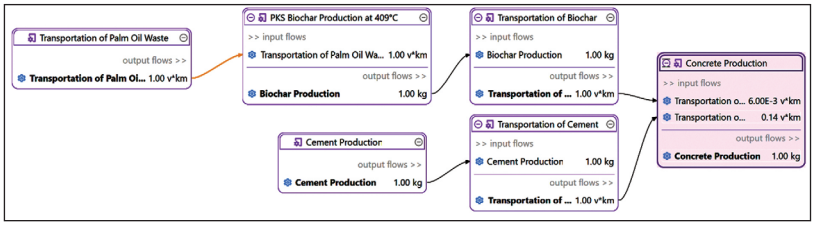

Figure 3.3: OpenLCA model: scenario of 4% palm kernel shell at 409°C pyrolysis

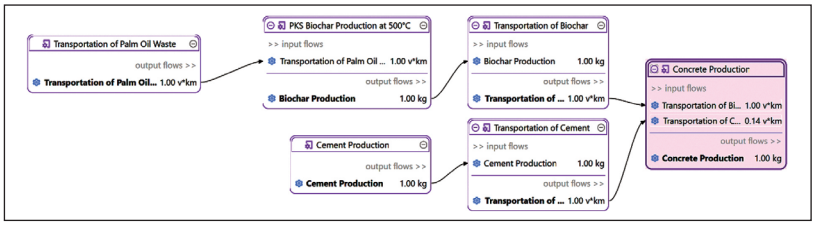

Figure 3.4: OpenLCA model: scenario of 4% palm kernel shell at 500°C pyrolysis

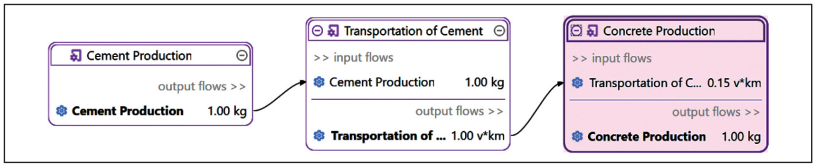

Figure 3.5: OpenLCA model: scenario of 100% cement

5.0 RESULTS ANALYSIS

Based on Figure 4.1, by setting 100% to the maximum result for each indicator, normal concrete production as the control study shows 100% on all impact categories. This clearly shows that the use of biochar as partial cement replacement indeed lowers the impact of greenhouse gas emissions during concrete production. For acidification potential, the use of empty fruit bunch biochar for both 455°C and 500°C produced a result of 80.65% and 87.76% respectively whereas for the use of palm kernel shell biochar for both 409°C and 500°C produced a result of 70.87% and 87.76% respectively. The greatest difference in percentage is between normal concrete production and the use of palm kernel shell biochar for both 409°C with difference of 29.17%.

Following the environmental impact of eutrophication potential, normal cement production remains 100% while other four scenarios ranging in between 60% to 80%. The use of empty fruit bunch biochar for both 455°C and 500°C shows a result of 70.42% and 75.61% respectively while the use of palm kernel shell biochar for both 409°C and 500°C shows a result of 65.21% and 75.61% respectively. The results for global warming potential and photochemical oxidation for scenarios with biochar used performs around the same with a small difference within 3%. Assessing human health impact, both biochar with 500°C has a percentage of 94.94% while the use of empty fruit bunch biochar for 455°C has a percentage of 86.69% and the use of palm kernel shell biochar for 409°C has a percentage of 74.21%.

Table 5.1: TRACI analysis without transportation

	Concrete Production	EFB Concrete Production at 455°C	EFB Concrete Production at 500°C	PKS Concrete Production at 409°C	PKS Concrete Production at 500°C	Unit
AP	1.979e-1	1.596e-1	1.736e-1	1.402e-1	1.736e-1	Moles of H+-Eq
EP	1.075e-4	7.538e-5	8.094e-5	6.980e-5	8.094e-5	kg N
GWP	1.382e+0	9.894e-1	1.073e+0	9.081e-1	1.078e+0	kg CO2-Eq
PO	2.420e-3	1.705e-3	1.831e-3	1.580e-3	1.833e-3	kg NOx-Eq
HH	5.906e-4	5.120e-4	5.607e-4	4.383e-4	5.607e-4	kg PM2.5-Eq

Table 5.2: TRACI analysis with transportation

	Concrete Production	EFB Concrete Production at 455°C	EFB Concrete Production at 500°C	PKS Concrete Production at 409°C	PKS Concrete Production at 500°C	Unit
AP	1.979e-1	1.837e-1	1.978e-1	1.644e-1	1.978e-1	Moles of H+-Eq
EP	1.075e-4	1.021e-4	1.076e-4	9.651e-5	1.076e-4	kg N
GWP	1.382e+0	1.318e+0	1.401e+0	1.240e+0	1.410e+0	kg CO2-Eq
PO	2.420e-3	2.308e-3	2.434e-3	2.185e-3	2.438e-3	kg NOx-Eq
HH	5.906e-4	5.397e-4	5.884e-4	4.659e-4	5.884e-4	kg PM2.5-Eq

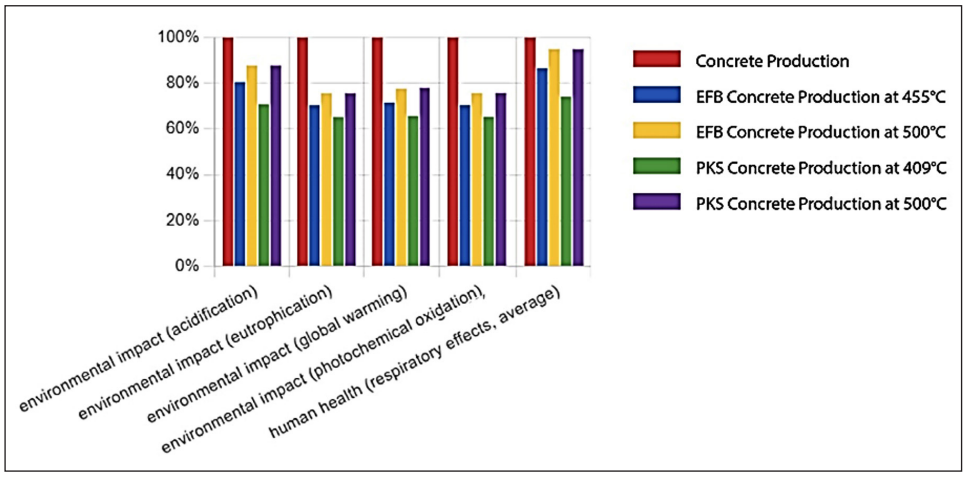

Figure 4.1: Relative results without transportation

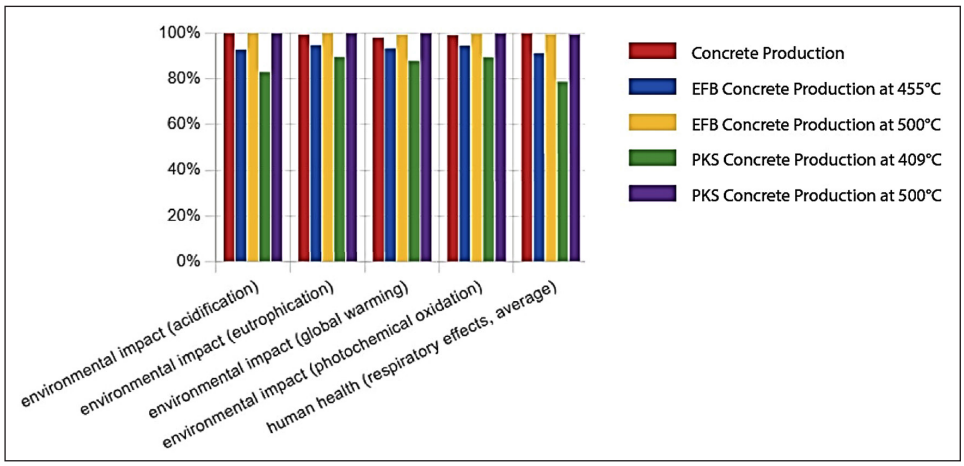

Figure 4.2: Relative results with transportation

Based on the results produced, the use of palm kernel shell biochar for 409°C shows the lowest impact of greenhouse gases emissions among all other scenarios with 29.16% lower for acidification potential, 35.07% lower for eutrophication potential, 34.3% lower for global warming potential, 34.71% lower for photochemical oxidation, and 25.79% lower for human health with transportation not taken into consideration compared with normal concrete production. With transportation taken into consideration, the impact of greenhouse gases emissions is lowered by 16.93% for acidification potential, 10.22% for eutrophication potential, 10.27% for global warming potential, 9.71% for photochemical oxidation, and 21.11% for human health compared with normal concrete production.

6.0 OVERALL IMPACT

Based on Table 5.1, the amount of each impact categories for all five scenarios are shown side by side for easier comparison. Based on the result, global warming potential shows the higher impact among all other categories. This can be explained by the environmental impact of greenhouse gas emissions relative to CO_2 is the highest among all other greenhouse gases. With 1kg of concrete produced, 1.382kg CO2-Eq is produced for normal concrete production where the CO_2 emissions includes cement production. As for the other four scenarios, the emission of CO_2 produced is 0.99kg CO2-Eq, 1.073kg CO2-Eq, 0.908kg CO2-Eq, and 1.078kg CO2-Eq respectively.

The subsequent greater impact would be acidification potential. All five scenarios ranging from 1.403e-1 moles of H+-Eq for the use of empty fruit bunch biochar for 455°C to 1.978e-1 moles of H+-Eq for normal concrete production. The other three impact categories which includes eutrophication potential, photochemical oxidation, and human health impact has very small value as shown in Table 5.1.

By comparing Table 5.1 and Table 5.2, it clearly shows that the impact of transportation towards the impact categories is great. The value for all four use of biochar scenarios increases significantly. This is mainly due to the transportation of palm oil waste from palm oil mill to biochar plant has an average of 69.94km where the emissions of greenhouse gases from truck. The difference of GWP values between with and without transportation for the use of empty fruit bunch biochar for 455°C is 0.329kg CO2-Eq and for 500°C is 0.328kg CO2-Eq and for the use of palm kernel shell biochar for both 409°C and 500°C is 0.332kg CO2-Eq. The difference of AP values between with and without transportation for the use of empty fruit bunch biochar for 455°C is 0.241 moles of H+-Eq and for 500°C is 0.242 moles of H+-Eq and for the use of palm kernel shell biochar for both 409°C is 0.242 moles of H+-Eq and for 500°C is 0.242 moles of H+-Eq.

7.0 FUTURE RECOMMENDATIONS

Future research studies on biochar should focus areas that are able to maximise its potential and address existing gaps including investigation on the suitability of diverse biomass sources, including agricultural residues, municipal waste, and industrial byproducts, to produce biochar with tailored properties for specific applications. Furthermore, enhancement on pyrolysis process by studying the effects of varying pyrolysis conditions (temperature, heating rate, duration) on biochar's physical, chemical, and structural properties to optimise its performance in different uses. Study of soil-biochar interactions by conducting long-term field studies to understand biochar's impact on soil health, microbial activity, nutrient cycling, and crop productivity across different soil types and climates. Moreover, study of the efficiency of carbon sequestration by quantifying biochar's long-term carbon storage potential and its role in reducing greenhouse gas emissions, including its stability and degradation rates in various environments. Additionally, explore biochar's effectiveness in wastewater treatment, contaminant removal, and its potential in renewable energy systems, such as bioenergy production and carbon capture technologies and assess the economic feasibility, scalability, and environmental impacts of biochar production and application through lifecycle assessments (LCA) and cost-benefit analyses. Investigation of potential risks associated with biochar, such as the presence of heavy metals or polycyclic aromatic hydrocarbons (PAHs), and develop safe production and application guidelines and research on strategies to integrate biochar production into circular economy models, focusing on waste valorisation and resource efficiency. By addressing these research areas, the scientific community can unlock the full potential of biochar as a sustainable solution for agriculture, environmental management, and climate change mitigation.

8.0 CONCLUSIONS

The assessment on the results produced from OpenLCA software for the five modelled scenarios, palm oil waste biochar as partial cement replacement in concrete production does shows lower impact on all categories. With the results produced, it is able to identify that palm kernel shell biochar with 409°C shows the best results among all other scenarios. However, due to incorporation of transportation, the effect of biochar as partial cement replacement is unable to perform a better result as expected. Hence, more detail study can be initiated in future to resolve the issue caused by taking account of transportation. Overall, these conclusions align with the aim of implementing palm oil waste biochar as partial cement replacement in concrete production. Justifications provided adhere to the study's objectives, encouraging the use of palm oil waste biochar in the Malaysian construction industry.

ACKNOWLEDGEMENT

Sincere appreciation to colleagues, technical staff and the University of Nottingham Malaysia for supporting the study with necessary resources. ■

REFERENCES

[1] Ali, M.B., Saidur, R., & Hossain, M.S. (2011). A review on emission analysis in cement industries. *Renewable and Sustainable Energy Reviews. 15(5),* pp.2252–2261.

[2] Anon (1996). Arrangement of Regulations Part I-Preliminary Regulation 1. Citation and commencement. Regulation 2. Interpretation. Part II-Control of diesel engine on motor vehicle. Regulation 3. Application of Part II. Regulation 4. Restriction on installation or replacing of engine system. Regulation 5. Application of regulation 4.

[3] Arshad, F. (2019). Energy consumption during transportation along the palm oil supply chain in Malaysia. *Journal of Oil Palm Research, 31 (4),* p. 641-650

[4] Benhelal, E., Zahedi, G., Shamsaei, E., & Bahadori, A. (2013). Global strategies and potentials to curb CO2 emissions in cement industry. *Journal of Cleaner Production 51,* pp.142–161.

[5] Chan, Y.H., Tan, R.R., Yusup, S., Lam, H.L., & Quitain, A.T. (2016). Comparative life cycle assessment (LCA) of bio-oil production from fast pyrolysis and hydrothermal liquefaction of oil palm empty fruit bunch (EFB). *Clean Technologies and Environmental Policy. 18(6),* pp.1759–1768.

[6] Ding, T., Xiao, J., & Tam, V.W.Y. (2016). A closed-loop life cycle assessment of recycled aggregate concrete utilization in China. *Waste Management, 56,* pp.367–375.

[7] Gupta, S., Kua, H. W., & Low, C. Y. (2018). Use of biochar as carbon sequestering additive in cement mortar. *Cement and Concrete Composites, 87,* 110-129.

[8] Gursel, A.P., & Ostertag, C.P. (2016). Impact of Singapore's importers on life-cycle assessment of concrete. *Journal of Cleaner Production. 118,* pp.140–150.

[9] Ramsden, K. (2020). *Cement and Concrete: The Environmental Impact.* Access via https://psci.princeton.edu/tips/2020/11/3/cement-and-concrete-the-environmental-impact

[10] Lehmann, J., & Joseph, S. (2015). *Biochar for Environmental Management: Science, Technology, and Implementation.* 2nd Edition. Routledge.

[11] Li, S., & Tasnady, D. (2023). Biochar for Soil Carbon Sequestration: Current Knowledge, Mechanisms, and Future Perspectives. *C- Journal of Carbon Research, 9(3),* 67

[12] Mora-Villalobos, J.A., Aguilar, F., Carballo-Arce, A.F., Vega-Baudrit, J.R., Trimino-Vazquez, H., Villegas-Peñaranda, L.R., Stöbener, A., Eixenberger, D., Bubenheim, P., Sandoval-Barrantes, M., & Liese, A. 2023. Tropical agroindustrial biowaste revalorization through integrative biorefineries—review part I: coffee and palm oil by-products. *Biomass Conversion and Biorefinery. 13(2),* pp.1469–1487.

[13] Mustapa, S.I., & Bekhet, H.A. (2016). Analysis of CO2 emissions reduction in the Malaysian transportation sector: An optimisation approach. *Energy Policy, 89,* pp.171–183.

[14] Nasrin, A.B., Vijaya, S., Loh, S.K., Astimar, A.A., & Lim, W.S. (2017). Quality compliance and environmental impact assessment of commercial empty fruit bunch (EFB) pellet fuel in Malaysia. *Journal of Oil Palm Research. 29(4),* pp.570–578.

[15] Nilimaa, J. (2023). Smart Materials and Technologies for Sustainable Concrete Construction. *Developments in the Built Environment, 15,100177.* https://doi.org/10.1016/j.dibe.2023.100177

[16] Qureshi, K.M., Kay Lup, A.N., Khan, S., Abnisa, F., & Daud, W.M.A.W. (2022). Pyrolysis of palm kernel shell using screw-assisted fluidization: effect of heating rate. Brazilian *Journal of Chemical Engineering. 39(3),* pp.619–629.

[17] Ritchie, H. (2020). Palm Oil.

[18] Ritchie, H. and Roser, M. (2021). Palm Oil - Our world in data.

[19] Rusdianasari, Utarina, L., Kalsum, L., Wulandari, D., & Bow, Y. (2022). Environmental Potential Impact on Biofuel Production from Thermal Cracking of Palm Shell Using Life Cycle Assessment. *Journal of Ecological Engineering. 23(12),* pp.61–67.

[20] Sutar, S.N., Patil, P.V., Chavan, R.V., & Maske, M.M. (2021). Study and Review of Ordinary Portland Cement. *ASEAN Journal of Science and Engineering. 1(3),* pp.153–160.

[21] Zakaria, M.R., Ahmad Farid, M.A., Andou, Y., Ramli, I., & Hassan, M.A. (2023). Production of biochar and activated carbon from oil palm biomass: Current status, prospects, and challenges. *Industrial Crops and Products. 199.*

PROFILES

ASHLEY YIING YI CHOW is a Project Engineer specialising in civil engineering, with a focus on building and infrastructure projects. She holds a Master's degree in Civil Engineering (2024) from the University of Nottingham Malaysia, where her research investigated sustainable construction materials, particularly "biocharcoal production and its application as a cement replacement" to promote renewable resource utilisation. With practical engineering expertise, she is committed to advancing sustainable infrastructure development.
Email address: ashleyyiing27@gmail.com

AAN MOHAMMAD NUSRAT AMAN holds a PhD in Sustainable Building Materials from the University of Nottingham Malaysia, where she also earned her Bachelor's degree. Her research focused on using biochar from palm oil waste as a supplementary cementitious material. Her work contributes to sustainable construction and waste valorisation from the palm oil industry, and further environmental impact.
Email address: aan.mohammad@outlook.com

ANURITA SELVARAJOO is an Associate Professor in Civil Engineering at the University of Nottingham Malaysia. She holds a B.Eng. (Hons) in Civil Engineering (Environmental) from Universiti Teknologi Malaysia (2006) and a Ph.D. in Fuels and Sustainability from the University of Nottingham Malaysia (2013). Her research focuses on biomass and biochar, particularly through pyrolysis for applications in energy, water and wastewater treatment, soil remediation, and climate change mitigation. She also works on natural coagulants for agricultural wastewater and enhanced landfill mining. She has published over 70 works, including journal papers, conference proceedings, and book chapters. She is an affiliate of the Young Scientists Network–Academy of Sciences Malaysia (YSN-ASM), a registered Professional Technologist with MBOT, and a Graduate Engineer with BEM.
Email address: anu_rita83@yahoo.com

MANUSCRIPT PREPARATION GUIDELINES FOR IEM JOURNAL AUTHORS

The aim of publishing the Journal of the Institution of Engineers Malaysia (or IEM Journal) is to promote the advancement of science, engineering, and technology; disseminate new and current knowledge; share novel findings among practising engineers, researchers and other interested colleagues. Hence, the IEM Journal covers a wide range of practical and diversified engineering disciplines, including publishing papers on any subjects relevant to the engineering and technology of today. As in other journals, all paper submissions to the IEM journal will be peer-reviewed by professionals.

Submission of a contribution is taken to manifest the fact that the submission has not been submitted, accepted, published, or copyrighted elsewhere. To avoid publication delays, please send all manuscripts to the Editor (via the Online Journal Submission) and observe the following guidelines. Each paper is independently peer-reviewed.

Types of Papers

IEM Journal will accept any submissions that fall within the three types of papers shown below:

- **Research Paper**

Significant research and development or applications in any field of engineering and/or technology. Submissions should be about 8-14 pages.

- **Review Paper**

Articles which summarises the state-of-the-art of a specific area of research. Submissions should be about 10-20 pages.

- **Brief Paper**

A concise description of new technical concepts or applications within the scope of the journal. Submission should be about 4 pages

Together with the paper submission, at least four (4) reviewers complete with their contact details (official postal and email address, and telephone number) are to be proposed by authors. Reviewers should be the experts in their research areas.

Plagiarism Policy

IEM Journal strictly prohibits any form of Plagiarism.

If the manuscript has been presented, published, or submitted for publication elsewhere, please inform the Editor. Our primary objective is to publish technical materials not available elsewhere.

Format and Elements of Submitted Texts

a) Initial Submission

For initial submission and reviewing, ALL papers are accepted regardless of the formatting used.

b) Final Submission

Upon final submission of paper, authors are required to follow the manuscript instruction guidelines and paper template as presented below.

Please prepare your main text document in Microsoft Word and PDF format, text should be single line spaced, line numbered and pages should be numbered. You can download the paper template here.

Please note that the style that you submit your paper in (e.g. any additional italics or bold fonts, bullet points, etc.) may be changed on publication to accommodate our publication style.

Manuscript Style

Language:

- The language of the IEM Journal is in English. However, a paper in Bahasa Melayu is also accepted. For accepted papers, an abstract in English and Bahasa Melayu must be included.
- The manuscript should be able to be readily understood by an engineer and researchers alike and should avoid any colloquialisms.
- The terms, including nomenclature and abbreviations, and style should be consistent throughout your journal paper. If you collaborate with other writers, please communicate clearly with them.
- Avoid referring directly to the names of individuals, organisations, products, or services unless essential to the comprehension of the manuscript. Gratuitous flattery or derogatory remarks about a person or organisation should not be included.
- Symbols and Units: SI and derived units should be used, if possible.
- Abbreviations: the use of internationally recognised abbreviations is allowed in the text. The abbreviations should be defined on first use. Abbreviations should not be used in the title.

Manuscript Guide

The following is a detailed manuscript preparation guide for articles submitted to IEM Journal; however, they can, in the most part, be used as a basis for other article types amending to concur with the page limit and premise of the formats, as appropriate.

The manuscript should be typewritten using single-spacing, font of 12 Times Roman; on one side of sheet only and in a single column format.

Title

Titles are limited to 150 characters, including spaces. Please avoid the use of any abbreviations, acronyms, or formulae. Titles should clearly reflect the content of the manuscript and any search terms that readers may use should be considered and incorporated.

List of Authors Name

List down all the names of authors (who has contributed to the paper) and the respective affiliations. From the list of authors, place an asterisk (*) next to the corresponding author's name. Provide an official email address of the corresponding author. **Please DO NOT include your personal telephone number on the title page.**

Abstract

Provide an informative 100 to 250 words abstract at the head of the manuscript. This should be a concise reflection of the aims, findings, conclusions and any interesting or important results. Carefully incorporate any terms that may be used by potential interested readers to improve the article's discoverability online (search engine optimisation). The abstract should contain no reference. Abbreviations that are not commonly used should be defined (for the benefit of the non-specialist reader) at first use.

Keywords

These are used for indexing. Please include between 3-5 keywords.

List of Notations

Please provide a list of symbols and definitions used in the text. This will ease our readers.

Introduction

A concise summary of current background knowledge, with reference to relevant previous works in the field should be presented. Please also describe the objectives of and justification for the work contained in the submitted manuscript.

Main Text

The methods and processes applied to investigate and achieve the objectives should be communicated in sufficient detail that readers could repeat the work successfully. The results should be reported clearly and interpreted accurately and analysed thoroughly. Figures/tables can be used to support these results.

It is important that all research articles include a section at the end of the main text that highlights the novelty of the results to the engineering field and any potential applications.

All sections should be numbered in Arabic such as 1, 2, etc. with the title in capitals. Sub-sections should be numbered such as 1.1, 2.3, etc. Numbered all equations in round brackets ( ) flush to the right. The equation should be in the centre.

Style for Illustrations (Tables and Figures)

Try to include the illustrations in between the text. Each illustration must be numbered such as "Figure 1, Figures 2-3, etc." and have a meaningful caption at the bottom. For tables, the caption must be at the top.
On graphs, show only the coordinate axes, or at most the major grid lines, to avoid a dense hard-thread result.

All lettering should be large enough to permit legible reduction of the figure to column width. Typing on figures is not acceptable. Photographs should be glossy prints, of good contrast and gradation and any reasonable size.

Conclusions

A concise summary of the results of case studies or research project papers and the lessons learned should be discussed. If necessary, please elaborate the applicability / relevance of your article to readers in other countries.

Research journals must discuss the practical relevance and potential applications of the engineering work described. This is important to readers working in engineering related practice.

Please also include relevant references to demonstrate how previous engineering research work has been used. These references could be standards, codes or relevant past journal papers.

Appendices

Additional information, such as tables or mathematical derivations can be included. These will be included in the article.

Acknowledgements

Please provide acknowledgement details to those persons or organization that contributed to the paper. Additional details required by funding bodies can be included.

References

The references to other literature that you have cited in your main text should be based on the APA style of referencing (Author, Date) as described below. Please refer https://apastyle.apa.org/ for a detailed guide on the referencing style.

- Single author: (Author, Year) or Author (Year)
- Two authors: (Author 1 & Author 2, Year) or Author 1 and Author 2 (Year)
- Three and more authors: (Author 1 et al., Year) or Author 1 et al. (Year)

In the text, the author and year of the reference should be put in parentheses immediately after the work referred to, for example 'Controlled tests on the Millennium Bridge (Chapman et al., 2005; Murray & Geddes, 1987; Wilby et al., 2011) during which.....' or 'as mentioned by Lim et al. (2018), the NCA derived from the agricultural wastes...'

All references must be listed, in full, at the end of the paper in alphabetical order, irrespective of where they are cited in the text.

In the reference section, the references should be written in full, as follows:

Books: Author 1 surname, author 1 initials, & Author 2 surname, author 2 initials. (Year of publication). Book title. Publisher, City, Country. doi reference. For example:

Kobayashi, K., Khairuddin, A. R., Ofori, G. & Ogunlana, S. (Eds.). (2009). *Joint ventures in construction*. Thomas Telford, London, UK.

Owen, G. & Totterdill, B. (2008). *The dispute board hearing. In Dispute Boards: Procedures and Practice*. Thomas Telford, London, UK.

Journal, magazine and newspaper articles: Author 1 surname, author 1 initials, & Author 2 surname, author 2 initials. (Year of publication). Paper title. Journal title, Volume (Issue number), First page-Last page. doi reference. Unpublished papers and theses should not be cited as they are not readily available.

Lim, J. L. G., Raman, S. N., Lai, F. C., Zain, M. F. M., & Hamid, R. (2018).

Synthesis of nano cementitious additives from agricultural wastes for the production of sustainable concrete. *Journal of Cleaner Production*, 171, 1150-1160. https://doi.org/10.1016/j.jclepro.2017.09.143.

Soon, F. C., Khaw, H. Y., Chuah, J. H., & Kanesan, J. (2018). Hyper-

parameters optimisation of deep CNN architecture for vehicle logo recognition. *IET Intelligent Transport System*, 12(8), 939-946. https://doi.org/10.1049/iet-its.2018.5127.

Conference proceedings: Author 1 surname, author 1 initials, & Author 2 surname, author 2 initials. (Year of publication). Paper title. Proceedings title, Volume (Issue number), First page-Last page. doi reference. Unpublished conference proceedings (i.e. that were only given to delegates) should not be cited as they are not generally available.

Chuah, J. H., Khaw, H. Y., Soon, F. C., & Chow, C. (2017). Detection of Gaussian noise and its level using deep convolutional neural network. *Proceedings of the TENCON 2017 - 2017 IEEE Region 10 Conference*, 2447-2450. https://doi.org/10.1109/TENCON.2017.8228272.

Unpublished material should not be included in the Reference list.

Please refer to https://apastyle.apa.org/ for a detailed guide on the referencing style. Authors should strictly adhere to the referencing style specified herein.

Mathematical Equations

Only relevant equations should be included in the main text and should be numbered. An equation editor program can be used to type in a formula.

Figures and tables caption list: Please supply a figure caption list at the end of your journal paper. Figures and tables must be put in the text in consecutive order. All figures must have a brief title accompanied with a short description.

Brief Profile

At the end of the manuscript, each author should provide a brief profile (less than 150 words), together with recent photographs (preferable less than 3 MB).

Corresponding Authors

We only permit one corresponding author per submission.

Conflict of Interest

Conflict of interest occurs when an author (or the author's institution) has personal or financial relationships that inappropriately influence the statements in the publication. Authors should ensure that publications will be written in an unbiased, ethical and responsible manner. The authors working on any sponsored engineering work or publications should declare such work under Conflict of Interest during submission.

Submission of Paper

Authors are required to submit via the IEM Online Journal Submission

(OJS) through the following link:

https://iemjournal.com.my/index.php/iem/about/submissions.

Together with the manuscript, the corresponding author should

enclose a cover letter containing the significance of the paper, the postal and email address, and telephone number for correspondence. In the cover letter, kindly provide four (4) names as reviewers. The selected reviewers must have the relevant knowledge and research experience. Provide the reviewers postal and email addresses and telephone numbers (if possible).

Further Enquiries

For further enquires, please contact Secretariat at the address shown below:

The Institution of Engineers, Malaysia
Bangunan Ingenieur, Lots 60 & 62, Jalan 52/4
Peti Surat 223 (Jalan Sultan), 46720 Petaling Jaya, Selangor Darul Ehsan
Tel: 03–78900130 Fax: 03–79577678
E-mail: pub@iem.org.my or iemjournal@gmail.com

PUBLICATION DISCLAIMER

The publication has been compiled by IEM and Dimension with great care and they disclaim any duty to investigate any product, process, service, design and the like which may may be described in this publication. The appearance of any information in this publication does not necessarily constitute endorsement by IEM and Dimension. They do not guarantee that the information in this publication is free from errors. IEM and Dimension do not necessarily agree with the statement or the opinion expressed in this publication.

COPYRIGHT

IEM Journal is the official magazine of The Institution of Engineers, Malaysia and is published by Dimension Publishing Sdn. Bhd. The Institution and the Publisher retain the copyright in all material published in the magazine. No part of this magazine may be reproduced and transmitted in any form, or stored in any retrieval system of any nature without the prior written permission of IEM and the Publisher.

EDITOR-IN-CHIEF

Ir. Ts. Prof. Dr Teo Fang Yenn
University of Nottingham Malaysia

EDITORIAL BOARD MEMBERS

Ir. Dr Bhuvendhraa Rudrusamy
Heriot-Watt University (HWU), Malaysia

Ir. Ts. Dr Hong Kai Sze
Tunku Abdul Rahman University of Management and Technology (TAR UMT)

Ts. Assoc. Prof. Dr Tee Boon Tuan
Universiti Teknikal Malaysia Melaka (UTEM)

Ir. Assoc. Prof. Dr Hassimi Abu Hassan
National University of Malaysia (UKM)

Ir. Ts. Wong Chee Fui
Universiti Tunku Abdul Rahman (UTAR)

Ir. Ts. Assoc. Prof. Dr Hum Yan Chai
Universiti Tunku Abdul Rahman (UTAR)

Ir. Dr Nor Ilia Anisa Aris
Taylor's University

Ir. Dr Sara Lee Kit Yee
Tunku Abdul Rahman University of Management and Technology (TAR UMT)

Ir. Assoc. Prof. Dr Moey Lip Kean
SEGi University

Ir. Dr Lim Siong Kang
University Tunku Abdul Rahman (UTAR)

Dr. Suchithra Thangalazhy Gopakumar
University of Nottingham Malaysia

Ir. Assoc. Prof. Dr Syamsul Rizal Abd Shukor
Universiti Sains Malaysia

Ir. Assoc. Prof. Dr Hasril Hasini
Universiti Tenaga Nasional (UNITEN)

Ir.Ts. EUR. ING. Dr Syuhaida Ismail
Maritime Institute of Malaysia

ASSOCIATE EDITORIAL BOARD MEMBERS

Prof. Khoo Hooi Ling
University Tunku Abdul Rahman (UTAR)

Ir. Assoc. Prof. Dr Teow Yeit Haan
Universiti Kebangsaan Malaysia

Ir. Ts. Dr Serene Lock Sow Mun
Universiti Teknologi PETRONAS

Assoc. Prof. Dr Sarajul Fikri Mohamed
University Teknologi Malaysia

Ir. Ts. Gs. Dr Chang Chun Kiat
Universiti Sains Malaysia

Assoc. Prof. Ir. Ts. Dr Jeffrey Yap Boon Hui
University Tunku Abdul Rahman (UTAR)

Assoc. Prof. Dr Anurita Selvarajoo
University of Nottingham Malaysia

INTERNATIONAL ADVISORY BOARD MEMBERS

Prof. Roger Falconer
Cardiff University, United Kingdom

Prof. Michael Parrett
University of Salford, United Kingdom

Professor Lynne B. Jack
Heriot-Watt University, United Kingdom

Prof. Dr Van Thanh Van Nguyen
McGill University, Canada

Prof. Dr Michael Nones
Institute of Geophysics Polish Academy of Sciences, Poland

Prof. Upaka Rathnayake
Altlantic Technological University, Ireland

Prof. Tanaka Yasuo
Kobe University, Japan

Ir. Ts. Prof. Dr Show Pau Loke
Khalifa University, Abu Dhabi, United Arab Emirates

Prof. Li Jiake
Xi'an University of Technology, China

Prof. Khu Soon Thiam
Tianjin University, China

Prof. Jung-Jeng Su
Dept. of Animal Science and Technology, National Taiwan University

Prof. Dr Jayaprakash Jaganathan
Vellore Institute of Technology, India

Prof. Dr Ignasius D.A. Sutapa
Soegijapranata Catholic University, Semarang, Indonesia

Prof. Dr Ooi Kim Tiow
Nanyang Technological University (NTU), Singapore

Prof. Haizhou Li
National University of Singapore (NUS)

INTERNATIONAL ASSOCIATE BOARD MEMBERS

Dr Chong Perk Lin
Teesside University, United Kingdom

AP Dr Khalid Hashim
Liverpool John Moores University, United Kingdom

Dr Syed Muzzamil Hussain Shah
King Fahd University of Petroleum & Minerals, (KFUPM), Saudi Arabia

Assoc. Prof. Dr Winardi Sani
Universitas Sangga Buana, Indonesia

Prof. Dr rer.nat Battsengel Baatar
German-Mongolian Institute for Resources and Technology, Mongolia

Assoc. Prof. Ir. Dr Intan Supraba
Universitas Gadjah Mada, Indonesia

Dr Nona Merry Merpati Mitan
Universitas Pertamina, Indonesia

Dr Tarig Faisal
Higher Colleges of Technology, United Arab Emirates

The Institution of Engineers, Malaysia

Bangunan Ingenieur, Lots 60/62, Jalan 52/4, Peti Surat 223 (Jalan Sultan), 46720 Petaling Jaya, Selangor Darul Ehsan
Tel: 03-78900130 Fax: 03-79577678 E-mail: sec@iem.org.my IEM Homepage: http://www.myiem.org.my

REFEREES FOR VETTING OF IEM PUBLICATIONS

Dear IEM Members/Readers,

The Standing Committee on Information and Publications is revising the list of referees to assist in the vetting of articles received from members and non-members. The referees should preferably be at least Corporate Members of The Institution or graduates with higher degrees.

The aim of appointing the referee is to ensure and maintain a standard in the IEM Publications namely the bulletin and the Journal.

Members who are interested to be placed in the database of referees are to return the registration form to the IEM Secretariat, providing details of their degrees and particular expertise and experience in the engineering fields.

We need your services to look into the vetting of articles received for Publications and due acknowledgement would be announced yearly in the Bulletin. Referees must be committed to return the papers within a month from date of appointment.

Chairman
Standing Committee on Information and Publications

All correspondences are to be addressed to: -

The Chief Editor
Standing Committee on Information and Publications
The Institution of Engineers, Malaysia
Bangunan Ingenieur, Lots 60 & 62, Jalan 52/4
P.O. Box 223 (Jalan Sultan)
46720 Petaling Jaya
Selangor Darul Ehsan

Email: pub@iem.org.my

AREAS OF INTEREST FOR VETTING OF PAPERS

Please tick (√) the appropriate area of interest that you are able to vet the papers.

- □ Acoustics
- □ Engineering Education
- □ Military Vehicles
- □ Room Temperature
- □ Aerodynamics
- □ Environmental Engineering
- □ Mini Pressure Meters
- □ Safety Engineering
- □ Air Conditioning
- □ Fine Chemical
- □ Mining Engineering
- □ Scaffolding Works
- □ Air Pollution Control
- □ Finite Element
- □ Naval Architecture
- □ Seepage
- □ Aircraft
- □ Fire Detection
- □ Navigation
- □ Sewerage
- □ Airport Engineering
- □ Fire Engineering
- □ Oil & Gas Engineering
- □ Shipbuilding
- □ Aluminium Design
- □ Floods
- □ Operation Research
- □ Signal Processing
- □ Arbitration
- □ Food Processing
- □ Palm Oil Industries
- □ Solar Energy Technology
- □ Automation
- □ Foundation Engineering
- □ Petrochemicals
- □ Steelworks Design
- □ Automotive Engineering
- □ Fuzzy Logic
- □ Petroleum Engineering
- □ Stream Turbine Power Plant
- □ Biochemical Engineering
- □ Gas Engineering
- □ Pharmaceuticals
- □ Sructural Analysis
- □ Biotechnology
- □ Geotechnical
- □ Piling
- □ Structural Rehabilitation
- □ Boiler Engineering
- □ Heat Exchanger
- □ Plumbing Engineering
- □ Survey Engineering
- □ Bridge Engineering
- □ Highway
- □ Pollution Control
- □ Taligates
- □ Building Services
- □ Hydraulics
- □ Ports & Harbour Engineering
- □ Telecommunication
- □ Coastal Engineering
- □ H.V. Electrical Distribution
- □ Power Electronics
- □ Thermal Engineering
- □ Co-Generation
- □ Industrial Engineering
- □ Power Generation
- □ Timber Design
- □ Computer Engineering
- □ Industrial Transport
- □ Pressure Vessels
- □ Tool Engineering
- □ Concrete Design
- □ Industrial Ventilation
- □ Prestressed Concrete
- □ Transfer Tunnels
- □ Concrete Technology
- □ Information Technology
- □ Project Management
- □ Transportation Engineering
- □ Construction Management
- □ Instrumentation
- □ Public Administration
- □ Urban Planning
- □ Control Engineering
- □ Lighting System
- □ Public Health Engineering
- □ Vehicles
- □ Drainage Engineering
- □ L.V. Electrical Distribution
- □ Quarry Engineering
- □ Vertical Transportation
- □ Dynamics Design
- □ Manufacturing
- □ Railways
- □ Waste Treatment
- □ Earthworks
- □ Mass Transit
- □ Reclamation Works
- □ Waste Water
- □ Edible Oil Refining
- □ Mechanical Handling Equipment
- □ Refrigeration
- □ Water Resources Engineering
- □ Electrical Transmission
- □ Management
- □ Reinforced Concrete Beams
- □ Water Pollution Control
- □ Electrochemical
- □ Metal Fabrication
- □ Road Transport
- □ Wind Engineering
- □ Electrotechnology
- □ Metallurgy
- □ Robotics
- □ Others (please specify)
- □ Energy Technology
- □ Micro Electronics
- □ Roof Structures

DISCIPLINES / SUB-DISCIPLINES OF VETTER

Please tick (√) the appropriate boxes.

- □ Aerospace
- □ Electrical
- □ Marine
- □ Petroleum
- □ Aeronautical
- □ Electronics
- □ Mechanical
- □ Production
- □ Agricultural
- □ Environmental
- □ Mining
- □ Structural
- □ Chemical
- □ Industrial
- □ Naval Architecture
- □ Others (Please specify)

VETTER'S DETAILS

Name : _____

Membership No. : _____ *(if applicable)*

Grade : □ Graduate □ Member □ Fellow □ Affiliate □ Others

(please specify) _____

Qualifications : _____

Addresses : *(Office)* _____

_____

(Residence) _____

_____

Contact No. : _____ *(Handphone)* _____ *(Office)* _____ *(Residence)*

E-mail Address : _____

Please mail all correspondences to the below. Please tick (√) the appropriate boxes.

Mail to : □ Office □ Residence

Brief Biodata (not longer than 50 words) (to be appended with this Reply Slip).

_____

_____

_____

_____

_____

Have you ever reviewed submissions for publication in any Journal(s) before? □ Yes □ No

If YES, name the Journal(s) _____

Do you have papers published in any Journal(s)? □ Yes □ No

If YES, name the Journal(s) _____

Date: _____ Signature : _____

IEM BRANCHES

PENANG	**IEM PENANG BRANCH SECRETARIAT** 1-04-02 E-Gate, Lebuh Tunku Kudin 2, 11700 Gelugor, Pulau Pinang	Tel : 04-606 599 iempenangbranch@gmail.com http://iempenang.org
SOUTHERN	**IEM SOUTHERN BRANCH SECRETARIAT** 24-B, Jalan Abiad, Taman Tebrau Jaya, 80400 Johor Bahru, Johor Darul Takzim	Tel : 07-331 9705 Fax : 07-331 9710 iemsouthern@gmail.com www.iemsb.org.my
PERAK	**IEM PERAK BRANCH SECRETARIAT** No. 60B, Jalan Lapangan Siber 1, Bandar Cyber (Business Centre), 31350 Ipoh, Perak Darul Ridzuan	Tel : 05-313 8459 iemperakbranch@gmail.com
EASTERN	**IEM PAHANG BRANCH SECRETARIAT** Ketua Penolong Pengarah Kanan Elektrik, JKR Cawangan Elektrik, Jalan Kamunting 2, Seri Kemunting, 25100 Kuantan, Pahang	Tel : 09-513 3533 Fax : 09-514 1594 mazman@jkr.gov.my
TERENGGANU	**IEM TERENGGANU BRANCH SECRETARIAT** 23-05, KT Business Centre, Padang Hiliran, Jalan Sultan Mohamad, 21100 Kuala Terengganu	Tel : 09-620 4500 Fax : 09-620 4502 iemterengganu@gmail.com
NEGERI SEMBILAN	**IEM NEGERI SEMBILAN BRANCH SECRETARIAT** No. 77-A-1, Lorong Haruan 5/3, Oakland Commerce Square, 70300 Seremban, Negeri Sembilan	Tel : 06-631 1011 Fax : 06-631 4619 iemnsembilan@gmail.com www.iemns.org.my
MELAKA	**IEM MELAKA BRANCH SECRETARIAT** C/O Sri Perunding Consulting Engineers, No. 2, Jalan Malinja 2, Taman Malinja Bukit Baru, 75150 Melaka	Tel : 06-284 8028 Fax : 06-283 8919 spcesb@gmail.com
SARAWAK	**IEM SARAWAK BRANCH SECRETARIAT** International Engineering Centre (IntEC), A2-G-19 & A2-1-19, Isthmus Raintree Square, Lot 3249, MTLD Block 7, Jalan Keruing, 93450 Kuching, Sarawak	Tel : 082-288 856 Fax : 082-288 856 iemsarawak@gmail.com
SABAH	**IEM SABAH BRANCH SECRETARIAT** Lot 25, 3rd Floor, Block C, Damai Point Commercial Centre, Lorong Damai Point, Off Jalan Damai, 88100 Kota Kinabalu, Sabah	Tel : 088-259 122 Fax : 088-236 749 iemsabah@gmail.com www.iemsabah.org.my
MIRI	**IEM MIRI BRANCH SECRETARIAT** 2nd Floor, Unit 14 (906-3-14), Soon Hup Tower Complex, (Mega Hotel), Jalan Merbau, 98000 Miri Sarawak	Tel : 085-423 718 Fax : 085-424 718 iem.miri@gmail.com www.iem-miri.org.my
KEDAH / PERLIS	**IEM KEDAH/PERLIS BRANCH SECRETARIAT** No. 164, Tingkat 2, Kompleks Alor Setar, Lebuhraya Darul Aman 05100 Alor Setar, Kedah Darul Aman	Tel : 04-734 3420 Fax : 04-733 3962 iemckps@gmail.com
PAHANG	**IEM PAHANG BRANCH SECRETARIAT** No. 114, Block F, Lorong Seri Teruntum, Medan Warisan, 25100 Kuantan, Pahang Darul Makmur	Tel : 019-855 6509 Fax : 09-514 6493 iempahang@gmail.com
KELANTAN	**IEM KELANTAN BRANCH SECRETARIAT** Lot 5139, Kompleks Niaga INOtrus Kawasan Perindustrian Pengkalan Chepa II, 6100 Kota Bharu, Kelantan	Tel : 09-773 0899 Fax : 04-733 3962 iemckps@gmail.com

www.iemjournal.com.my

IEM
The Institution of Engineers, Malaysia

IEM JOURNAL IS CALLING FOR PAPERS!

- Be part of a 60-year-old peer-reviewed journal with opportunities to enlighten the world with your research findings or expertise
- Be part of a well-recorded journal publication contributing towards the application of Scopus-Indexing
- Be recognised for your scientific credibility to preserve your work in the field of Engineering
- Authors will enjoy an incentive of RM500 for each successful published paper *(T&C apply)

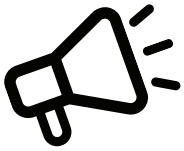

Scan the QR Code for Info

DOAJ Crossref doi iThenticate

THE INSTITUTION OF ENGINEERS, MALAYSIA
Bangunan Ingenieur, Lots 60 & 62, Jalan 52/4, P.O. Box 223 (Jalan Sultan),
46720 Petaling Jaya, Selangor Darul Ehsan.
Tel: 03-7890 0130 | Fax: 03-7957 7678 | E-mail: sec@iem.org.my

www.myiem.org.my

Published and Printed by
DIMENSION PUBLISHING SDN. BHD. (449732-T)
Level 18-01, PJX-HM Shah Tower, No.16A, Persiaran Barat,
46050 Petaling Jaya, Selangor Darul Ehsan.
Tel: 03-7493 1049 | Fax: 03-7493 1047 | E-mail: info@dimensionpublishing.com